Dendritic spines as chemical and electrical compartments:

A two-photon imaging study in the hippocampus of the rat

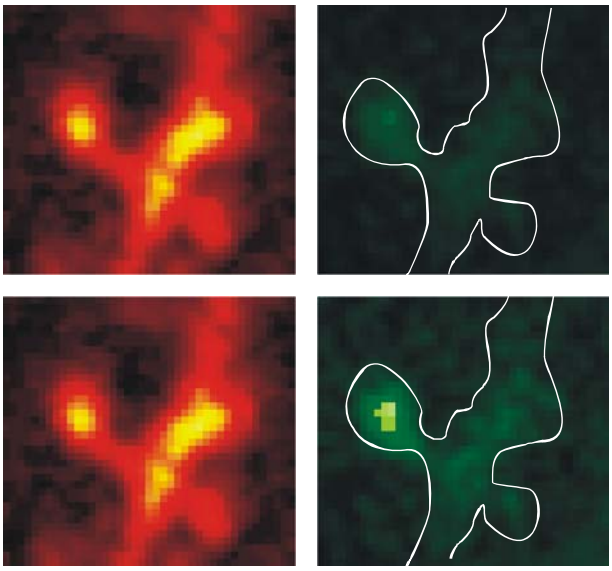

Inauguraldissertation

zur
Erlangung der Würde eines Doktors der Philosophie
vorgelegt der
Philosophisch-Naturwissenschaftlichen Fakultät
der Universität Basel

von

Åsa Müller-Grunditz
aus Linköping, Schweden

Basel, 2008

Genehmigt von der Philosophisch-Naturwissenschaftlichen Fakultät
auf Antrag von
Prof. Denis Monard
Prof. Andreas Lüthi
Prof. Fritjof Helmchen
Dr. Thomas Oertner

Basel, den 19. Februar 2008

Prof. Hans-Peter Hauri
Dekan der Philosophisch-
Naturwissenschaftlichen Fakultät

Summary

Most excitatory synapses are located on small dendritic protrusions called spines. So far, the function of dendritic spines is not fully understood. Imaging experiments have shown that spines can compartmentalize second messengers such as Ca^{2+}. In addition to chemical compartmentalization, spines could play a role in shaping excitatory postsynaptic potentials (EPSPs) by activating voltage-dependent conductances in the spine head, thus serve as electrical amplifier. The electrical resistance of the spine neck is essential for influencing synaptic potentials. We measured the diffusion coupling between spine heads and parent dendrites of CA1 pyramidal cells using fluorescence recovery after photobleaching (FRAP) to estimate the resistance of the spine neck. Our data indicate that the diffusional coupling between spine and parent dendrite is highly plastic. Postsynaptic depolarization led to dramatic reduction in the diffusional coupling between spine head and parent dendrite, indicating a proportional rise in the electrical resistance. But is the ohmic resistance sufficent to electrically isolate the synapse? We used two-photon Ca^{2+} imaging combined with modeling to address this question.

We found two different classes of synapses in the CA1 region of the hippocampus. One class producrd clearly detectable Ca^{2+} transients in current clamp (functional spines), whereas an other class showed hardly any Ca^{2+} influx under current clamp conditions ('Ca^{2+}-silent spines'). Interestingly, this group of Ca^{2+}-silent spines showed Ca^{2+} responses following a brief burst of presynaptic action potentials that were much larger than in functional spines, indicating differences in both presynaptic release properties and postsynaptic receptor densities.

The Ca^{2+} transients in the funciotnal spines were inhibited by blocking either NMDA receptors, AMPA receptors, or R-type Ca^{2+} channels. We concluded that Ca^{2+} transients were dependent on the joint activation of these channels, which all contributed to spine depolarization in a synergistic fashion. To estimate the depolarization in individual functional spines, we used the voltage-dependence of the NMDA receptors. Two-photon imaging allowed us to measure NMDA receptor-mediated Ca^{2+} currents in individual spines. The voltage-dependence of synaptic NMDA receptors was steeper than previously thought. Using the Ca^{2+} imaging data

combined with modeling, we predicted that EPSPs reach amplitudes of ~55 mV in functional spines, approaching the synaptic reversal potential. Functional spines are electrically isolated from the parent dendrite by a high resistance neck and amplify synaptic currents through the activation of high-voltage activated Ca^{2+} channels.

The spine neck resistance appears to have a strong effect on the Ca^{2+} transients needed to induce synaptic plasticity. Our biophysical model predicted that only spines with high spine neck resistance experience supralinear Ca^{2+} transients after paring presynaptic activity with a postsynaptic action potential. Furthermore, spines with a high spine neck resistance are more sensitive to the precise timing the presynaptic and the postsynaptic action potentials then in spine with low neck resistance.

By integrating data from diffusion measurements, calcium imaging and pharmacology into a single quantitative model, we have gained new insights into the complex interaction between chemical and electrical signaling at individual synapses. The newly discovered spine neck plasticity might be an important mechanism to set the threshold for the induction of functional synaptic plasticity. To test this hypothesis in the future, new methods are currently being developed to quantify plasticity on the single-synapse level.

Table of contents

SUMMARY **1**

TABLE OF CONTENTS **3**

INTRODUCTION **5**

GENERAL INTRODUCTION 5
THE NEURON 6
THE CHEMICAL SYNAPSE IS A PLACE OF COMMUNICATION 7
DENDRITIC SPINES 8
Structure of dendritic spines *8*
Postsynaptic density (PSD) *9*
Smooth endoplasmatic reticulum (sER) and other organelles in spines *9*
Function of a dendritic spine *10*
Ca^{2+} signaling in dendritic spines *16*
AMPA RECEPTORS 17
NMDA RECEPTORS 18
SILENT SYNAPSES 19
VOLTAGE-DEPENDENT CA^{2+} CHANNELS 20
THE HIPPOCAMPUS 22
CA1 PYRAMIDAL NEURONS 24
Dendritic morphology *24*
Excitatory synaptic input *25*

AIM OF THE THESIS **26**

SPINE NECK PLASTICITY CONTROLS POSTSYNAPTIC CALCIUM TRANSIENTS THROUGH ELECTRICAL COMPARTMENTALIZATION **28**

SUMMARY 28
ABSTRACT 28
SUPPORTING MATERIAL 39

OPTICAL INVESTIGATION OF FUNCTIONAL AND SILENT SYNAPSES **44**

ABSTRACT 44
INTRODUCTION 45
RESULTS 46
Synaptically evoked Ca^{2+} transients in individual spines *46*
Classification of spines according to their Ca^{2+} response profiles *47*
Properties of Ca^{2+}-silent spines *50*
DISCUSSION 53
Differences between Ca^{2+}-silent and functional spines *53*
Do all Ca^{2+}-silent spines carry silent synapses? *54*
EPSP amplitude in functional spines is uniform *54*

SPINE NECK RESISTANCE SETS TIME WINDOW FOR THE DETECTION OF COINCIDENT ACTIVITY **56**

ABSTRACT 56
INTRODUCTION 56
RESULTS 58

Backpropagation of action potentials evoke Ca^{2+} transients in the proximal apical dendrites of a CA1 pyramidal cell *58*
Modeling Ca^{2+} transients *59*
Ca^{2+} transients after pairing of EPSPs and bAPs are dependent on the spine neck resistance *62*
Ca^{2+} transients evoked by an EPSP preceding a bAP are strongly enhanced in spines with high spine neck resistance *63*
DISCUSSION 66

CONCLUSIONS AND OUTLOOK 68

1. SPINE CA^{2+} TRANSIENTS DEPEND ON ELECTRICAL SYNERGISM BETWEEN AMPA RECEPTORS, NMDA RECEPTORS, AND VDCCS 68
2. THE VOLTAGE-DEPENDENCE OF SYNAPTIC NMDA RECEPTORS IS STEEP 68
3. CA^{2+}-SILENT SPINES DIFFER PRE- AND POSTSYNAPTICALLY FROM THEIR FUNCTIONAL NEIGHBORS 69
4. HIGH CA^{2+} LEVELS TRIGGER CHANGES IN THE SPINE NECK RESISTANCE 70
OUTLOOK: IS SPINE NECK PLASTICITY ESSENTIAL FOR FUNCTIONAL SYNAPTIC PLASTICITY? 70

METHODS 72

ACUTE SLICE PREPARATION 72
ORGANOTYPIC SLICE CULTURE 72
ELECTROPHYSIOLOGY 73
PHARMACOLOGY 73
TWO-PHOTON LASER SCANNING MICROSCOPY 74
CA^{2+} IMAGING 75
DATA ANALYSIS 75
DYE SATURATION 75
ESTIMATION OF SPINE VOLUME 77
ESTIMATION OF SPINE NECK RESISTANCE 77
FRAP MEASUREMENTS IN ACUTE SLICES 78
IN VIVO FRAP MEASUREMENTS 78
COMPARTMENTAL MODELING 79
AMPA receptor current *79*
NMDA receptor current *80*
Voltage-dependent Ca^{2+} channels *81*
The sodium current (I_{Na}) *81*
A-type potassium current ($I_{KA(prox)}$) and ($_{IKA(dist)}$) *82*
Noninactivating potassium current (I_{KDR}) *83*
Noninactivating, nonspecific cation current (I_h) *83*
Simulation of spine Ca^{2+} transients *84*

REFERENCES 86

LIST OF ABBREVIATIONS 96

ACKNOWLEDGMENTS 97

CURRICULUM VITAE 98

Introduction

General introduction

The brain is an extremely complex structure containing billions of cells. It is constantly receiving information via sensory organs and makes decisions based on the sensory input. However, the behavior resulting from this processing is not hardwired, but can be adapted in response to previous experience. The ability of an organism to make decisions, to modify its behavior based on previous experiences and to store these modifications is in general called learning and memory. The mechanism for learning and memory has been a subject of intense interest and has to be investigated on different levels of complexity. These levels range from the behavior of an animal, the anatomy of neuronal networks, the properties of a single cell down to single molecules.

More than a century ago, Ramon y Cajal observed the presence of small dendritic protrusions, which he called ‘espinas’ (spines). He believed that they connected the nerve cells in the brain (Ramon y Cajal, 1891) and that they are involved in the process of learning (Ramon y Cajal, 1893). Sixty years later, Donald Hebb postulated that altering the strength of the connections between nerve cells could be the cellular basis of learning and memory (“Hebbian rule”, (Hebb, 1949)). The process of creating, strengthening, and discarding synaptic contacts among nerve cells is called synaptic plasticity, and it is nowadays acknowledged that synaptic plasticity is involved in mediating learning and memory (Morris et al., 1986; Moser et al., 1998). It is assumed that memory traces are stored in the strength of synaptic contacts. The hippocampus is an ideal model for studying the function of synaptic contacts because of its importance for memory processing and because of its relatively simple feed-forward circuit, involving a small cast of excitatory cell types. The aim of this thesis was not to answer the question as to how memory is stored in the brain but rather to better understand the function of individual synaptic contacts, using the Schaffer collateral pathway in the hippocampus as a model system.

The neuron

The basic building block of the brain is the neuron, which is a highly specialized cell that encodes information in the form of electrical activity. A typical neuron can have connections with up to 10'000 other neurons (Stevens, 1979). Although the human brain contains an extraordinary number of these cells that can be classified into many different types depending on location and function, they all share the same basic architecture. Neurons consist of three distinct domains; the soma (cell body), the dendrites and the axon. The soma contains the nucleus and the organelles for homeostasis and protein synthesis. In contrast to most other cell types, neurons are highly polarized cells and have regions specialized for input and output. The regions where neurons receive input from other neurons are the dendrites. A highly branching, treelike shape characterizes the dendrites. The neuron's output region is the axon. It extends out from the soma and provides the pathway over which signals can travel from the soma for long distances to other parts of the brain (Fig. 1.1).

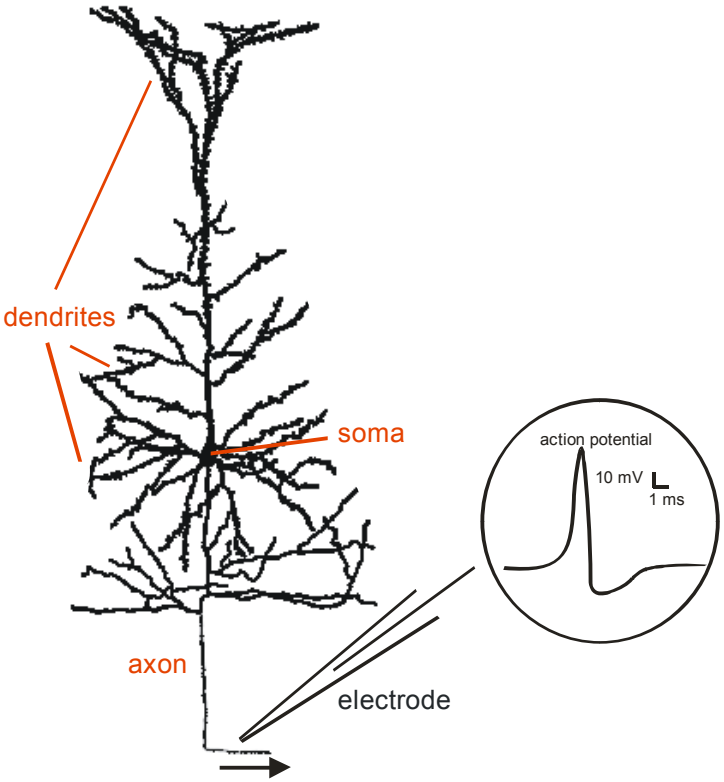

Figure 1.1. ***Single neuron in a drawing by Ramón y Cajal.*** *Dendrite, soma, and axon can be clearly distinguished. The inset shows an example of a neuronal action potential (schematic). The action potential is a short voltage pulse of 1-2 ms duration and amplitude of about 100 mV. (Adapted from Cajal, 1909).*

Neurons communicate via chemical and electrical synapses in a process known as synaptic transmission. Every neuron receives signals from a large number of upstream

neurons and integrates this input in order to decide whether or not to send out its own signal. An understanding of the brain demands a wide-ranging knowledge, which stretches from the molecular events that occur within a single neuron, to the highly complex synaptic interactions between thousands of neurons. Higher brain functions such as learning and memory can be studied on the level of single spines up to the level of large neuron populations.

The chemical synapse is a place of communication

The synapse is the point of functional contact between two neurons; it is the primary place at which information is transmitted from neuron to neuron. The synapse composes of a pre- and a postsynaptic cellular component. At a chemical synapse the communication between two cells relies on the use of a neurotransmitter, which is secreted following an action potential by the presynaptic terminal. An action potential is a regenerative electrical signal and when triggered by depolarization travels along the axon of the presynaptic cell (inset in Fig. 1.1). When the action potential reaches the presynaptic terminal, voltage-dependent Ca^{2+} channels (VDCC) transiently open and can cause a synaptic vesicle to fuse with the cell membrane and release neurotransmitter into the synaptic cleft. The transmitter then diffuses across the synaptic cleft and binds to receptors on the postsynaptic membrane. These receptors are often ion channels, which after binding the neurotransmitter change their conformation resulting in a transient opening of their conducting pore. These pores are selective for different ions, whose influx across the membrane generates either an inward or an outward current in the postsynaptic cell, depending on the charge of the ion and the net direction of flux. A transmitter can therefore result in either an increase (excitatory synapse) or a decrease (inhibitory synapse) in the probability that the postsynaptic cell itself generates an action potential and thus transmits the signal. The number of synaptic connections a neuron forms can be large and many afferents can interact and influence a postsynaptic neuron by either excitatory or inhibitory effects. The responses are classified as excitatory postsynaptic potentials (EPSPs) or inhibitory postsynaptic potentials (IPSPs), depending on whether they drive the cell towards or away from its firing threshold. Because a single EPSP is usually too small

to induce an action potential, neurons typically integrate signals from many synapses . If the summation of all incoming excitatory and inhibitory postsynaptic potentials reaches the spiking threshold, an action potential is initiated. The action potential is then actively transmitted along the axon in an all-or-non fashion.

Action potentials do not only travel along the axon to cause neurotransmitter release at the presynaptic terminal, but they also invade the dendritic tree which is mainly the input region of the neuron. Voltage-dependent sodium and Ca^{2+} channels in the dendrites allow an active back-propagation of an action potential initiated at the soma (Stuart and Sakmann, 1994). This back-propagating action potential (bAP) is an effective feedback signal providing the input region with information about the output state of the neuron (Magee and Johnston, 1997; Stuart and Hausser, 2001).

Dendritic spines

The majority of excitatory synapses are located on dendritic spines which are tiny protrusions extending from the dendrite (Harris and Kater, 1994; Nimchinsky et al., 2002). Dendritic spines were first described by Ramon y Cajal more than a century ago. He discovered that cerebellar Purkinje cells had small thorns that project from dendrites like leaves from a tree (Ramon y Cajal, 1888). At that time, he thought that the spines serve as connections between axons and dendrites and that they might be involved in the process of learning (Ramon y Cajal, 1891, 1893). Half a century later, three landmark studies using electron microscopy verified Cajal's neuronal theory and his prediction that spines were the sites of synaptic contact between axons and dendrites (DeRobertis and Bennett, 1955; Palay, 1956; Gray, 1959).

Structure of dendritic spines

A typical hippocampal CA1 spine consists of a narrow neck, ranging in length from 0.2 to 2 μm, in diameter from 0.04 to 5 μm and with a voluminous head. The total spine volume ranges from 0.004 to 0.6 μm^3 (Harris and Kater, 1994). Spines exist in a variety of morphological forms. Spine necks can be long or short, thick or thin, straight or bent, cylindrical or irregular, and branched or unbranched in all combinations. Spine heads can be small or large, and spherical, oval, or irregular in

shape (Fig. 1.2). This heterogeneity in spine structure occurs both along a single dendrite and across the different cell types. How this heterogeneity in morphology of the spines effects their function is yet not known.

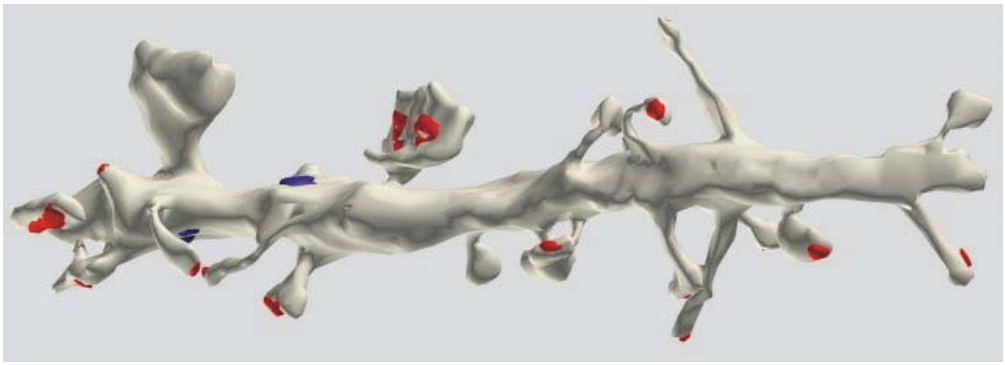

Figure 1.2. ***Spiny dendrite from a hippocampal pyramidal cell.***
Three-dimensional reconstruction of a segment of dendrite with dendritic spines from a CA1 neuron in the stratum radiatum of a rat. Excitatory synapses are shown in red. Inhibitory synapses are shown in blue. (Adapted from http://synapses.clm.utexas.edu)

Postsynaptic density (PSD)

Spines are structures specialized for synaptic transmission. They contain the postsynaptic components of the synapse. The postsynaptic density (PSD) is the site on the postsynaptic cell where neurotransmitter receptors are clustered together with scaffolding and signaling molecules. The PSD appears as an electron-dense thickening which is concentrated on the surface of spines in electron micrographs (EM). The protein composition of PSDs consists of hundreds of components such as receptors, cytoskeletal and adaptor proteins, as well as associated signaling molecules which are involved in several signaling pathways implicated in synaptic plasticity (Walikonis et al., 2000).

Smooth endoplasmatic reticulum (sER) and other organelles in spines

Most smooth endoplasmatic reticulum (sER) is located in the dendrites but approximately 20% of the spines in an adult CA1 pyramidal cell contains extensions of sER (Cooney et al., 2002). In a subset of these spines the sER elaborates into a structure called the spine apparatus (Gray and Guillery, 1963). The spine apparatus consists of two or more disks of sER laminate separated by sheets or plates of dense material. The sER is thought to be involved in Ca^{2+} uptake and Ca^{2+} release (Pozzan

et al., 1994; Emptage et al., 1999; Korkotian and Segal, 1999), but its exact role has still to be investigated. Less than a fifth of the thin spines contain sER (Spacek and Harris, 1997), whereas the majority of the large mushroom spines contain a spine apparatus. As sER is thought to be involved in the Ca^{2+} handling, thin spines could therefore experience different forms of Ca^{2+} dynamics compared to large mushroom spines (Knott et al., 2006).

Clathrin-coated vesicles, multivesicular bodies and endosomes are found in a subset of spines, indicating that protein degradation and recycling can occur within dendritic spines (Spacek and Harris, 1997; Cooney et al., 2002). Free ribosomes are rarely found in the spines but polyribosomes are frequently accumulated in the spine head, indicating that protein synthesis can take place within dendritic spines (Steward and Falk, 1985; Steward and Reeves, 1988).

Although spines lack neurofilaments, the spine head contains a dense network of actin filaments (Fifkova and Delay, 1982; Matus et al., 1982). In the neck actin filaments are oriented lengthwise along the spine apparatus (Fifkova, 1985). The actin cytoskeleton determines the structure of a spine and is regulated by transmembrane receptors through their actions on Rho family GTPbinding proteins, including RhoA, RhoB, Rac and Cdc42 (reviewed in (Carlisle and Kennedy, 2005)). Cellular organelles such as the mitochondria are usually absent in spines but are present in dendrites (Li et al., 2004). Therefore ATP, which is essential for several processes in the spine, must diffuse from the dendritic shaft into the dendritic spines.

Function of a dendritic spine

Since the synapses could sit directly on dendritic shafts, spines must have an additional function besides receiving synaptic inputs. Because of their small size, the function of dendritic spines has only recently become accessible to the experimentalist. Over the last fifty years, spine properties have been investigated through analytical and computational studies based on morphological data (Harris and Kater, 1994). More recently, the development of high-resolution two-photon Ca^{2+} imaging in dendrites and spines allows the scientists to directly study the function of spines in intact neural tissue.

However, we are only beginning to understand their complexity and functionality. Below I will describe some hypotheses on what the function of a spine might be.

Do dendritic spines simply increase the dendritic surface area available for synaptic contacts?

Ramon y Cajal first postulated that the spines could increase the surface area available for new synapses to be formed (Ramon y Cajal, 1991). His idea has mostly been dismissed, because electron-microscopic images of spiny dendrites show that the dendritic membranes between the spines often lack synapses. Based on three-dimensional electron-microscopic reconstructions, Harris and Stevens estimated that only 5-9% of the dendritic membrane area of CA1 pyramidal cells would have been covered by synapses if all the spines had been removed and the associated synapses moved onto the dendrites (Harris and Stevens, 1988). These results argue against the hypothesis that the spines are necessary in order to increase the dendritic membrane area available for the synaptic contacts.

Do dendritic spines enhance the connectivity between neurons?

Dendritic spines allow dendrites to reach not only synapses on axons close to the dendrites but also to reach synapses on axons 1-2μm away. Thus the choice of potential axons available to a given dendrite is increased for a spiny dendrite compared to a nonspiny dendrite (Stepanyants et al., 2002) (Fig 1.3). In a neuropil densely packed with axons and dendrites, the existence of spines allows more synaptic connections to be compacted into a limited brain volume. Therefore, the function of spines could be to increase the density of connections between dendrites and axons (Swindale, 1981).

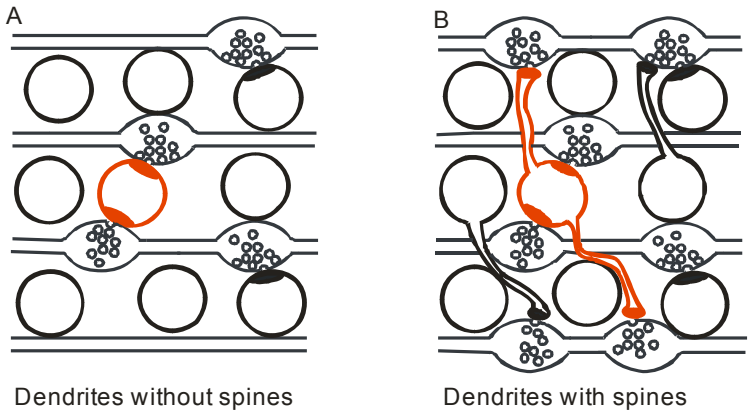

Figure 1.3. ***Spines exist to increase the density of connections between dendrites and axons.***
(A) *A cross section through a nonspiny dendrite (red) illustrating the number of axons available for that dendrite to make contacts with (in this case 2 axons).*
(B) *A spiny dendrite (red) can reach more axons (in this illustration 4 axons).*
The total number of axons from which a segment of dendrite without spines (A) could select contacts is determined by the diameter of the dendrite. On the other hand, the total number of axons from which a segment of dendrite with spines (B) could select contacts is not only determined by the diameter of the dendrite but also by the length of the attached spine. (Adapted from Sorra and Harris 2000).

Are dendritic spines primarily biochemical compartments?

The narrow spine neck might limit the diffusion of molecules into and out of the spine. Spines might therefore serve as biochemical compartments for second-messengers such as Ca^{2+}. The introduction of Ca^{2+} imaging techniques has shown that Ca^{2+} influx after synaptic stimulation is restricted to the stimulated spine head (Sabatini et al., 2001; Nimchinsky et al., 2002) (Fig. 1.4).

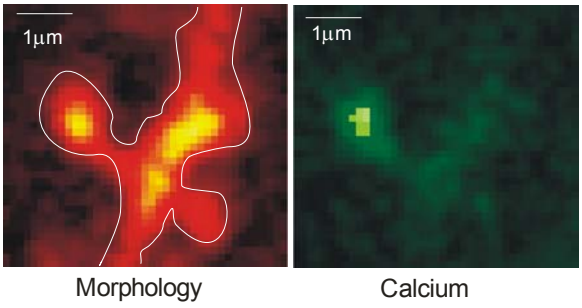

Figure 1.4. ***The Ca^{2+} signal is restricted to the stimulated spine.*** *Measurement of changes in [Ca^{2+}] evoked by synaptic stimulation. The red Ca^{2+}-insensitive dye (Alexa-FLuor 594) helps to visualize the morphology (left). The green Ca^{2+} indicator (Fluo5F) shows a large fluorescence changes in the stimulated spine (right). The Ca^{2+} signal is almost completely restricted to the spine head*

Ca^{2+} imaging experiments and diffusion measurements of other proteins by different groups support the idea that spines can act as biochemical compartments (Gray et al., 2006; Santamaria et al., 2006).

Postsynaptic elevation of Ca^{2+} concentration triggers a variety of activity-dependent long-lasting synaptic modifications (Mulkey and Malenka, 1992; Bliss and Collingridge, 1993). The amplitude and duration of the Ca^{2+} rise inside a dendritic spine is assumed to determine the magnitude of long-term changes in synaptic efficacy (Nevian and Sakmann, 2006). In addition, limiting the spread of Ca^{2+} could provide input specificity (Yuste and Denk, 1995), and protect the dendritic shaft and the soma, both of which are sensitive to Ca^{2+}-induced excitotoxicity. The regulation of Ca^{2+} concentration in spines is therefore important and might be a key function of the spines.

The spine neck not only functions as a diffusion barrier for Ca^{2+} but also for other second messengers and activated enzymes like CaMKII. CaMKII has been suggested to act as a Ca^{2+}-triggered switch (Miller and Kennedy, 1986; Lisman, 1989). Studies have shown that the postsynaptic CaMKII activity is necessary and sufficient to generate long-term potentiation (LTP) (Silva et al., 1992; Pettit et al., 1994). Thus, by trapping activated kinase molecules close to their target proteins in the PSD, narrow spine necks might facilitate the induction of synaptic plasticity.

Do dendritic spines also act as electrical compartments?

In addition to chemical compartmentalization, spines might also have an impact on the electrical signal generated by the synapse. Chang was the first to point out that the spine neck shapes the electrical signal generated by the synapse (Chang, 1952). He suggested that a high spine neck resistance can attenuate the effect of a synapse on the rest of the cell. Therefore, a cell can only fire when a large number of synapses fire together.

Do spines attenuate the synaptic potential?

A longstanding hypothesis has been that the thin spine neck might act as an internal resistance limiting the spread of synaptic currents (Rall and Shepherd, 1968; Coss and Perkel, 1985). Changes in spine neck constriction could then modulate synaptic

strength and provide a mechanism for short-term memory (Crick, 1982). The passive property of a single spine has been analyzed in many modeling studies (Wilson, 1984; Shepherd et al., 1985; Segev and Rall, 1988). Compartmental models based on three-dimensional reconstructions of serial electron micrographic sections of spines (Harris and Stevens, 1989) have however suggested that most spine necks are not thin and long enough to significantly reduce the charge transfer to the parent dendrite (Wickens, 1988; Koch and Zador, 1993).

Are dendritic spines excitable?

Even if the spine neck resistance does not affect the sizes of synaptic currents reaching the dendrite, it could still compartmentalize the membrane potential in the spine head. The spine neck could slow down the current passing through and produce a voltage difference between spine head and the parent dendrite. If the spine head membrane is equipped with excitable channels, the amplitude of the membrane potential in the spine head should then be sufficient to selectively activate these channels (Wilson, 1984; Segev and Rall, 1988) (Fig. 1.5). This active conductance should then allow spines to isolate synaptic inputs or to generate localized action potentials in response to their synaptic inputs, thus acting as synaptic amplifiers (Miller et al., 1985; Perkel and Perkel, 1985; Shepherd et al., 1985). The idea of spines acting as amplifiers for synaptic input has been tested in many modeling studies and among others by Segev and Rall (Segev and Rall, 1988). The presence and the amount of amplification depend on the density of the active channels and on the spine neck resistance.

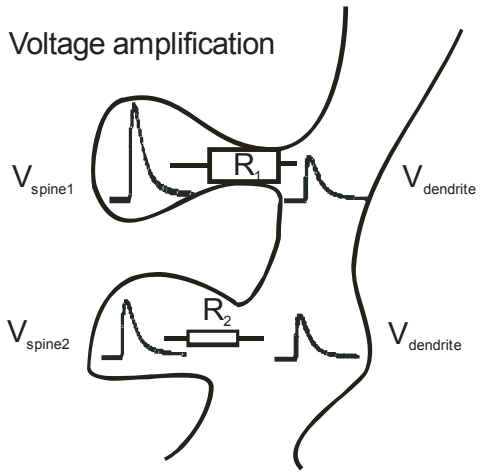

Figure 1.5. ***Spines exist to amplify electrical potential at the synapse.***
Spine shape and resistance of the spine neck may influence the electrical potential (V) in the spine head. The upper mushroom spine has a high spine neck resistance (R_1), enough to slow down the flow of the electric current and activate voltage dependent conductances, thus act as a synaptic amplifier. The lower stubby spine with a low spine neck resistance (R_2) is not able to isolate synaptic input. (Adapted from Sorra and Harris, 2000).

The idea that spines can restrict electrical activation independent from the rest of the dendrite has long been in dispute. To what degree a spine restricts the depolarization depends strongly on the electrical resistance of the spine neck, which can not be measured directly. But measurements of diffusion through the spine neck can be used to estimate the electrical resistance of spine necks (Svoboda et al., 1996).

The diffusion through the spine neck has been probed using different methods, either by measuring the fluorescence recovery after photobleaching (FRAP) in the spine (Svoboda et al., 1996; Sobczyk et al., 2005) or by using a photoactivatable green fluorescence protein (PAGFP) (Bloodgood and Sabatini, 2005). In FRAP experiments a freely diffusible fluorophore is bleached in the spine head and the time for fluorescence recovery by diffusion from the parent dendrite is measured. Photoactivation experiments, measuring the clearance of activated PAGFP from the spine head by diffusion, should in principle result in similar estimates of spine neck resistance, but the outcomes of the studies are controversial. Whereas some groups claimed that the spine neck is not restrictive enough to allow for substantial voltage drop across the neck after synaptic activation (Svoboda et al., 1996), other groups claim that the diffusional coupling between spine head and the parent dendrite is heterogeneous and that some spines are diffusionally isolated (Bloodgood and Sabatini, 2005). These diffusionally isolated spines seem to have a high spine neck resistance that may compartmentalize the membrane potential in the spine head.

Do dendritic spines act as single units for synaptic plasticity?

Spines show a large diversity in both shape and size (Fig. 1.2). It is believed that these differences between neighboring spines are reflections of differences in synaptic strength. Supporting this idea different groups have shown that there is a relation between spine volume, PSD area and the number of AMPA receptors in the PSD (Nusser et al., 1998; Takumi et al., 1999; Matsuzaki et al., 2001). Many studies have focused on the correlation between spine morphological change and synaptic plasticity. Although alternations in spine morphology have been found (Fifkova, 1985; Moser et al., 1994; Toni et al., 1999), it has been difficult to directly show a correlation between specific morphological changes (such as enlarged spine heads) and different stages of induction or maintenance of synaptic plasticity. Light-induced release of glutamate from caged compounds has been a useful tool to investigate the

induction and maintenance of long-term potentiation (LTP) in single spines by using this novel approach. Matsuzaki *et al.* have shown that it is the smaller and weaker spines that preferentially undergo LTP, whereas larger and stronger spines are more stable and show less plasticity (Matsuzaki et al., 2004). Such observations have led to the idea that the small 'plastic' spines are preferential sites for plasticity and large mushroom spines represent 'memory' spines (Kasai et al., 2003). Thus, LTP is input-specific at the level of individual synapses but does the induction of LTP at one synapse influence the neighboring synapse? In a recent study from Harvey and Svoboda (Harvey and Svoboda, 2007) they show that neighboring synapses can influence each other: LTP at one synapse reduces the threshold for potentiation at neighboring synapses.

Ca^{2+} signaling in dendritic spines

Postsynaptic Ca^{2+} transients play a major role in many forms of activity-dependent synaptic plasticity (Zucker, 1999). Because the spine neck serves as a barrier to Ca^{2+} exchange between the spine head and the dendrite, spine Ca^{2+} may play an important role in activating synapse-specific regulatory mechanisms (Noguchi et al., 2005). So far, the entry of Ca^{2+} into the spine is known to activate signaling cascades that regulate the strength of the synapse, the morphology of the spine, the trafficking of proteins and of organelles (reviewed in (Kennedy and Ehlers, 2006; Tada and Sheng, 2006; Bloodgood and Sabatini, 2007a). The resting Ca^{2+} concentrations in neurons are only around 80 nM, which means that approximately 3 free Ca^{2+} ions are present in an average spine head volume of 0.05 μm^3, and this is 20.000 fold lower than the 2 mM Ca^{2+} found extracellularly. Synaptic stimulation leads to Ca^{2+} influx from the following sources (Fig 1.6):

1. The release of glutamate leads to the opening of Ca^{2+} permeable receptors, such as NMDA receptors or Ca^{2+}-permeable AMPA receptors.
2. Voltage-dependent Ca^{2+} channels (VDCC) are opened by the depolarization produced mainly through AMPA receptors.
3. The release of Ca^{2+} from intracellular stores can be triggered by metabotropic neurotransmitter receptors or by Ca^{2+}-induced Ca^{2+}-release (CICR). Two types of receptors located in the sER membrane, the ryanodine-receptor (RyR)

family and the inositol-1,4,5-triphosphate receptor (IP_3R) family, seem to control this process.

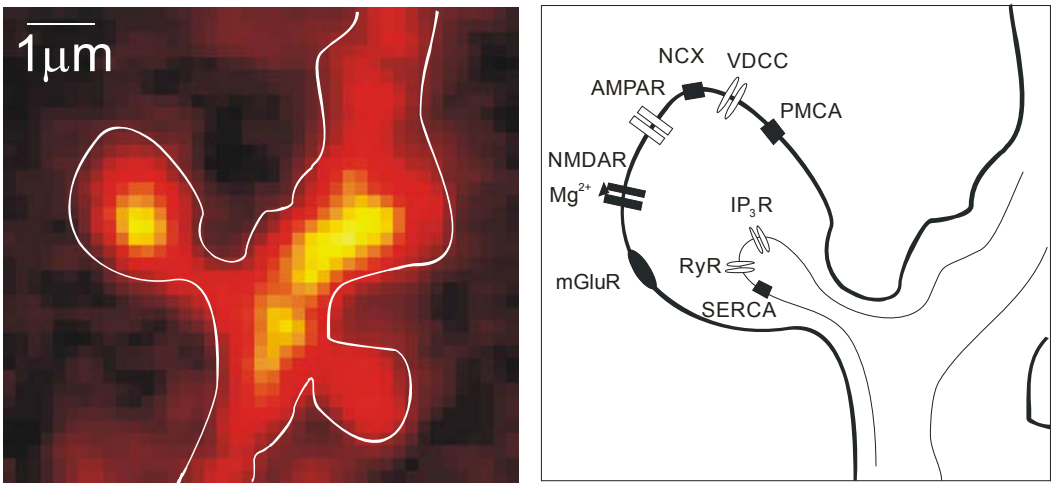

Figure 1.6. ***Schematic drawing of a postsynaptic spine with different*** Ca^{2+} ***sources.***
The NMDA receptor is the main source of Ca^{2+} *influx into the spine. The NMDA receptors are blocked by* Mg^{2+} *at resting membrane potential, only opening if glutamate is bound and the membrane is depolarized. The glutamatergic AMPA receptors are permeable to* Na^+ *and* K^+ *and mediate depolarizing of the postsynaptic membrane. Another source of* Ca^{2+} *influx into the posynaptic spine is through voltage-dependent* Ca^{2+} *channels (VDCC). The mGluRs exhibit second messenger cascades that among others can trigger* Ca^{2+} *release from internal IP3-sensitive stores. The low basal* Ca^{2+} *level inside the spine is restored by the* Na^+ */* Ca^{2+} *exchanger (NCX), plasma membrane* Ca^{2+} *pumps (PMCA) and by SERCA pumps refilling the internal stores.*

The source of synaptic Ca^{2+} has been controversial because it is difficult to selectively inhibit each of these components. For example, blocking NMDA receptors not only disrupts the direct Ca^{2+} influx through the NMDA channels but also reduce the depolarization in the spine head that leads to VDCCs opening and to the initial Ca^{2+} influx that triggers CICR. Compartmental modeling opens the possibility to unravel the relative contributions and temporal sequence of ligand-gated and voltage-gated channels to spine depolarization and Ca^{2+} transients.

AMPA receptors

The release of glutamate activates two different types of ligand-gated ion channels, the α-amino-3-hydroxy-5-methyl-4-isoxazoleproprionate (AMPA) receptors and the

N-methyl-D-aspartate (NMDA) receptors. The AMPA receptors act as the main initial charge during excitatory transmission and they are activated in less then a millisecond, while NMDA receptors generate a slower current. The AMPA receptors are hetero-oligomeric proteins made of the subunits GluR1-4. Each receptor is a complex of four subunits (Kaczmarek et al., 1997). They are permeable to cations, to both K^+ and Na^+ ions. The presence of a GluR2 subunit makes hetero-oligomeric receptors impermeable to Ca^{2+}. Only channels lacking GluR2 show a significant permeability for Ca^{2+} in addition to the permeability for Na^+ (Burnashev et al., 1992). AMPA receptors in most CA1 pyramidal cells contain the GluR2 subunit and are therefore Ca^{2+} impermeable (Geiger et al., 1995).

NMDA receptors

The ionotropic NMDA receptor requires the binding of both the transmitter (glutamate) and the coagonist (glycine) for its activation (Dingledine et al., 1999). In contrast to the AMPA receptor, the activation of the NMDA receptor occurs on a slow time-scale of several milliseconds and is long-lasting. Around a resting membrane potential of -70 mV the NMDA receptor is nonconducting due to a voltage-dependent Mg^{2+} block. This block is relieved by depolarization, revealing the channel with an unusually slow activation/deactivation kinetic and a high permeability to Ca^{2+} ions as well as Na^+ and K^+ ions (Kaczmarek et al., 1997). Thus glutamate binding can only lead to influx of Ca^{2+} ions when the membrane is depolarized to a more positive membrane potential at the same time as glutamate is released. Therefore, NMDA receptors act as coincidence detectors for depolarization and synaptic release of glutamate.

The NMDA receptor consists of the subunits NR1 and NR2A-D. The subunit composition determines the Ca^{2+} permeability of the receptor and is regulated during development. NMDA receptors have a larger Ca^{2+} permeability in the early developmental stages due to the subunit NR2B which is later replaced by the NR2A subunit and thereby reducing the Ca^{2+} permeability (Dingledine et al., 1999).

Silent synapses

From electrophysiological experiments using minimal stimulation, it is known that not all synapses produce both AMPA and NMDA responses. Some synapses seem to lack AMPA receptors (Isaac et al., 1995; Liao et al., 1995; Durand et al., 1996). These synapses are called 'silent' to indicate that they do not produce postsynaptic currents at the resting potential, but only if the cell is artificially depolarized. Silent synapses have been suggested to play a role in long-term potentiation (LTP) and they are thought to convert into functional ones by either insertion of new AMPA receptor proteins in the synaptic membrane or by activation of nonfunctional receptors (Liao and Malinow, 1996). The hypothesis that the membrane of silent synapses lacks AMPA receptors but expresses functional NMDA receptors is widely accepted (postsynaptic silent, 'deaf' synapse, Fig. 1.7A). But there is also an alternative explanation for the silent mechanism; silent synapses can be presynaptically silent meaning they do not respond either because the probability of glutamate release (p_r) is almost zero ('mute' synapse, Fig. 1.7B) or the concentration of released glutamate is insufficient to produce a detectable quantal response, Q ('whispering' synapses, Fig. 1.7C) (reviewed in (Voronin and Cherubini, 2004)). In a presynaptically silent synapse, both NMDA and AMPA receptors are functionally expressed in the synaptic membrane and they are simultaneously activated. The amount and the temporal profile of the transmitter in the cleft determine the degree of receptor activation. In case of a low concentration of glutamate either because of a slow adapting fusion pore (Choi et al., 2000) or because of spillover from neighboring synapses (Kullmann, 2003) (Fig. 1.7C), the amount of glutamate in the cleft would be sufficient to activate the high affinity NMDA receptors but not to activate the low affinity AMPA receptors. A presynaptically silent synapse may convert into an excitable one by enhancing the release of glutamate during LTP (Gasparini et al., 2000). Previous silent synapse studies are based on electrophysiology data pooled from many synapses and even for many cells. We used an optical method to monitor synaptic transmission at individual synapses.

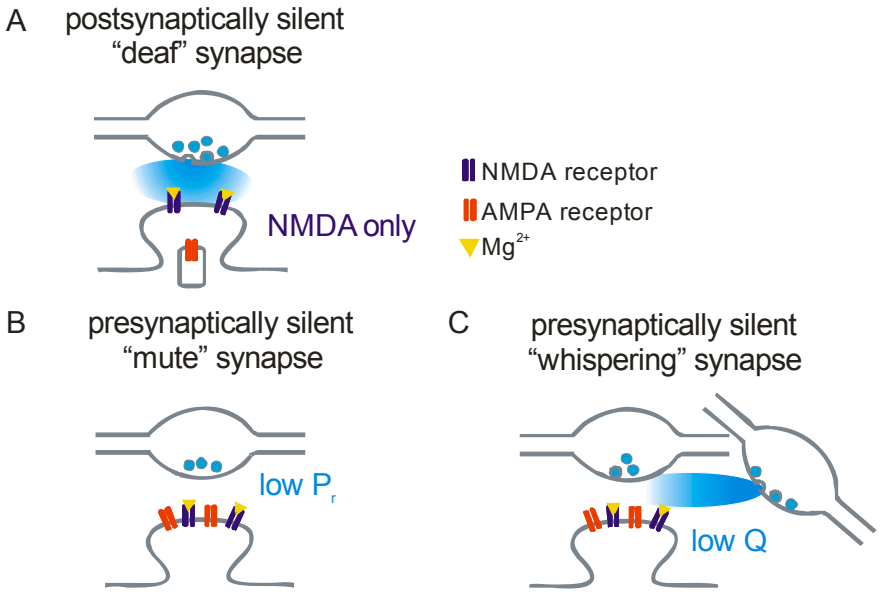

Figure 1.7. ***Alternative explanations for silent synapses.***

(A) *A postsynaptically silent synapse ('deaf') lacking AMPA receptors, but expressing functional NMDA receptors.*

(B) *A presynaptically silent ('mute') synapse. In this case, both AMPAR and NMDAR are expressed on the synaptic membrane, but they get activated only rarely because of the very low release probability (p_r) (no docked vesicles).*

(C) *A presynaptically silent ('whispering') synapse. Both AMPA and NMDA receptors are expressed but either the amount of glutamate released by one vesicle is too small and the release is too slow to be detected by the low affinity AMPA receptors. This could occur either because of a low conductance fusion pore or because of glutamate spillover from remote synapses (shown in this figure).*

Voltage-dependent Ca^{2+} channels

Voltage-dependent Ca^{2+} channels (VDCCs) mediate Ca^{2+} influx in response to depolarization of the membrane. The general classification of VDCCs is done according to their activation threshold: Low-Voltage Activated Ca^{2+} channels (LVA) are activated already during low depolarization of the cell, whereas High-Voltage Activated Ca^{2+} channels (HVA) need a higher depolarization to be activated (Catterall, 2000).

VDCCs are further subdivided into T, L, N, P, Q/R type channels according to their pharmacological sensitivity (Table 1.1). The names derive from the electrical properties of the channels and the tissue distribution:

- T-type channels have tiny and transient currents (8 pS single channel conductance)
- L-type channels have large and long lasting currents (25 pS single channel conductance)
- N-type channels have an intermediate voltage-dependence and rate of inactivation (more negative and faster then L-type but more positive and slower than T-type) and they are neuron specific
- P-type channels were first described in Purkinje cells and P-type channels have a high sensitivity to the spider toxin ω-agatoxin IVA
- Q-type Ca^{2+} current were first recorded in cerecellar granule neurons and are less sensitive to ω-agatoxin IVA
- R-type channels were resistant to all antagonists of VDCCs known at the time of their finding (Catterall, 2000; Catterall et al., 2005)

The T-type channel, which is activated by low depolarization, is an LVA channel, whereas all the others belong to the HVA class of channels (Table 1.1). Ca^{2+} channels undergo an inactivation which is usually fast for the T-type channel and slow for the L-type channel. The inactivation of L-type channels is sensitive to intracellular Ca^{2+}, thus acting as a negative feedback loop which prevents extensive accumulation of Ca^{2+} in the intracellular space (Imredy and Yue, 1994). For the other channel types, inactivation is mainly voltage-dependent.

The different subtypes of VDCCs are localized to different parts of a CA1 pyramidal cell. T-type, N-type and L-type channels are present in dendrites and spines, whereas the R-type channels are only present in the spines (Bloodgood and Sabatini, 2007b) (Table 1.1).

Activation voltage	Channel type	location in CA1 cells	antagonists
HVA	L	Dendrites and spines (Yasuda et al., 2003; Bloodgood and Sabatini, 2007b)	Dihydropyridines, phenylalkylamines, benzothiazepines, nimodipine
	P/Q		ω-agatoxin IVA, ω-conotoxin-MVIIC
	N	Dendrites and spines (Bloodgood and Sabatini, 2007b)	ω-conotoxin-MVIIC
	R	Spines (Yasuda et al., 2003; Bloodgood and Sabatini, 2007b)	SNX-482, mibefradil (partial blocker), Ni^{2+} (at low concentration)
LVA	T	Dendrites and spines (Bloodgood and Sabatini, 2007b)	mibefradil (partial blocker), Ni^{2+} (at low concentration)

Table 1.1. ***Nomenclature of VDCC types***

The hippocampus

The hippocampal structure forms a part of the limbic system and is located within the medial temporal lobe. It consists of several regions: CA1, CA2, CA3 (the hippocampus, CA orginates from Cornu Ammonis), dentate gyrus, subiculum, perisubiculum, parasubiculum, and entorhinal cortex. The hippocampus with its three subdivisions (CA1, CA2, and CA3) is probably one of the most studied regions in the brain.

The hippocampus receives inputs from numerous limbic, cortical and subcortical areas, primarily via the entorhinal cortex and the subiculum. The primary pathway of neural activity entering the hippocampus is from the entorhinal cortex via the perforant path to the dentate granule cells, with collaterals to CA1 and CA3 pyramidal cells. Mossy fibers from the granule cells in the dentate gyrus excite the CA3 pyramidal cells and the hilar interneurons. CA3 connects with CA1 pyramidal cells

via the Schaffer collateral from the ipsilateral hippocampus and via the commissural fibers from the contralateral hippocampus. CA1 pyramidal cells (output region of the hippocampus) project efferent fibers to subiculum, entorhinal cortex and several subcortical areas (Amaral and Witter, 1989) (Fig. 1.8).

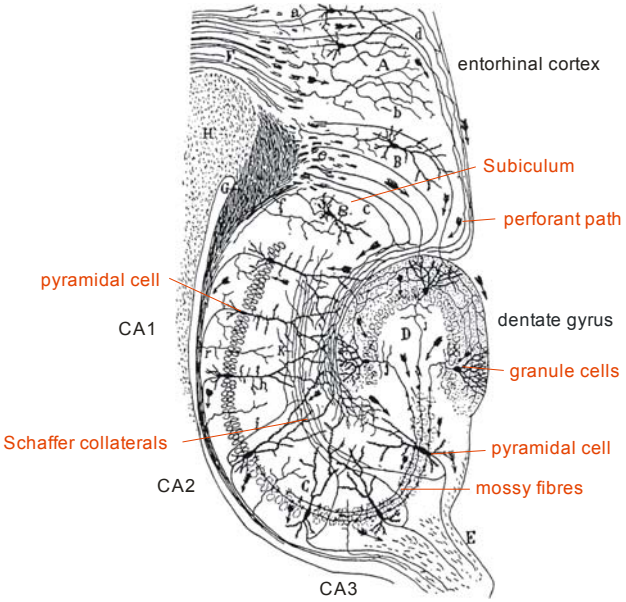

Figure 1.8. ***The Hippocampus.***
All regions of the hippocampus and the dentate gyrus receive input from the entorhinal cortex along the perforant path. Granule cells in the dentate gyrus send mossy fibers to CA3 pyramidal cells. The pyramidal cells in the a CA3 region send Schaffer collaterals to the CA1 pyramidal cells and project to other CA3 pyramidal cells and to the contralateral hippocampus through the commissural fibers. (Adapted from Zador and Brown, 1990 after original drawing by Cajal).

The hippocampus is believed to play a central role in the declarative memory consolidation, a process for converting short-term memory into cortically stored, long-lasting memory in the mammalian brain. Studies of amnesiac patients have revealed two consequences of hippocampal damage: loss of the ability to form new declarative memories and loss of recently formed memories (Scoville and Milner, 1957; Zola-Morgan et al., 1986; Rempel-Clower et al., 1996). These findings have lead to the general notion that the hippocampus is essential for the brain to convert short-term memory into long-lasting memory.

In rodents, there is abundant evidence that the hippocampus is involved in spatial orientation. Lesion of the hippocampus in rats leads to poor performance in various spatial navigation tasks (Czurko et al., 1997; Moses et al., 2005). The observation of ‘place cells’ by O`Keefe and collegues strongly supports the idea that the hippocampus represents the spatial environment as a cognitive map (O'Keefe and Dostrovsky, 1971). Place cells are neurons that fire depending on the location of the animal within its environment, meaning that a certain cell only fires when the animal

is moving through a particular location in space. Different neurons have different receptive fields.

For the purpose of this dissertation we will focus on the function of excitatory synapses between the Schaffer collaterals, which are axons of CA3 pyramidal cells, and the dendrites of CA1 pyramidal cells. The Schaffer collateral axons form a homogenous pathway which is easily activated in order to study synaptic transmission.

CA1 pyramidal neurons

The CA1 pyramidal cell of the hippocampus has become one of the most intensively studied neuron in the brain. As a result, we know much about its neurotransmitter receptors, ion channels, micro-circuitry and morphology.

Dendritic morphology

Two elaborately branching dendritic trees emerge from the pyramidal-shaped soma of a CA1 neuron. The basal dendrites occupy the stratum oriens, and the apical dendrites occupy the stratum radiatum (proximal apical) and the stratum lacunosum-moleculare (distal apical) (Fig. 1.9).

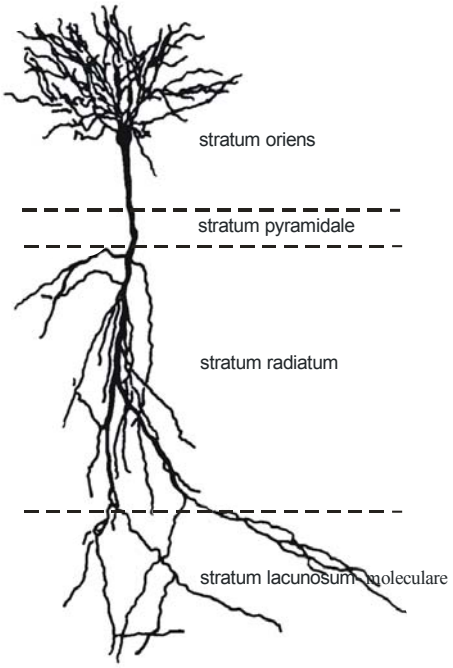

Figure 1.9. ***A CA1 pyramidal cell.***
The hippocampus is divided into stratum oriens, stratum pyramidale, stratum radiatum and stratum lacunosum moleculare. (Adapted from Bannister and Larkman, 1995)

Excitatory synaptic input

CA1 neurons receive input from both excitatory and inhibitory presynaptic neurons. The principle excitatory inputs derive from the entorhinal cortex and the CA3 pyramidal neurons. The perforant path input from the entorhinal cortex to CA1 selectively innervates the distal apical dendrites in the stratum lacunosum-moleculare (Blackstad, 1958). Input from the CA3 pyramidal neurons via the Schaffer collaterals forms synapses on the apical dendrites in the stratum radiatum and on the basal dendrites in stratum oriens (Blackstad, 1956). In CA1, spines are usually contacted by a single presynaptic terminal. In the rare cases when more than one presynapse make contact with the same spine, they are usually from different neurons (Harris and Stevens, 1989).

Aim of the thesis

The majority of excitatory synapses on a CA1 pyramidal neuron are located on dendritic spines which have a great diversity in shape and size. Although we have plenty of information about the fine anatomy, the function of dendritic spines is still poorly understood. Imaging experiments have demonstrated that spines can serve as biochemical compartments for molecules such as Ca^{2+} and thus might play a role in synaptic plasticity. In addition to chemical compartmentalization, spines could also play an electrical role in transforming synaptic inputs. So fare, very little is known about the electrical properties of the spines and the idea of the electrical isolation of the spines has only been supported by theoretical studies. The goal of this thesis is to better understand the electrical role of the spines and to answer the following questions:

1) How strongly does the spine head get depolarized during synaptic transmission?
2) Do spines act as electrical amplifiers?
3) Is the spine neck resistance fixed or is it dynamic?

The soma allows recording of electrical activity with conventional electrophysiological methods but for smaller structures such as thin dendrites or spines these methods are not applicable. Optical imaging of membrane potential using voltage-sensitive dyes would be an experimental method to directly study electrical properties of a spine during synaptic transmission. However, there are some technical limitations by using the present optical probes. To start with, the existing voltage-sensitive dyes are not sensitive enough for studying sub-threshold synaptic potentials in fine neuronal structures such as the dendritic spines. Spines are tiny structures and the size of the optical signal is related to the membrane area, therefore the signal in a single spine is very small. Further more, voltage-sensitive dyes bleach rather easily, which results in phototoxic damage and limits the time that labeled structure can be imaged. Finally, the signal-to-noise ratio is typically small, so that averaging of responses is usually required. In contrast to voltage-sensitive dyes Ca^{2+}-sensitive dyes can exhibit large changes in fluorescence. A main source of spine Ca^{2+} following glutamate release is influx through NMDA receptors. Two-photon imaging allows us to measure NMDA receptor-mediated Ca^{2+} currents in individual spines of CA1

pyramidal cells. We used the voltage-dependence of NMDA receptors to estimate the depolarization in individual spines.

There is no simple linear relation between spine head depolarization and Ca^{2+} level. Therefore, in the first part of this thesis, we developed an experimental protocol to estimate the fraction of NMDA receptors that became unblocked during the EPSP: We normalized the average Ca^{2+} signal at resting membrane potential to the average of the Ca^{2+} signal at depolarized potential. Since different types of channels are active during the EPSP, we built a biophysical model to extract the relative contributions of different channels to spine head depolarization. Our main finding was that Ca^{2+} transients and thus spine head depolarization can be very different in individual spines, reaching from completely 'Ca^{2+}-silent' spines to spines that can generate 50% of the maximum Ca^{2+} influx during the EPSP. We found that the spine neck resistance plays a major role, and that spine necks change dramatically in response to depolarization of the postsynaptic cell. This unexpected plasticity of the spine neck can potentially explain several long-standing controversies in the field.

Interestingly, several Ca^{2+}-silent spines had also unusual presynaptic properties, providing the first evidence that individual synapses can be both 'silent' and 'mute' at the same time, and responded very vigorously to trains of presynaptic action potentials. In the second part of the thesis, we compare morphometric and functional properties of Ca^{2+}-silent and functional spines.

In the third part of my thesis, we investigated the role of the spine neck in spike-timing-dependent plasticity (STDP). The main result is a much enhanced Ca^{2+} signal in spines with high neck resistance, restricted to a very narrow time window. These findings suggest that the spine neck, besides restricting the diffusion of second messengers away from the synapse, also sharpens the coincidence detection by NMDA receptors.

Spine neck plasticity controls postsynaptic calcium transients through electrical compartmentalization

Åsa Grunditz[1], Niklaus Holbro[1], Lei Tian[1], Yi Zuo[2], Thomas G. Oertner[1*]
[1]Friedrich Miescher Institute, Maulbeerstrasse 66, CH-4058 Basel, Switzerland
[2]Dept. for Molecular Cell & Developmental Biology, UC Santa Cruz, CA 95064
Submitted to Science

Summary

Dendritic spines of CA1 pyramidal cells increase their neck resistance in response to postsynaptic depolarization, causing local electrical amplification of postsynaptic potentials and massively increased Ca^{2+} influx.

Abstract

Dendritic spines are miniature protrusions of nerve cells that have been proposed to serve as electrical compartments for the active processing of local synaptic signals. However, estimates of the resistance between the spine head and the parent dendrite suggest that compartmentalization is not tight enough to electrically de-couple the synapse. Here we show that depolarization of hippocampal pyramidal cells leads to a dramatic reduction of the diffusional coupling between spines and dendrites, indicating a proportional rise in electrical resistance. As a functional consequence, a large fraction of NMDA receptors is activated during synaptic activity in spines with high resistance necks. We conclude that Ca^{2+} influx into spines, a key trigger for synaptic plasticity, is dynamically regulated by spine neck plasticity via electrical compartmentalization.

Most excitatory synapses on cortical pyramidal cells are formed on small protrusions called dendritic spines. It is well established that mushroom-shaped spines act as chemical compartments: Their narrow necks form a diffusional barrier that slows down the exchange of second messengers between spine head and dendrite (Muller and Connor, 1991). A second potential function of dendritic spines is more controversial: Since they are equipped with different types of voltage-gated channels, spines could in principle serve as active electrical amplifiers (Segev and Rall, 1988). According to this theory, active spines could locally boost synaptic currents at minimal metabolic cost, providing a substrate for information storage as well as information processing (Koch and Poggio, 1985; Koch, 1999). However, estimates of the resistance between the spine head and the parent dendrite suggest that in the majority of spines, the ohmic resistance of the spine neck is not high enough to electrically de-couple the synapse (Koch and Zador, 1993).

The electrical resistance of individual spine necks can be estimated by optical measurements of the diffusional coupling between spine head and dendrite, using fluorescence recovery after photobleaching (FRAP) or photoactivation. Estimates from different preparations, however, did not reach agreement about the typical resistance of a spine neck (Harris and Stevens, 1989; Svoboda et al., 1996; Bloodgood and Sabatini, 2005). To test for systematic differences in spine properties, we compared FRAP time constants (τ_{FRAP}) in acute hippocampal slices, hippocampal slice cultures, and in vivo (Fig. 3.1A, Fig. S3.2). In acute slices, τ_{FRAP} was fast (range 16-159 ms), consistent with previous studies (Svoboda et al., 1996; Sobczyk et al., 2005). In organotypic slice cultures and in vivo, on the other hand, we found much broader distributions of time constants, with a median value 2.3 and 3 times higher than in acute slices, respectively (see methods). Acute slices are completely deafferentiated and the level of spontaneous activity is very low. We therefore tested whether a step depolarization to 0 mV, evoked by somatic current injection, would affect spine neck properties in the acute slice. To our surprise, 5-10 min after the end of a 4 min depolarizing pulse, τ_{FRAP} was increased by a factor of 12, on average (Fig. 3.1A). Recovery after photobleaching depends on the ratio of spine neck length L to neck cross-sectional area A, but also on the spine head volume V such that $\tau = VL/AD$, where D is the diffusion coefficient of the fluorescent molecule (Svoboda et al., 1996). However, V did not significantly change in our experiments (3% decrease, on average;

Fig. S3.1), indicating that the dramatic increase in τ_{FRAP} was due to an increase in the *L*/*A* ratio of the spine neck. Blocking AMPA, NMDA and $GABA_A$ receptors reduced, but did not prevent depolarization-induced spine neck changes, indicating that the induction mechanism was not dependent on synaptic activity (Fig. S3.1). In Ca^{2+}-free extracellular solution, on the other hand, spine neck plasticity was completely blocked (Fig. S3.1). In our population study, we could not address the question whether the neck resistance changed in every individual spine. Therefore, we proceeded by measuring τ_{FRAP} in individual spines before and after a depolarizing pulse (Fig. 3.1B). We observed a consistent increase in τ_{FRAP} in all spines (Fig. 3.1C), but the magnitude of the effect was variable: The diffusional resistance increased by a factor of 10, on average, ranging from 2 to 25-fold changes. This large range points to subtle differences in neck plasticity between individual spines.

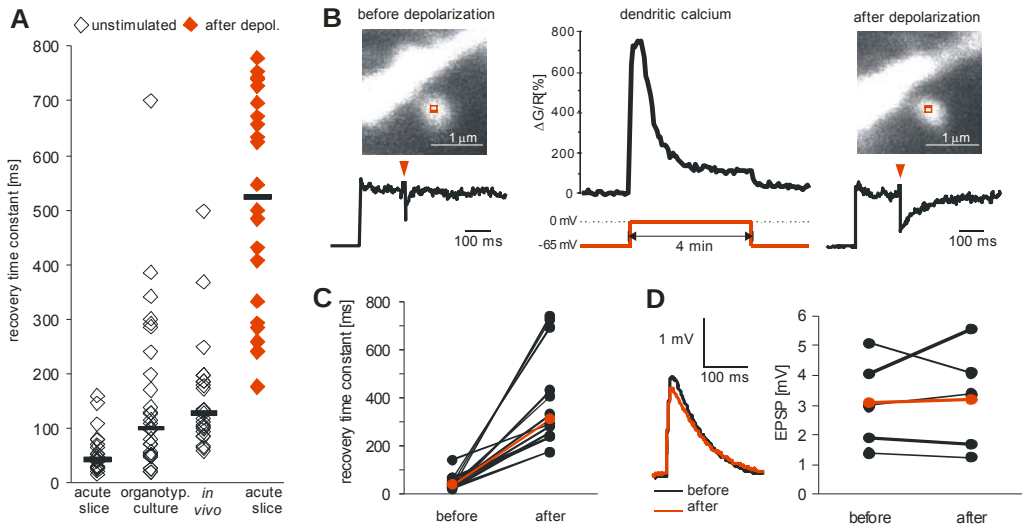

Figure 3.1. ***Postsynaptic depolarization changes diffusional coupling between spine head and dendrite.***

(A) *Time constants of fluorescence recovery after photobleaching (τ_{FRAP}) in spines from CA1 cells in acute hippocampal slices (median τ_{FRAP} = 43 ms, range, 16-159 ms, n = 23), in hippocampal slice cultures (median τ_{FRAP} = 100 ms, range, 20-700 ms, n = 29), in cortical pyramidal cells in vivo (median τ_{FRAP} = 129 ms, range, 56-498 ms, n = 24), and in acute hippocampal slices after step depolarization (median τ_{FRAP} = 524 ms, range, 177-778 ms, n = 22). Measurements in vivo are based on YFP bleaching and have been multiplied with 4.85 to facilitate comparison (see Methods).*

(B) *Example of a spine FRAP experiment using Alexa-Fluor 594. Red arrow heads indicate time of bleaching. During the step depolarization, intracellular Ca^{2+} concentration was monitored by two-photon Ca^{2+} imaging. Line scans across the spine head were used to measure fluorescence recovery.*

(C) *In individual spines, τ_{FRAP} increased by a factor of 10, on average (before depolarization: median τ_{FRAP} = 40 ms, range, 22-146 ms; after depol: median τ_{FRAP} = 312 ms, range, 177-743 ms, n = 12).*

(D) *EPSP amplitude at the soma was not significantly affected by step depolarization (n = 5).*

To test whether spine neck plasticity affects the electrical function of the synapses, we first measured excitatory postsynaptic potentials (EPSPs) in CA1 pyramidal cells. Individual Schaffer collateral synapses in CA1 can generate 40 pA of current at the soma (Conti and Lisman, 2003). In a passive cell, a 10-fold increase in spine neck resistance would be expected to strongly attenuate EPSPs measured at the soma (Koch and Zador, 1993). In our experiments, however, EPSP amplitudes changed only slightly after the depolarizing pulse (Fig. 3.1D). A potential explanation could be active electrical amplification in spines with high resistance necks, compensating for the electrotonic attenuation along the spine neck. Electrical amplification is provided by ion channels that open at depolarized potentials and lead to additional depolarization, thus creating a positive feedback loop. A candidate channel is the

NMDA receptor which is blocked by Mg^{2+} ions in a strongly voltage-dependent fashion (Jahr and Stevens, 1990) (Fig. S3.3). Since NMDA receptors are permeable for Ca^{2+} ions, we could monitor NMDA receptor activation in individual spines by two-photon Ca^{2+} imaging (Fig. 3.2A and B). However, there is no simple relation between spine depolarization and spine Ca^{2+} levels: Number and subunit composition of NMDA receptors, as well as spine head volume, are heterogeneous, leading to differences in absolute Ca^{2+} concentrations in individual spines even for identical EPSP amplitudes (Sobczyk et al., 2005). We developed an experimental protocol to compensate for this variability: Synaptically evoked Ca^{2+} transients (CaTs) were measured under two conditions: Depolarized to the synaptic reversal potential (voltage clamp) and free running (current clamp) (Fig. 3.2C). The ratio between the Ca^{2+} signal amplitude in current clamp and the Ca^{2+} signal amplitude at the reversal potential we call the fractional Ca^{2+} transient (fCaT). The stronger the spine depolarizes during the EPSP, the larger the fCaT will be. In a sample of 33 spines, the amplitude of fCaTs ranged from 0.02 – 0.51 (Fig. 3.2D), pointing to large differences in spine head depolarization. Interestingly, the distribution was bimodal, suggesting that spines with small fCaTs (< 0.15) are not stable and turn into 'Ca^{2+}-silent' synapses (fCaT < 0.05), possibly through a loss of AMPA receptors.

If spines act as electrical compartments, spine head depolarization should be correlated with spine neck resistance. We used the decay time constant of the Ca^{2+} signal under depolarized conditions (τ_{decay}, Fig. 3.2C) as a measure of spine neck resistance (see methods and Fig. S3.4). Spines with low diffusional resistance of the spine neck (wide necks) generated small fCaTs (Fig. 3.2E), indicating weak depolarization of the spine head. This is consistent with the idea that a high spine neck resistance is necessary to enable strong spine head depolarization. In electrically isolated spines, AMPA receptor currents can generate EPSPs of high amplitude and thus efficiently remove the Mg^{2+} block of NMDA receptors. About half of the variability in fCaT amplitude could be explained by differences in spine neck resistance ($R^2 = 0.419$, Fig. 3.2E), but spine depolarization is also influenced by other factors: From immunogold studies and glutamate uncaging experiments, it is known that that the number of AMPA receptors is highly variable between synapses and scales with spine size (Matsuzaki et al., 2001; Tanaka et al., 2005). In our experiments, however, we found no correlation between spine head volume and fCaT amplitude

(R^2 = 0.008, Fig. S3.4). It is worth to point out that vesicular transmitter release, unlike glutamate uncaging, activates AMPA receptors very locally, so that the amplitude of the postsynaptic responses is not necessarily correlated with the total number of AMPA receptors (Raghavachari and Lisman, 2004).

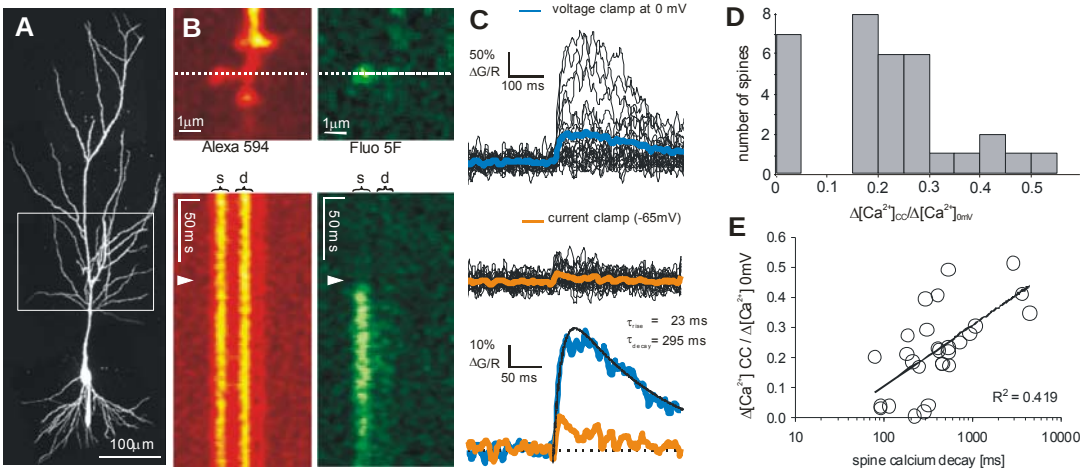

Figure 3.2. ***Spine neck resistance controls NMDA receptor activation during the EPSP.***

(A) *Spines on oblique dendrites of CA1 pyramidal cells (white box) were used for* Ca^{2+} *imaging experiments.*

(B) *Synaptically evoked spine* Ca^{2+} *transients. For ratio measurements, cells were filled with a green* Ca^{2+}*-sensitive dye (Fluo5F) and a red dye (Alexa-Fluor 594).* Ca^{2+} *signals were measured in line-scan mode.*

(C) *Synaptically evoked* Ca^{2+} *transients were measured first under depolarized conditions (voltage clamp at synaptic reversal potential, blue trace), then in current clamp (orange trace).* τ_{decay} *was extracted by fitting the difference of 2 exponentials to the average response under depolarized conditions (blue trace).*

(D) *Histogram of* Ca^{2+} *transient amplitude in current clamp, normalized by the* Ca^{2+} *transient amplitude at the synaptic reversal potential (*$[Ca^{2+}]_{CC}$ / $[Ca^{2+}]_{0mV}$*), in 33 different spines.*

(E) *Fractional* Ca^{2+} *transient amplitude was correlated with spine neck properties (decay time constant of the* Ca^{2+} *transient at the synaptic reversal potential)*

From a series of imaging experiments using specific antagonists, we concluded that at least three types of channels contributed to the EPSP in the spine head: AMPA receptors, NMDA receptors, and R-type Ca^{2+} channels (Fig. 3.3A, Fig. S3.5). In current clamp experiments, blocking a single type of channel will affect depolarization and thus change all other currents. The only way to dissect the relative contributions of different channels to spine depolarization is biophysical modeling. We used the NEURON simulation environment to set up a model spine equipped with

AMPA receptors, NMDA receptors and R-type channels and connected to a passive CA1 pyramidal cell (Hines and Carnevale, 1997; Golding et al., 2001) (Fig. 3.3A). The spine neck resistance was initially set to R_n = 1.2 GΩ, according to our estimate from the fluorescence signal decay (see methods). The voltage-dependent blocking function of the NMDA receptor was experimentally determined (Fig. S3.3). Channel densities were adjusted to reproduce the amplitude of fluorescence transients measured in our pharmacological experiments. The time courses of the Ca^{2+} signals were also faithfully reproduced in our simulations (Fig. 3.3A and B), indicating that the simple model captured the essential mechanism of spine Ca^{2+} transient generation. From the simulation, we could extract the individual currents (Fig. 3.3C) and the typical EPSP in the spine head (Fig. 3.3D), which had an amplitude of 55 mV and lasted ~10 ms (full width at half maximum). Depolarization was actively amplified and prolonged by the joint activation of NMDA receptors and R-type Ca^{2+} channels. At the soma, the EPSP was attenuated to ~1 mV (Fig. 3.3E).

Secondly, we run the same model with a 10-fold lower spine neck resistance (R_n = 120 MΩ), to simulate spine neck properties before step depolarization. The EPSP in the spine head decreased by ~20 % in peak amplitude and was also much briefer (Fig. 3.3D). Electrical amplification was weak the 120 MΩ spine, leading to a 71% reduction in the simulated Ca^{2+} signal (Fig. 3.3F). We conclude that only in strongly isolated spines, Ca^{2+} signals were boosted by the voltage-dependent activation of NMDA receptors and high-threshold Ca^{2+} channels. The smaller depolarization in the 120 MΩ spine increased the AMPA receptor current due to the larger driving force, leading to a slightly larger somatic EPSP (Fig. 3.3E). In summary, our simulation suggests that a 10-fold increase in spine neck resistance boosts synaptically evoked Ca^{2+} transients by a factor of 3.4, but only weakly affects somatic EPSP amplitudes. Thus, active changes in spine neck resistance are a powerful mechanism to modulate local chemical signaling largely independent of electrical signaling to the soma.

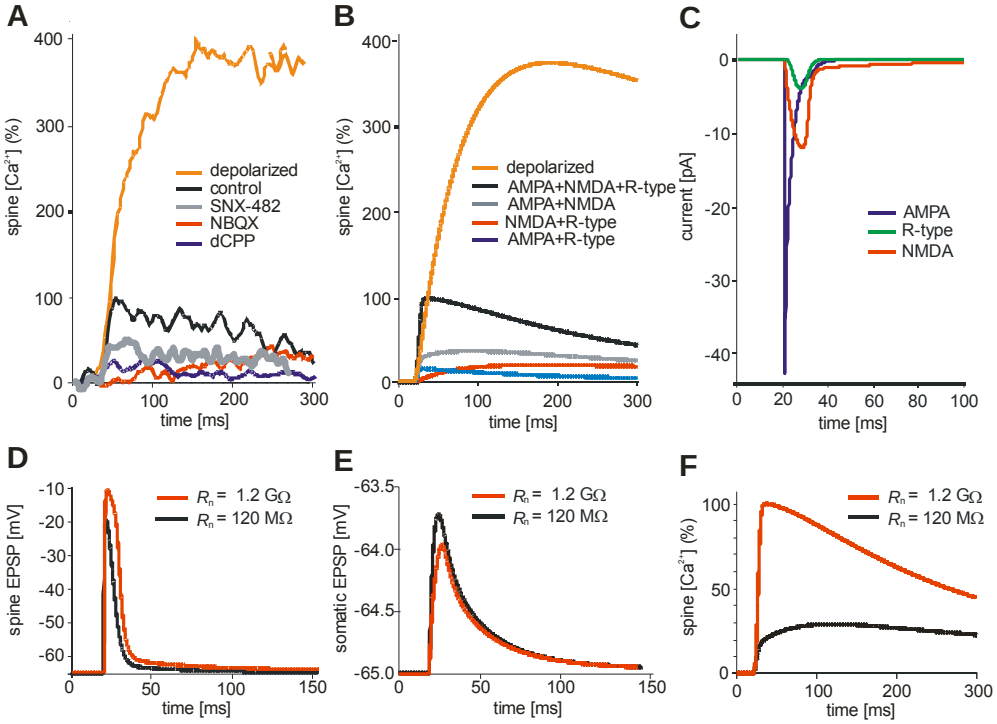

Figure 3.3. ***Assessing the impact of spine neck resistance changes by compartmental modeling.***

(A) *Pharmacological block of R-type* Ca^{2+} *channels (gray curve), AMPA receptors (red curve), or NMDA receptors (blue curve) partially blocks spine* Ca^{2+} *signals. Traces from 3 different experiments (average of 40-54 responses each) were normalized to the control response in current clamp (100%; black trace). For comparison, the average response in voltage clamp (0 mV) is also shown (yellow trace)*

(B) *NEURON model reproduces not only the amplitude, but also the time course of the fluorescence transients under all conditions tested (*R_{neck} *= 1.2 GΩ).*

(C) *The model reveals the sequence of currents during the EPSP. NMDA and R-type currents lead to a substantial prolongation of the depolarization.*

(D) *EPSP in the spine head, for the high spine neck resistance used in B and C (red curve), and for a 10 fold lower resistance, typical for naïve acute slices (black curve). Note prolonged depolarization in the 1.2 GΩ neck spine due to electrical amplification.*

(E) *At the soma, EPSP amplitudes are fairly independent of spine neck resistance.*

(F) *The simulated* Ca^{2+} *transient is much lower in the spine with* R_{neck} *= 120 MΩ.*

Our spine model suggested that even in a spine with R_n = 1.2 GΩ, synaptic activation will not trigger runaway depolarization, i.e. activation of all voltage-gated channels. Increasing the AMPA receptor current, however, could lead to such a 'spine spike' (Fig. S3.6). We boosted synaptic AMPA receptor currents experimentally by bath application of cyclothiazide, which induced a dramatic increase in the amplitude of spine Ca^{2+} signals (Fig. 3.4A). In many spines, Ca^{2+} transients under cyclothiazide

reached or even exceeded the amplitude of transients recorded at the reversal potential, suggesting the generation of Ca^{2+} spikes in the spine head. A second insight from the model was that in low neck resistance spines, the decay of the EPSP is accelerated (Fig. 3.3D). In such spines, AMPA receptor block should have a weaker effect on postsynaptic Ca^{2+} transients, since much of the Ca^{2+} influx is due to the 'leakiness' of the NMDA receptor at the resting potential. To test this prediction, we sorted our AMPA receptor block experiments into two groups: Spine that had a fast decaying Ca^{2+} signal (τ_{decay}) at 0 mV, indicating low resistance necks, and spines with τ_{decay}>1 s. In diffusionally isolated spines, AMPA receptor block reduced the Ca^{2+} signal to 8% of the control amplitude, on average, indicating that 92% of the control Ca^{2+} transient was dependent on AMPA receptor mediated depolarization (Fig. 3.4C). In spines with faster decay of the Ca^{2+} signal (open necks), influx after AMPA receptor block was abolished after wash-in of dCPP, consistent with a leak current through NMDA receptors (Fig. 3.4B). Taking into account the dynamic changes in spine neck resistance (Fig. 3.1), these findings provide a plausible explanation for a striking discrepancy between previous imaging studies: While some laboratories reported a weak effect of AMPA receptor block on postsynaptic Ca^{2+} signals (Koester and Sakmann, 1998; Kovalchuk et al., 2000), others studies demonstrated nearly complete block of Ca^{2+} transients after AMPA receptor block (Emptage et al., 1999; Yuste et al., 1999; Nevian and Sakmann, 2004). In Ca^{2+} imaging experiments, the search for responsive spines is facilitated by clamping the membrane potential of the postsynaptic cell to 0 mV (Yasuda et al., 2004), a procedure that will, however, dramatically alter spine neck properties (Fig. 3.1). Thus, subtle differences in the experimental strategy used by different laboratories could have considerably altered the outcome of AMPA receptor blocking experiments.

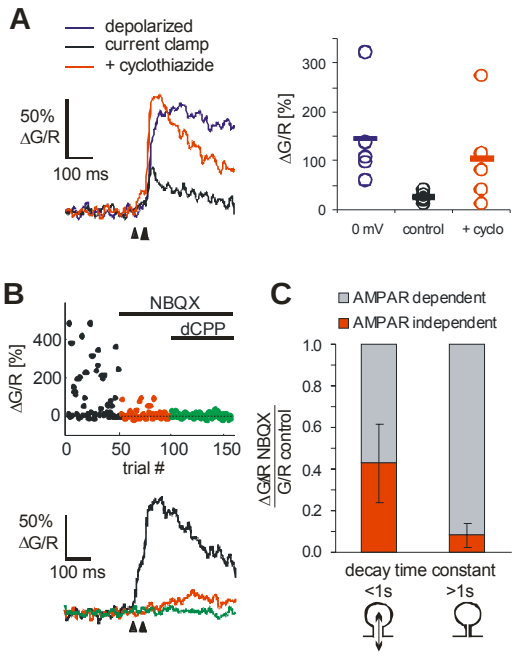

Figure 3.4. ***The voltage-dependence of spine calcium signals.***

(A) *Increasing AMPA receptor affinity by cyclothiazide led to a dramatic boosting of the spine* Ca^{2+} *signals in current clamp (red curve). The current clamp recordings were preceded by recordings at the reversal potential (0 mV, blue trace).*

(B) *AMPA receptor antagonist NBQX (10 µM) reduces amplitude and changes time course of spine* Ca^{2+} *transients. Remaining* Ca^{2+} *transient is NMDA receptor dependent (10 µM dCPP). Traces are averages over all trials (failures and successes). Paired-pulse stimulation was used to increase the number of successful synaptic transmission events.*

(C) *Sorting of NBQX experiments according to spine neck properties (n = 7). Effect of AMPA receptor block on* Ca^{2+} *transients was weaker in spines with low resistance necks (τdecay > 1 s, residual CaT: 0.43 ± 0.18) than in spines with high resistance necks (CaT: 0.08 ± 0.05).*

If step depolarization of a CA1 pyramidal cell is paired with activation of presynaptic axons, synapses undergo long-term potentiation (LTP) (Petersen et al., 1998; Chen et al., 1999). Could spine neck plasticity be an essential step in this process? It has been noted that pairing with presynaptic activity is very effective at the end of a long depolarizing pulse, but not at its beginning (Chen et al., 1999), pointing to a slow, Ca^{2+}-dependent postsynaptic process that enables plasticity and is triggered by postsynaptic depolarization. Furthermore, disturbing actin filament turnover in the postsynaptic cell with latrunculin B or phalloidin inhibits the induction of LTP, demonstrating the importance of cytoskeletal rearrangements for synaptic plasticity (Kim and Lisman, 1999). The 10-fold change in diffusional resistance we report here leads -activated second messengers, e.g. αCaMKII, in the active spine. It is plausible that electrical and chemical isolation induced by high spine neck resistance cooperate to facilitate the induction of long-term plasticity at spine synapses. In this 'metaplasticity' scenario (Abraham, 1996), local dendritic Ca^{2+} spikes (Schiller and

Schiller, 2001) or Ca^{2+} waves (Nakamura et al., 1999) could induce local spine neck changes, which would 'prime' spine synapses for later functional plasticity. Here we show that spine neck resistance controls local depolarization of the spine head, but has little effect on somatic EPSPs, which might explain why this form of structural plasticity has been overlooked for many years.

Supporting material

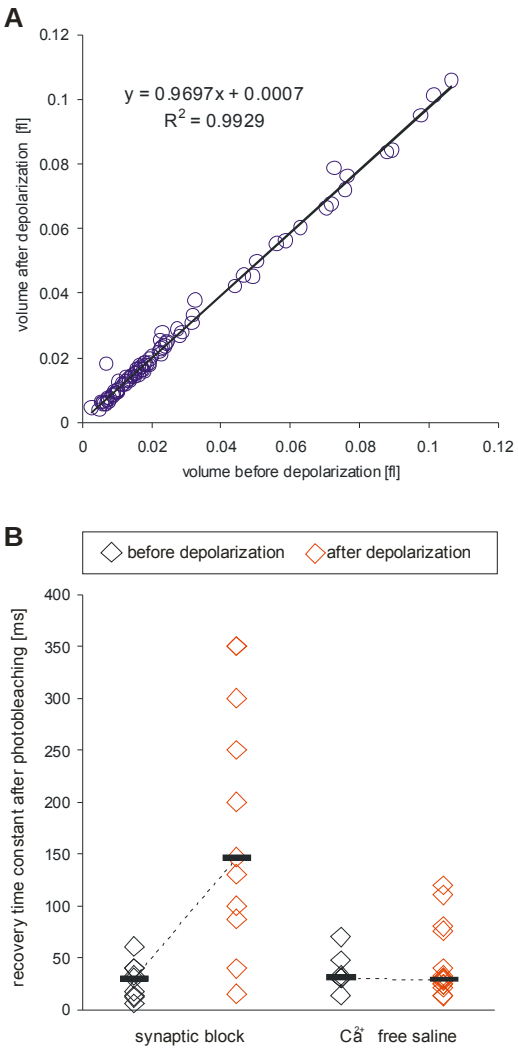

Figure S3.1. ***Morphological changes after step depolarization of CA1 pyramidal cells in acute hippocampal slices.***

(A) *Spine head volume of individual spines before and after 4 min depolarization to 0 mV. No significant volume change was observed (n = 84). Linear fit indicates 3% decrease in spine head volume, on average.*

(B) *Step depolarization induces spine neck changes if synaptic transmission is blocked by dCPP (10 µM), NBQX (10 µM), and bicuculline (10 µM) (Control: median* τ_{FRET} *= 30 ms, range, 6-60 ms, n = 9; after depolarization: median* τ_{FRET} *= 147 ms, range, 15-350 ms, n = 11). Nominally* Ca^{2+}*-free ACSF blocks spine neck changes after step depolarization (Control: median* τ_{FRET} *= 31 ms, range, 14-70 ms, n = 6; after depolarization: median* τ_{FRET} *= 29 ms, range, 14-120 ms, n = 15).*

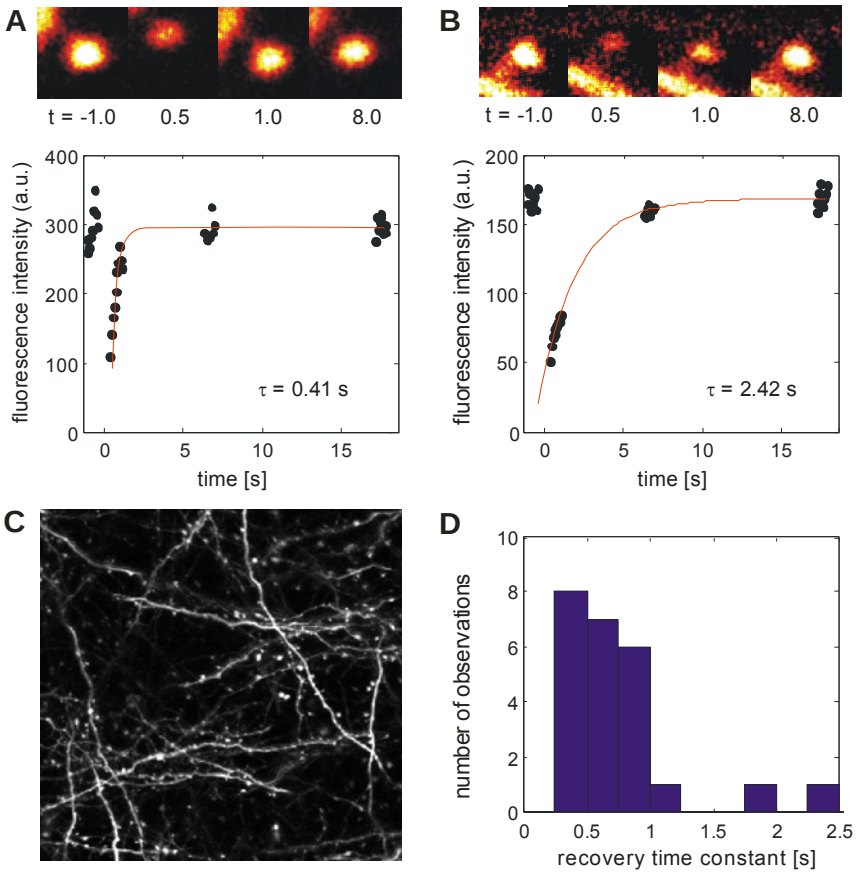

Figure S3.2. ***In-vivo FRAP experiments on thy1-YFPH mice.***

(A) *Bleaching of single spine in frame mode (13 Hz frame rate, 64x64 pixels). To extract the fluorescence time course and avoid heart beat artifacts, a region of interest (ROI) of fixed size was manually centered on the spine head in every frame. Red line: Mono-exponential fit.*

(B) *Example of spine with high diffusional resistance*

(C) *Overview of thy1-YFP expressing dendrites through the thinned skull. Maximum intensity projection.*

(D) *Histogram of recovery time constants. Median* τ_{FRET} *= 0.62 s, range, 0.27 -2.42 s, n = 24 spines, 3 animals.*

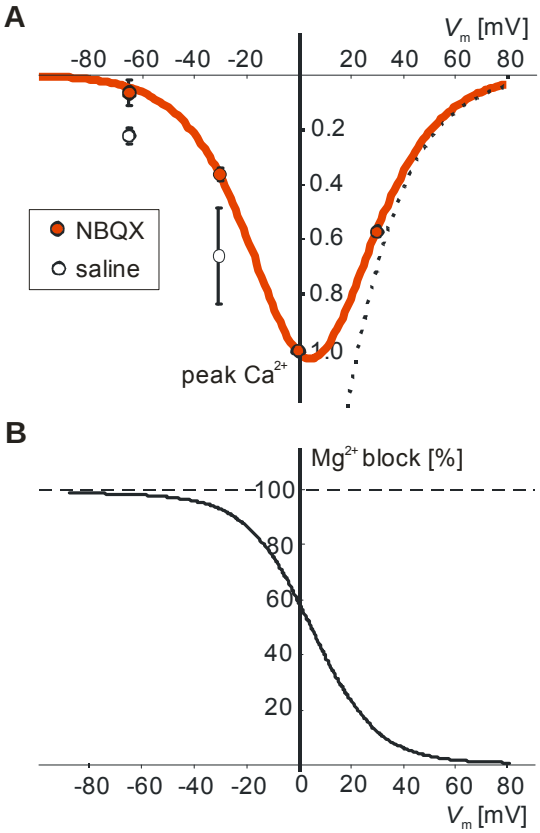

Figure S3.3. ***Voltage-dependence of synaptically evoked spine calcium transients.***

(A) *Red circles: Amplitude of spine calcium transients at different holding potentials normalized to the amplitude at the synaptic reversal potential (0 mV). To improve space clamp, Cs^+-based intracellular solution was used and AMPA currents were blocked by NBQX (10 µM). The voltage-dependence of the current is well fit by combining the Goldman-Hodgkin-Katz current equation for Ca^{2+} (dotted line) with the voltage-dependent gating function of the NMDA receptor (red curve). In experiments without AMPA receptor block (white circles), spines escaped the somatic voltage clamp and depolarized, resulting in larger calcium transients.*

(B) *Voltage-dependent gating function of synaptic NMDA receptors, extracted from fit in (A).*

$g(V_m) = 1/[1 + exp(-0.087V_m)(C/0.88)]$, where V_m is the membrane potential and C is the extracellular Mg^{2+} concentration in mM.

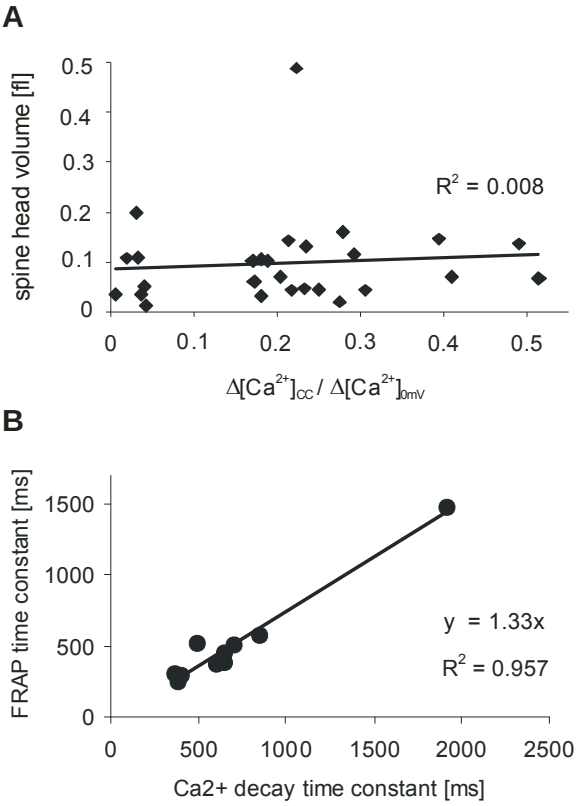

Figure S3.4.

(A) *No correlation between calcium transient amplitude and spine head volume. R^2 = 0.008 (Same dataset as in Fig. 3.2).*

(B) *Comparison of the recovery time constant after FRET (Alexa-Fluor 494) and the decay time constant of the calcium transient under depolarized conditions (Fluo5F). Two-photon uncaging of MNI-glutamate at 725 nm was used to stimulate individual spines. Time constants were highly correlated; indicating that diffusion of both fluorophores was controlled by spine volume and spine neck resistance.*

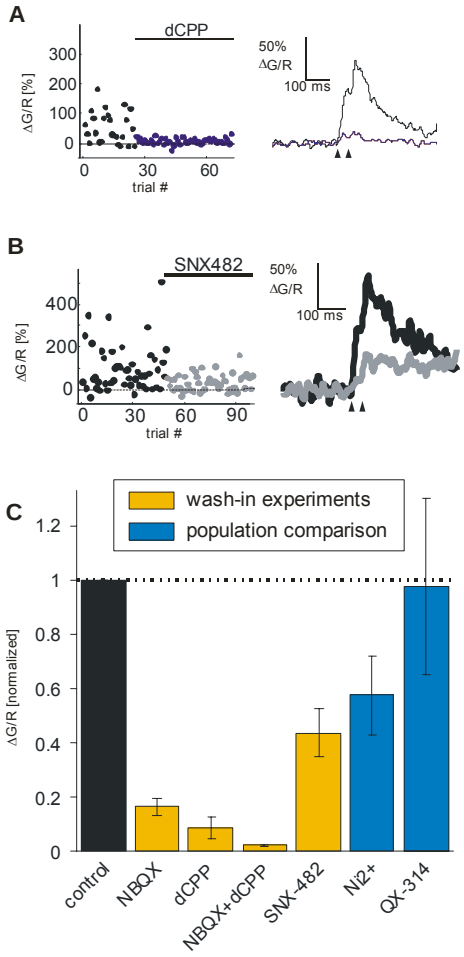

Figure S3.5 ***Pharmacology of spine calcium transients in current clamp.***

(A) *Example of NMDA receptor blocking experiment using dCPP (10 µM). Paired pulse stimulation was used to increase release probability.*

(B) *Example of R-type Ca^{2+} channel blocking experiment using SNX-482 (10 µM).*

(C) *Summary of blocking experiments. In wash-in experiments, the response amplitudes were normalized to the response amplitude in current clamp before drug application. NBQX (10 µM), 0.166 ± 0.029, n = 6; dCPP (10 µM), 0.087 ± 0.040, n = 3; NBQX+dCPP, 0.025 ± 0.003, n = 2, SNX-482 (10 µM), 0.437 ± 0.089, n = 4 (mean ± SEM). To exclude presynaptic effects of Ni^{2+}, we recorded trials at 0 mV and in current clamp in Ni^{2+} (10 µM), calculated the fCaT and compared it to the average fCaT in standard ACSF (0.576 ± 0.145, n = 6). The same strategy was used for the intracellular Na^{+} channel blocker QX-314 (5 mM, 0.976 ± 0.324, n = 4).*

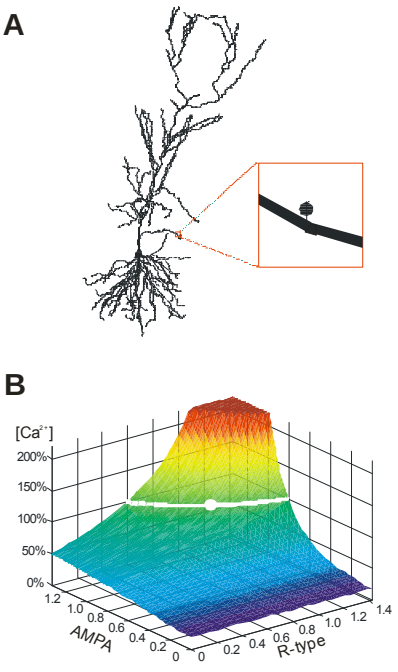

Figure S3.6. ***Parameter space of NEURON model.***

(A) *Single compartment spine attached to oblique dendrite of CA1 pyramidal cell.*

(B) *Parameter space: Dependence of simulated spine Ca^{2+} transients on AMPA receptor and R-type Ca^{2+} channel densities. White dot indicates channel densities used in Fig. 3.4. White line indicates other channel density combinations consistent with our experimental results.*

Optical investigation of functional and silent synapses

Åsa Grunditz, and Thomas G. Oertner

Abstract

Silent synapses are defined by their electrophysiological response profile, but it is unclear whether their silence is caused by pre- or postsynaptic mechanisms. Here we used an optical method to investigate pre- and postsynaptic properties, and the morphology of silent and functional synapses in acute hippocampal slices. Two-photon imaging allowed us to measure NMDA receptor-mediated Ca^{2+} currents in single spines during the excitatory postsynaptic potential (EPSP). Most spines produced clearly detectable Ca^{2+} transients during the EPSP, but we found a clearly distinct subset of spines that did not generate fast Ca^{2+} signals when stimulated in current clamp. Surprisingly, these 'Ca^{2+}-silent' spines were not significantly smaller than the functional spines, but apparently contained a higher density of NMDA receptors. A subset of these 'Ca^{2+}-silent' spines did not respond to single action potentials. This indicates a presynaptic specialization ('mute' synapses) that we never encountered among the functional spines.

Introduction

Silent synapses are characterized by the lack of electrophysiological responses at the resting potential, but the presence of NMDA receptor-mediated responses that can be detected at depolarized membrane potentials (Isaac et al., 1995; Liao et al., 1995; Durand et al., 1996). They are found most frequently in brain tissue from young animals and seem to disappear gradually with age, which has led to the hypothesis that they represent an immature state in the development of a synapse (Petralia et al., 1999; Gasparini et al., 2000; Losi et al., 2002). Several mechanisms have been suggested to explain the electrophysiological signature of silent synapses, the most obvious being a complete absence of AMPA receptors from the postsynaptic terminal ('deaf' synapse). Alternative explanations are based on the fact that NMDA receptors have a higher affinity for glutamate and could thus detect a lower concentration of the transmitter. Thus, it is possible that silent synapses are presynaptically silent ('mute'), release less transmitter ('whispering' synapse) or have a different cleft geometry (reviewed in (Voronin and Cherubini, 2004)).

To understand the mechanism of synaptic silence, it is attractive to use optical methods to compare functional and silent synapses, since both functional and morphological parameters of individual synapses can be measured simultaneously. Indeed, two-photon glutamate uncaging has been used to distinguish between functional and 'deaf' synapses (Busetto et al., 2008). Presynaptic properties, however, can not be investigated with this technique.

Here, we used two-photon Ca^{2+} imaging to investigate the release probability (p_r), the amplitude of the Ca^{2+} transients and the volume of individual spines. Excitatory postsynaptic potentials (EPSPs) in CA1 pyramidal cells were induced by local stimulation of the Schaffer collaterals. Most spines produced clearly detectable Ca^{2+} transients during EPSP. In contrast to these functional spines, we also found spines that generated fast Ca^{2+} transients only if provided with additional depolarization, either by somatic current injection or by tetanic activation of neighboring synapses. We were interested in correlations between spine head depolarization, release probability, and morphological parameters (e.g. spine volume).

Results

Synaptically evoked Ca^{2+} transients in individual spines

To quantify Ca^{2+} transients and measure morphological parameters of individual spines, we filled single CA1 pyramidal cells with a mixture of two dyes: A Ca^{2+}-insensitive red dye (Alexa-Fluor 594) to visualize the anatomy and to quantify spine volumes, and a green Ca^{2+} indicator dye with a large dynamic range (Fluo5F). The experiments were performed at 30-34° C using a custom-built two-photon microscope. We stimulated Schaffer collaterals with brief negative voltage pulses (-3 to -5 V, 0.2 ms) delivered through a glass microelectrode positioned close (15-25 μm) to the dendrite of the patched cell using laser-DIC. Single-pulse stimulations of Schaffer collaterals were interleaved with paired-pulse stimulations to assess properties of the presynaptic terminal (Fig. 4.1D). Since Ca^{2+} release from intracellular stores can amplify spine Ca^{2+} signals in a non-linear fashion (Emptage et al., 1999; Ward et al., 2006), we disabled intracellular Ca^{2+} stores by adding 2 μM thapsigargin to the bath solution. We measured synaptically evoked spine Ca^{2+} transients in line-scan mode under 2 conditions: First, we voltage clamped the soma of the cell to the potential where the excitatory postsynaptic current (EPSC) started to reverse its direction. Using this strategy, we could hold the stimulated synapses at a defined membrane potential (reversal potential of glutamate receptors, ~0 mV) independent of their location in the dendritic tree. In addition, since no net synaptic current is generated at the reversal potential, the spine head could not escape the voltage clamp during synaptic activity. After collecting a sufficient number of trials (50-60) under depolarized conditions, we switched to current clamp mode (CC) and collected a second set of Ca^{2+} responses (Fig. 4.1A and B). The average resting potential ($I = 0$) was -64.6 mV ± 3.0 mV, and we used small holding currents to adjust all cells to –65 mV. In all spines, the Ca^{2+}calcium transients measured at –65 mV were much smaller in amplitude (Fig. 4.1C) and the peak was reached significantly earlier. At the end of each experiment, we measured the fluorescence intensity in the apical dendrite of the cell as reference for the estimation of spine volume (see Methods).

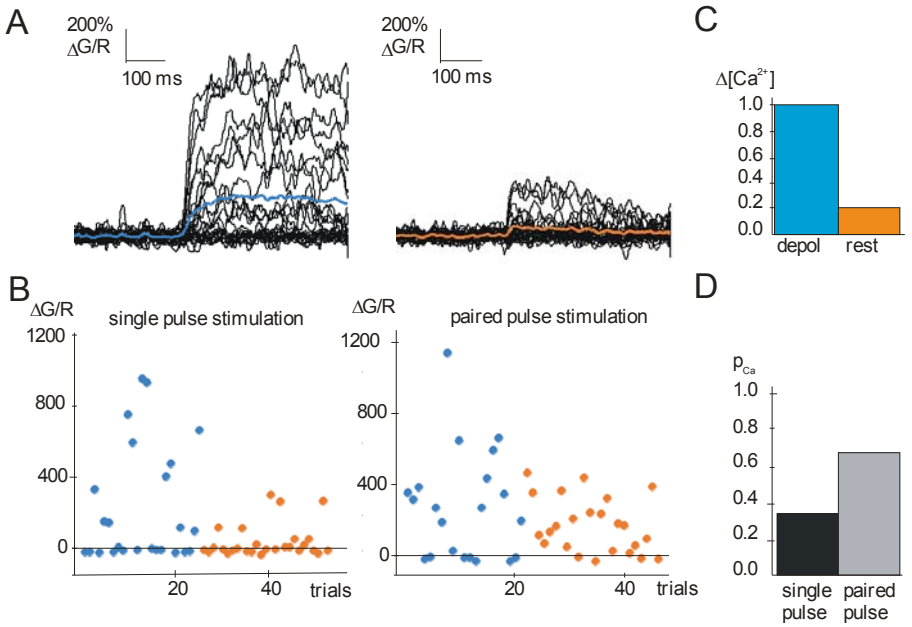

Figure 4.1. ***Spine Ca^{2+} measurements***

*(**A**) Synaptically evoked spine Ca^{2+} transients were measured first under depolarized conditions (voltage clamp at synaptic reversal potential, left panel), then in current clamp (right panel). With the cell depolarized to 0 mV, successful synaptic transmissions can be easily distinguished from failure trials (left panel). Under current clamp conditions, responses are smaller (right panel).*

***(B)** Peak spine Ca^{2+} amplitudes with postsynaptic cell depolarized (blue dots) and in current clamp (orange dots). Stimulations with single pulses and paired pulses (40 ms ISI) were interleaved, but are displayed in separate plots for clarity. The number of transmission failures (dots on 'zero' line) is lower with paired pulse stimulations (right plot). Response amplitudes are stable during the experiment (17 min total).*

***(C)** Normalized Ca^{2+} transient amplitude under depolarized conditions (blue) and in current clamp (orange).*

***(D)** The probability of a Ca^{2+} signal (P_{Ca}) after single pulse stimulation (black) and after paired pulse stimulation (grey).*

Classification of spines according to their Ca^{2+} response profiles

Most of the spines we investigated showed large Ca^{2+} transients at depolarized potentials and smaller Ca^{2+} transients under CC conditions (Fig. 4.1B and Fig. 4.2, upper panels). As expected, trials with paired-pulse stimulation had a higher probability of eliciting a Ca^{2+} response then single-pulse stimulations (single pulse: $p_{Ca} = 0.35 \pm 0.04$; paired pulse: $p_{Ca} = 0.68 \pm 0.05$; only depolarized trials evaluated). In contrast to these functional spines, we found several spines that did not show fast rising Ca^{2+} transients when recorded in current clamp (Fig. 4.2, middle and lower panels). We used the term 'Ca^{2+}-silent spines' (Nevian and Sakmann, 2004) to

describe this response profile, in analogy to electrophysiologically 'silent' synapses that do not generate currents at the resting potential (Voronin and Cherubini, 2004). In Ca^{2+}-silent spines, we could detect slow rising Ca^{2+} signals with peak amplitudes of less than 5% of the depolarized Ca^{2+} responses, very similar to the residual Ca^{2+} transients after pharmacological block of AMPA receptors. A subset of Ca^{2+}-silent spines were only responsive when the presynaptic axon was stimulated with at least 2 pulses (Fig. 4.2, lower panels). An analogous response profile has been described in electrophysiological experiments as 'mute' synapses (Voronin and Cherubini, 2004).

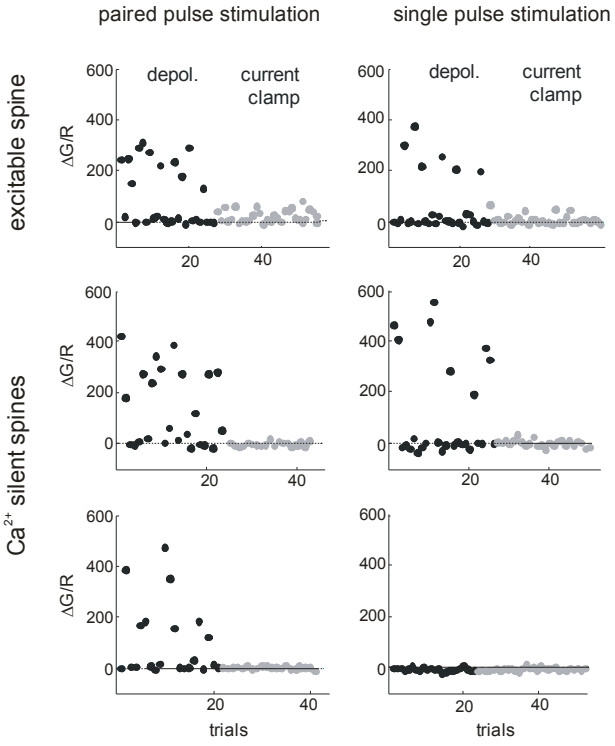

Figure 4.2. ***Representative examples of different Ca^{2+} response profiles in spines***

Functional spine: Ca^{2+} transients above detection threshold under all tested conditions. Ca^{2+}-silent spines: Detectable Ca^{2+} transients only under depolarized conditions (black markers), not under current clamp (gray markers). Lower panels: Example of 'mute' spine, producing Ca^{2+} transients only under depolarized conditions using paired pulse stimulation.

The fraction of NMDA receptors that become unblocked during the EPSP can be used as a reporter of spine head depolarization. To compare the efficiency of NMDA receptor unblocking between individual spines, we normalized the average Ca^{2+} signal amplitude under CC conditions to the average Ca^{2+} amplitude under depolarized conditions. The resulting histogram (Fig. 4.3A) shows a clear gap between the group of Ca^{2+}-silent spines (left, amplitude of Ca^{2+} transient < 5% of value at 0mV) and functional ones (right, amplitude of Ca^{2+} transient > 15% of value at 0mV). We were interested in potential correlations between the fractional NMDA receptor activation and other synaptic parameters, namely the volume of the spine and the probability of observing Ca^{2+} transients after single pulse stimulation at depolarized potentials (p_{Ca}).

Spine volume was a poor predictor of Ca^{2+} transient amplitude during the EPSP (Fig. 4.3B): In the group of functional spines (right group), large and small spines can be found, as in the group of Ca^{2+}-silent spines (left). Linear regression resulted in a correlation coefficient of 0.0082.

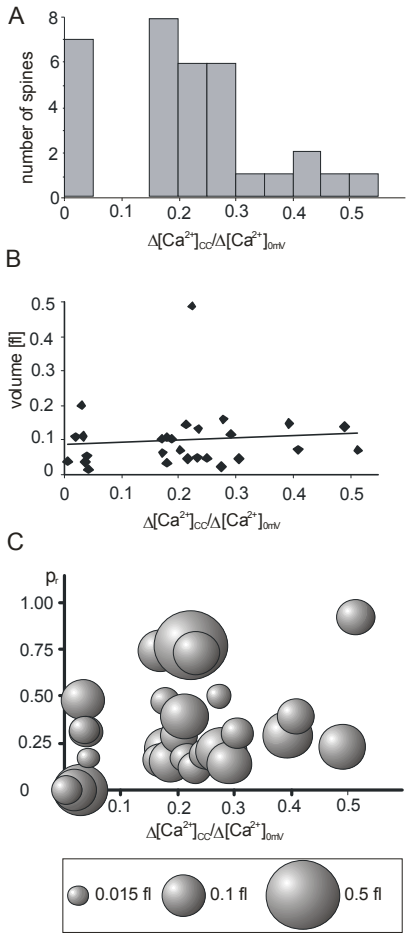

Figure 4.3. ***Summary of functional properties of 33 spines***

(A) *Histogram of average Ca^{2+} signal amplitude under current clamp conditions normalized by average amplitude under depolarized conditions (0 mV). In 7 spines, current clamp responses were < 5% of depolarized responses (leftmost bin).*

(B) *No correlation between relative Ca^{2+} signal amplitude and spine volume. Line is linear fit, $R^2 = 0.0082$.*

(C) *Correlation between relative Ca^{2+} signal amplitude and Ca^{2+} response probability (p_r), measured at depolarized potentials using single pulse stimulation. Marker size indicates spine volume. Several spines with very small Ca^{2+} responses (left group) have a Ca^{2+} response probability of zero ('mute' spines).*

The probability of observing a Ca^{2+} transient under voltage clamp (0mV) is a good measure of presynaptic release probability (p_r), since under depolarized conditions, individual responses were well above our detection threshold (Fig. 4.2). We noted a systematic difference in the presynaptic properties of functional versus Ca^{2+}-silent spines (Fig. 4.3C): 'Mute' spines ($p_r = 0$ with single pulse stimulation) were frequently found in the group of Ca^{2+}-silent spines (3 out of 7), but not among the 26 functional ones. This indicates a matching of functional properties between pre- and postsynaptic terminals at individual synapses.

Properties of Ca^{2+}-silent spines

Since spine Ca^{2+} transients are an essential trigger for synaptic plasticity (Nevian and Sakmann, 2006), we were interested to find conditions under which silent spines would experience high Ca^{2+} levels. We reasoned that additional activation of neighboring synapses could depolarize the dendrite sufficiently to activate NMDA receptors and VDCCs at Ca^{2+}-silent spines. To test this hypothesis, we used a burst of presynaptic stimulation pulses with ever shortening inter-stimulus intervals, leading to a ramp-like subthreshold depolarization as measured at the soma (Fig. 4.4A, black trace). To our surprise, the Ca^{2+}-silent spines responded with Ca^{2+} transients 2.8 times larger in amplitude than the functional spines, on average (Fig. 4.4A). These very large Ca^{2+} transients point to a high density of NMDA receptors or VDCCs at Ca^{2+}-silent spines. If NMDA currents were indeed larger at Ca^{2+}-silent spines, Ca^{2+} transients should also be larger when voltage clamped at the reversal potential. To test this, we averaged the Ca^{2+} responses (excluding failures) from all functional spines and all silent spines separately. Peak Ca^{2+} amplitudes were indeed significantly larger in Ca^{2+}-silent spines (160 % of average amplitude in functional spines), consistent with a higher NMDA receptor density in Ca^{2+}-silent spines (Fig. 4.4B).

We also noted that the decay of the Ca^{2+} transient was significantly faster in Ca^{2+}-silent spines (τ_{decay} = 0.23 s ± 0.07 s, Fig. 4.4B and C) compared to functional ones (τ_{decay} = 0.90 s ± 0.32 s). These measurements were taken at depolarized membrane potentials, above the reversal potential of the Na^{+}/Ca^{2+} exchanger (Blaustein and Lederer, 1999b), and with high added buffer capacity ($\kappa_{dye} \approx 750$). Under these conditions, extrusion of Ca^{2+} ions is compromised, and the decay of the fluorescence signal is mostly governed by diffusion of Ca^{2+}-bound dye molecules out of the spine head into the dendrite (Sabatini et al., 2002). Differences in the time constant of decay therefore point to differences in neck geometry. We conclude that Ca^{2+}-silent spines have wider or shorter necks than functional spines, on average. However, the range of time constants found in Ca^{2+}-silent spines (0.09 - 0.53 s) did not exceed the range found in functional spines (0.08 - 4.5 s), suggesting that neck geometry is not the only explanation for their silence. Most likely, channel configuration and neck geometry conspire to render a spine Ca^{2+}-silent.

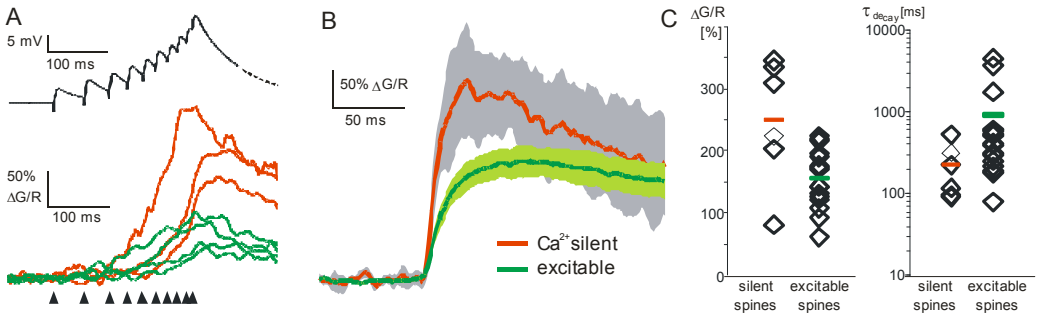

Figure 4.4. ***Functional properties of Ca^{2+}-silent spines***

(A) *Stimulation with a burst of presynaptic action potentials led to a ramp-like depolarization in postsynaptic cell (black curve), and triggered high amplitude Ca^{2+} transients in Ca^{2+}-silent spines (red curves) compared to functional spines (green curves).*

(B) *Average Ca^{2+} transients to paired-pulse stimulation at 0 mV in functional spines (green) and Ca^{2+}-silent spines (red). Shaded areas show 95% confidence interval.*

(C) *Ca^{2+}-silent spines have significantly larger Ca^{2+} responses under depolarized conditions and faster decay time constants, on average.*

How do the differences between Ca^{2+}-silent and functional spines relate to spine head depolarization? We used a biophysical model of a typical CA1 cell spine (Grunditz et al. 2008) to simulate Ca^{2+} transients. Varying the number of activated AMPA receptors between 5 and 500 allowed us to construct the transfer function between depolarization and calcium transient amplitude, keeping all other channel densities (NMDA receptors, R-type calcium channels) constant (Fig. 4.5).

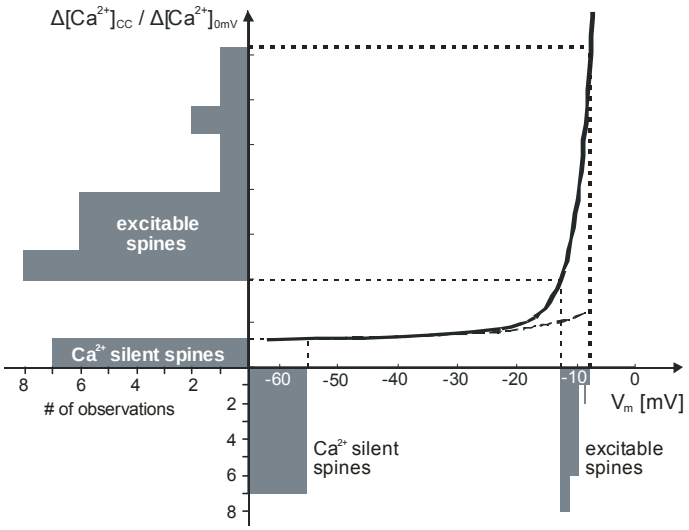

Figure 4.5. ***Transfer function between spine depolarization and peak [Ca^{2+}]***

Simulations were run for spines containing 10-500 AMPA receptors, keeping all other parameters constant. The broad distribution of Ca^{2+} concentrations measured in functional spines (histogram on ordinate) maps onto a narrow range of membrane potentials around +10 mV (abscissa), indicating relatively uniform EPSC amplitudes in all functional spines. Dashed line: Spine model without voltage-dependent Ca^{2+} channels cannot account for the high Ca^{2+} concentrations observed in functional spines.

The transfer function is very shallow in the beginning, where Ca^{2+} influx is due to imperfect Mg^{2+} block of NMDA receptors. Once depolarization reaches threshold for NMDA unblocking and Ca^{2+} channel activation, a positive feedback loop is activated, leading to a steep dependence of spine Ca^{2+} levels on membrane depolarization. The range of Ca^{2+} signals measured in functional spines maps onto a remarkably narrow range of spine membrane potentials (-7 to -13 mV), corresponding to EPSP amplitudes of ~ 55 mV. Interestingly, the gap in the distribution of spine Ca^{2+} signals corresponds to a much larger gap in the distribution of EPSP amplitudes, suggesting that spines with EPSP amplitudes between 10 and 50 mV are quite rare and might represent an unstable state.

Discussion

Differences between Ca^{2+}-silent and functional spines

We have classified spines according to the relative amplitude of synaptically evoked Ca^{2+} transients under current clamp conditions. The large gap in the distribution suggests two functional groups: Ca^{2+}-silent and functional spines (Fig. 4.3). Could these differences be simply due to stronger stimulation in some experiments, activating multiple synapses on the same dendritic branch? Firstly, we rejected experiments where more than one spine within the field of view (20 x 20 μm) showed Ca^{2+} responses. Secondly, synaptic activity under depolarized conditions leads to accumulation of Ca^{2+}-bound dye in the dendrite. In trials where no glutamate was released at the synapse under scrutiny (failure trials), activity of neighboring synapses could be detected as a slow increase in fluorescence in the dendrite. When we compared failure trials in Ca^{2+}-silent and functional spines, however, we found no significant difference in dendritic Ca^{2+}. These tests make it unlikely that neighboring stimulated synapses can account for the bimodal distribution of spine Ca^{2+} transients. Somatic EPSPs (4.2 ± 3.1 mV, mean ± STD) were not compared between groups, because we expected functional spines to contribute larger currents than Ca^{2+}-silent spines.

Furthermore, we found several other functional properties that distinguish Ca^{2+}-silent from functional spines and corroborate our classification: Firstly, many Ca^{2+}-silent spines were contacted by specialized presynaptic terminals which apparently did not release glutamate when stimulated by a single action potential (Fig. 4.2). None of the 26 functional spines displayed this 'mute' behavior (Voronin and Cherubini, 2004) when tested at depolarized potentials. Secondly, Ca^{2+}-silent spines consistently produced significantly larger Ca^{2+} transients than their functional counterparts following dendritic depolarization by strong presynaptic input in current clamp (Fig. 4.3B). Voltage clamped at the synaptic reversal potential, Ca^{2+}-silent spines also reached higher Ca^{2+} levels after single pulse stimulation (Fig. 4.4B and C). These two observations indicate larger NMDA receptor currents in Ca^{2+}-silent spines, which might be due to differences in receptor number, subunit composition, or phosphorylation state (Sobczyk et al., 2005; Kohr, 2006). Large NMDA currents at silent synapses were predicted in a recent modeling study (Rhodes, 2006), but this is,

to our knowledge, the first experimental evidence using optically identified Ca^{2+}-silent spines. A third difference was the significantly faster decay of the Ca^{2+} signal in Ca^{2+}-silent spines under depolarized conditions (Fig. 4.4B and C). The fast decay can not be attributed to more efficient removal of free Ca^{2+} ions from the cytoplasm, since:

i) the Na^{+}-Ca^{2+} exchanger is non-functional at a membrane potential of 0 mV (Blaustein and Lederer, 1999b)
ii) Ca^{2+} pumps in the plasma membrane were out-competed by the high concentration of Ca^{2+} buffer (Fluo5F)
iii) SERCA pumps were blocked by thapsigargin.

Under these conditions, the decay of the Ca^{2+} signal was largely governed by diffusion of Ca^{2+} bound dye molecules into the dendrite, and the fast decay of the fluorescence transient in Ca^{2+}-silent spines indicates a lower diffusional resistance of the spine neck, on average. These observations support our classification of spines into two functional groups, but what mechanism is responsible for the differences?

Do all Ca^{2+}-silent spines carry silent synapses?

The most straightforward explanation for the lack of fast Ca^{2+} transients in some spines is a very low number of postsynaptic AMPA receptors, an explanation that equates Ca^{2+}-silent spines with silent synapses (Liao et al., 1995; Ward et al., 2006). However, there is an alternative explanation: Spines could be Ca^{2+} silent due to insufficient electrical isolation from the parent dendrite by a wide spine neck. In this scenario, the AMPA receptor current can not depolarize the spine head sufficiently to relieve the Mg^{2+} block of the NMDA receptors because the current is drained by the low-impedance dendrite. Indeed, fluorescence transients decayed faster in Ca^{2+}-silent spines (τ_{decay} = 0.23 s ± 0.07 s), suggesting wider spine necks, on average (Fig. 4.4C). In summary, spine neck resistance and AMPA receptor density are the most critical parameters in controlling spine depolarization and spine Ca^{2+} levels, and low values of either one can account for Ca^{2+}-silent spines.

EPSP amplitude in functional spines is uniform

Studies using electron microscopy (EM) and glutamate uncaging have suggested that the AMPA receptor number is are highly variable among synapses and scales with spine size (Nusser et al., 1998; Matsuzaki et al., 2001; Tanaka et al., 2005). Therefore,

we expected to observe a widely range of spine head depolarization values. Surprisingly, we found no correlation between spine head volume and calcium transient amplitude. The bimodal distribution found in the Ca^{2+} imaging experiments points to an even more segregated distribution in the depolarization of the spine head during an EPSP (Fig. 4.5). This suggests a bistable situation, once a spine is Ca^{2+}-silent it might lose its remaining AMPA receptors. It remains to be seen what kind of stimulation can turn a Ca^{2+}-silent spine into a functional one and vice versa.

Spine neck resistance sets time window for the detection of coincident activity

Åsa Grunditz, and Thomas G. Oertner

Abstract

NMDA receptors are considered to act as detectors for coincident pre- and postsynaptic activity. Paring of pre- and postsynaptic action potentials has been shown to generate supralinear Ca^{2+} transients in dendritic spines. Here we show that the electrical resistance of the spine neck plays an important role in generating these non-linear effects. Only spines with a high neck resistance are sensitive to the precise timing of coincident activity.

Introduction

Long-term modifications in synaptic efficacy are thought to be the cellular mechanisms of learning and memory (Bliss and Collingridge, 1993; Whitlock et al., 2006). Changes in the strength of synaptic contacts can be induced by coincident presynaptic and postsynaptic activity (Magee and Johnston, 1997; Markram et al., 1997; Debanne et al., 1998) (Bi and Poo, 1998). The relative timing of postsynaptic action potentials and excitatory postsynaptic potentials (EPSPs) determines the magnitude and the direction of change in synaptic efficacy, a phenomenon known as spike-timing-dependent plasticity (STDP) (Markram et al., 1997; Bi and Poo, 1998; Feldman, 2000; Sjostrom et al., 2001). A lasting increase in synaptic strength (long-term potentiation, LTP) is usually observed when EPSPs are followed by an action potential and a decrease (long-term depression, LTD) when EPSPs are evoked after action potentials (Linden, 1999; Sourdet and Debanne, 1999; Paulsen and Sejnowski, 2000). STDP is thought to account for experience-driven changes on the connectivity in neuronal networks (Song and Abbott, 2001; Senn, 2002).

Ca^{2+} ions play a crucial role in the induction of long-term potentiation and long-term depression (Malenka and Nicoll, 1999). The elevation of postsynaptic Ca^{2+} acts as a second messenger that converts the Ca^{2+} induction signal into a long-lasting modification of synaptic efficacy. Ca^{2+} entry in spines is greatly enhanced when synaptic stimulation is paired with action potentials (Yuste and Denk, 1995; Koester and Sakmann, 1998; Yuste et al., 1999; Nevian and Sakmann, 2004), suggesting a potential mechanism for STDP. Postsynaptic NMDA receptors, which open only if bound to glutamate and with the postsynaptic membrane sufficiently depolarized to relieve the Mg^{2+} block, could act as coincidence detectors (Mayer et al., 1984; Nowak et al., 1984). NMDA receptors have a high permeability for Ca^{2+}, and spine Ca^{2+} transients are thought to determine the magnitude of long-term changes in synaptic strength (Nevian and Sakmann, 2006).

The neck of the spine can influence spine calcium transients by two mechanisms. Firstly, it acts as a diffusional barrier between spine head and dendrite (Holmes, 1990; Koch and Zador, 1993; Svoboda et al., 1996), compartmentalizing and prolonging spine calcium transients. Secondly, the spine neck poses an electrical resistance which allows the spine head to depolarize more strongly than its parent dendrite, enhancing voltage-dependent Ca^{2+} influx. There is conflicting evidence about the range of spine neck resistances in different preparations (Harris and Stevens, 1989; Svoboda et al., 1996; Bloodgood and Sabatini, 2005). As a further complication, it has been shown that strong stimulation, purely postsynaptic or paired, can change the diffusional coupling between spine and dendrite (Bloodgood and Sabatini, 2005) (Grunditz et al., 2008), making the spine neck resistance a dynamic variable. Thus, it is an open question to which degree the spine neck can affect the sensitivity of the spine synapse to STDP.

Here we use a biophysical model to examine the effects of the spine neck resistance on spine Ca^{2+} transients during coincident pre- and postsynaptic activity. Our modeling results indicate that spine Ca^{2+} transients are strongly dependent on the spine neck resistance, and that a high resistance spine neck makes the spine more sensitive to the precise timing of pre-and postsynaptic activity. Using two-photon imaging, we experimentally tested the timing dependence of spine Ca^{2+} transients in a CA1 pyramidal cell. Our experimental results show a pronounced, non-linear boosting

of the spine Ca^{2+} signal for positive (EPSP-bAP), but not for negative timing windows, indicate a spine neck resistance in the Gigaohm range.

Results

Backpropagation of action potentials evoke Ca^{2+} transients in the proximal apical dendrites of a CA1 pyramidal cell

To characterize backprotagating action potential (bAP) evoked Ca^{2+} transients CA1 pyramidal cells were filled with a green Ca^{2+} indicator dye (200 µM Fluo4) and a Ca^{2+}-insensitive red dye (30 µM Alexa-fluor 594) (Fig. 5.1). We performed current injections into the soma to induce action potentials that propagated to the dendrites and evoked Ca^{2+} transients (Fig. 5.1). Single action potentials caused Ca^{2+} accumulations with small amplitude (data not shown). To improve the signal-to-noise ratio, we used two action potentials (40 ms interstimulus interval) to study dendritic Ca^{2+} dynamics at different distances from the soma (Fig. 5.1). The peak Ca^{2+} transient amplitude in a CA1 pyramdial cell decreased with distance from soma in the apical dendrite (Fig. 5.1 right). We were able to detect Ca^{2+} transients in the proximal apical dendrites (Fig. 5.1 left) and spines but the amplitude decayed very fast in the thin dendrites. In the more distal dendrites no backpropagating action potential induced Ca^{2+} transients were measurable (data not shown). These results are in agreement with studies on CA1 and neocortical pyramidal neurons showing a distance-dependent reduction in the amplitude of bAPs and in the evoked Ca^{2+} transients in dendrites (Stuart and Sakmann, 1994; Spruston et al., 1995b; Svoboda et al., 1999; Golding et al., 2001). Therefore, we decided to study coincident activity only in spines on the first oblique dendrites where we were able to detect Ca^{2+} transients evoked by bAPs.

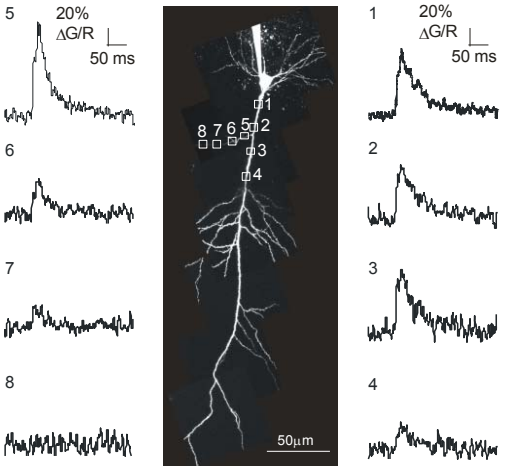

Figure 5.1. ***Two photon Ca^{2+} imaging of backpropagating APs at different distances from the soma in hippocampal CA1 pyramidal cell.***
A hippocampal CA1 pyramidal cell filled with 200 µM Fluo4 and 30 µM Alexa-fluor 594 via the patch pipette. White boxes indicate the positions of the line scans across the dendrites. The calcium transients were elicited by a pair of APs with an interstimulus interval of 40 ms. Calcium transients along the first oblique dendrite are plotted on the left (decay length constant l_{decay} = 12 µm). Calcium transients along the apical dendrite are plotted on the right (l_{decay} = 79 µm).

Modeling Ca^{2+} transients

We built a biophysical model of a dendritic spine attached through a variable spine neck to a CA1 pyramidal cell using the NEURON simulation environment (Hines and Carnevale, 1997) (Fig. 5.2) to study coincident activity and to investigate the effect of the spine neck resistance on the peak Ca^{2+} amplitude. To generate APs and its propagation through the neuron voltage gated sodium conductance (g_{NA}), a delayed rectifying potassium conductance ($g_{K(DR)}$) and an A-type potassium conductance ($g_{K(A)}$) were inserted in the axon, the soma and the dendritic compartments of a reconstructed CA1 pyramidal cell taken from the NEURON database (Golding et al., 2001). The propagation of an action potential along the apical dendrite is shown in Fig. 5.2. The backpropagating action potential innervated the proximal dendrites and the amplitude decreased with distance from soma.

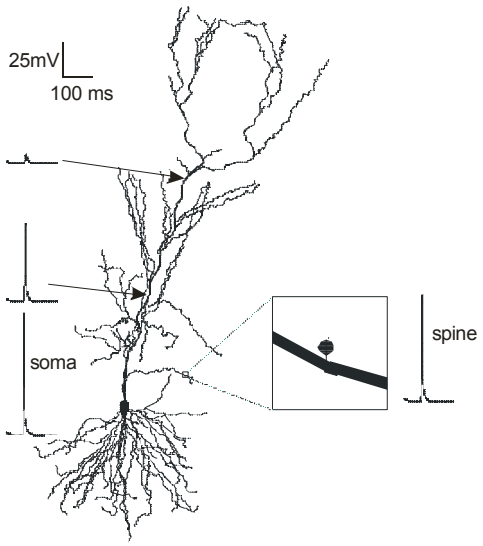

Figure 5.2. ***Simulation of a propagating action potential.*** *A multicompartment model of a CA1 pyramidal cell equipped with active channels was used for the simulations. The spine head further contains AMPA and NMDA receptors and R-type Ca^{2+} channels (see methods). A single action potential was evoked by a short current step (1 nA, 3 ms) delivered at the soma. The membrane potential is shown at the soma, at two different locations at the apical dendrite and at the spine head.*

In earlier pharmacological experiments, we have shown that at least three types of channels are important for the Ca^{2+} influx in a spine after synaptic stimulation: AMPA receptors, NMDA receptors and R-type Ca^{2+} channels (Grunditz et al., 2008). Furthermore, a model spine containing these three channels was able to reproduce the Ca^{2+} transients we observed in the imaging experiments. The R-type voltage gated Ca^{2+} channels have also been shown to produce the main fraction of the Ca^{2+} influx evoked by APs in spines (Yasuda et al., 2003). For these reasons, we decided to limit the conductance of the spine head to these three channels: AMPA receptors, NMDA receptors and R-type Ca^{2+} channels (see methods for more details of the model). The spine was attached to the first oblique dendrite as shown in Fig. 5.2. The dendrites did not contain any Ca^{2+} permeable conductance.

We first simulated the Ca^{2+} transients evoked by synaptic stimulation and the backpropagation of an action potential (AP) alone (Fig. 5.3A left panel and 5.3B left panel) in a spine with low spine neck resistance (R_{neck} = 120 MΩ). In the simulations of coincident activity the peak Ca^{2+} amplitude was larger ($A_{CaEPSP-AP}$ = 137%, black line in Fig. 5.3C left panel) than the Ca^{2+} transient evoked by synaptic stimulation and an AP alone (red line in Fig. 5.3C left panel) when the EPSP preceded the AP by an interstimulus interval of 5 ms. When the EPSP was followed by the AP (50 ms interstimulus interval) the amplitude hardly differed from the Ca^{2+} transient evoked by an EPSP and an AP alone ($A_{CaAP-EPSP}$ = 101%, Fig. 5.3D left).

Next, we did the same simulations for a spine with a higher spine neck resistance (R_{neck} = 1.2 GΩ). In the simulations where the EPSP preceded the AP the peak Ca^{2+} transient amplitude was strongly enhanced: the peak amplitude of the Ca^{2+} transient was 218% (black line in Fig. 5.3C right panel) compared with the Ca^{2+} amplitude evoked by an EPSP and an AP alone (red line in Fig. 5.3C right panel). When the bAP was followed by an EPSP the amplitude of the Ca^{2+} transient was smaller ($A_{CabAP-EPSP}$ = 94%, black line in Fig. 5.3D right panel) then the Ca^{2+} transients after synaptic stimulation and an AP alone (red line in Fig. 5.3D right). To summarize the simulations with the different spine neck resistance: First, in both spines the peak Ca^{2+} amplitude of the pairing simulations was dependent whether the bAP preceded or followed an EPSP. The amplitude of the peak Ca^{2+} transient was enhanced when the EPSP was followed by a bAP. In addition, the amplitude was stronger enhanced in the spine with high spine neck resistance then in the spine with the lower spine neck

resistance. Second, the Ca^{2+} transients in the spine with the higher spine neck resistance was generally bigger then the rise time of the Ca^{2+} transient in the spine with a lower spine neck resistance was in all simulations much slower then in the spine with the higher spine neck resistance.

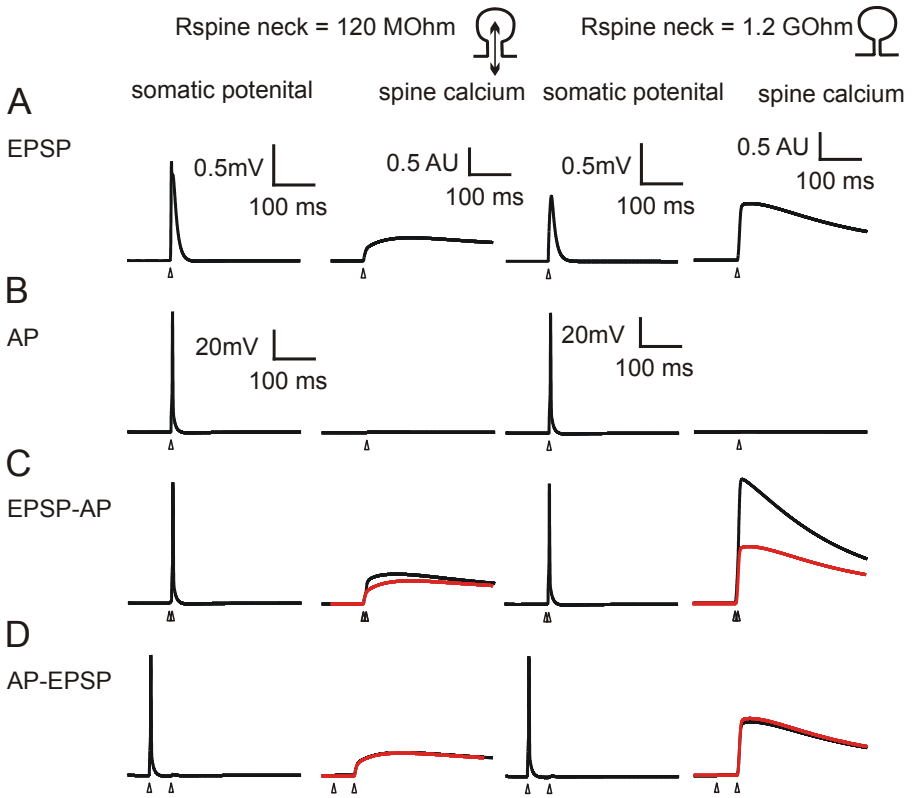

Figure 5.3. ***Modeling* spine Ca^{2+} *transients after EPSP and bAP in a spine with low spine neck resistance (120 MΩ) and in a spine with high spine neck resistance (1.2 GΩ)***

(A) *For each spine, the EPSPs at the soma after synaptic stimulation are plotted on the left and spine calcium transients on the right. The resting membrane potential was set to -65 mV for all simulations.*

(B) *Depending on its position in the dendritic tree, the calcium transient in response to a single bAP can be very small in a spine.*

(C) *Pairing of an EPSP with a bAP (Δt = 5 ms) results in supralinear amplification of the calcium signals (120 MΩ spine: 38% amplification, 1.2 GΩ spine: 103% amplification). For comparison, the linear sum of EPSP- and bAP-evoked calcium is shown (red line).*

(D) *A bAP preceding an EPSP (Δt = -50 ms) has no effect in the 120 MΩ spine and results in a small (6%) attenuation of the calcium transient in the1.2 GΩ spine.*

Are only NMDA receptors responsible for the enhanced Ca^{2+} transients? We run the model without R-type VDCC to investigate the contribution of these channels to the Ca^{2+} transients (data not shown). In the spine with high neck resistance the amplitude

of the Ca^{2+} transient was reduced to 37% and in the spine with low neck resistance the amplitude was reduced to 90%. Indicating that in spines with high neck resistance the R-type channels play an important role in the

Ca^{2+} transients after pairing of EPSPs and bAPs are dependent on the spine neck resistance

To emphasize the influence of the spine neck resistance on the Ca^{2+} transients evoked by pairing of EPSPs and bAPs, we run the model with the two different spine neck resistances (120 MΩ and 1.2 GΩ) at different time intervals of the EPSPs and bAPs (Fig. 5.4). When the EPSPs were followed by postsynaptic APs (positive spike timing), the Ca^{2+} transients were strongly enhanced in the spine with high spine neck resistance but only little in the spine with low spine neck resistance. The Ca^{2+} transient in the spine with a higher neck resistance was also much more sensitive to the exact timing of the EPSP and the bAP. Pairing with negative spike timing resulted in a stronger reduction of the Ca^{2+} transients in the spine with the higher spine neck resistance then in the spin with a lower neck resistance. But in both spines, positive spike timing had a stronger effect on the peak Ca^{2+} transients then negative spike timing.

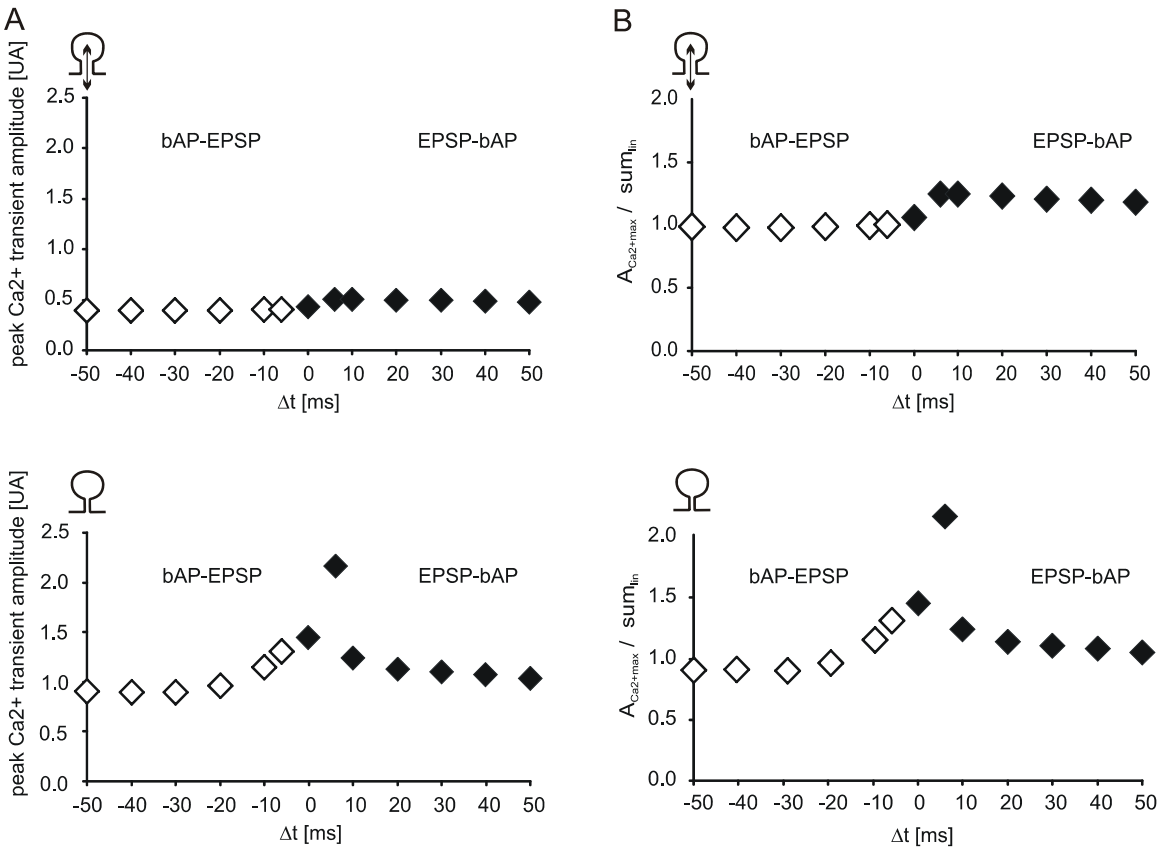

Figure 5.4. ***Modeling the effect of the spine neck on the peak Ca^{2+} transient amplitudes evoked by pairing of EPSPs with bAPs at different time intervals.***

(A) *The peak Ca^{2+} transients evoked by pairing of EPSPs with APs are plotted for the corresponding time intervals Δt in a spine with a low spine neck resistance (R_{neck} = 120 MΩ).*

(B) *Same as A, but R_{neck} = 1.2 GΩ. Note narrow time window for calcium transient amplification at t = 5 ms.*

Ca^{2+} transients evoked by an EPSP preceding a bAP are strongly enhanced in spines with high spine neck resistance

Next, we tested the prediction from our model that spines with high spine neck resistance strongly enhance the Ca^{2+} amplitude after EPSP paired with AP by measuring the Ca^{2+} transients evoked by synaptic stimulation and APs. To quantify the Ca^{2+} transients in single spines we filled a CA1 pyramidal cell with the green Ca^{2+} indicator dye (Fluo5F, 600 µM) for a large dynamic range and a red Ca^{2+}-insensitive dye (Alexa-fluor 594, 30 µM) (Fig. 5.5A). A glass microelectrode was positioned close to the dendrite of the patched cell using laser DIC. Responsive spines were found by a transient increase in fluorescence after synaptic stimulation. When searching for the stimulated spine the membrane potential was clamped to 0 mV. A

step depolarization to 0 mV leads to a large Ca^{2+} influx through the VDCC. We have shown in a previous study (Grunditz et al., 2008) that such a depolarization pulse changes the diffusional coupling between spine head and the parent dendrite; the spines are afterwards more isolated then before.

The Ca^{2+} transients evoked by synaptic stimulation were in contrast to the bAPs induced Ca^{2+} influx restricted to the stimulated spine (Fig. 5.5C). In the same spine we studied Ca^{2+} transients evoked by synaptic stimulation alone (Fig. 5.5D), Ca^{2+} transients induced by a bAP (Fig. 5.5E) and Ca^{2+} transients evoked by pairing of synaptic EPSP and bAP (Fig. 5.5F and G). The Ca^{2+} amplitudes were extracted by fitting of two exponentials to the average response (red line in Fig. 5.5D, E, F, G). Peak Ca^{2+} transient evoked by an EPSP in the spine head was larger ($\Delta G/R_{CaEPSP}$ = 0.678, Fig. 5.5D) than the corresponding transient evoked by a bAP ($\Delta G/R_{CabAP}$ = 0.149, Fig. 5.5E). In the pairing experiments the amplitudes of the Ca^{2+} transients depended on weather the bAP was evoked before ($\Delta G/R_{CabAP\text{-}EPSP}$ = 0.938, Fig. 5G) or after the EPSP ($\Delta G/R_{CaEPSP\text{-}bAP}$ =1.373, Fig. 5.5F). The peak Ca^{2+} amplitude was strong enhanced ($A_{CaEPSP\text{-}bAP}$ = 203%) when the EPSP preceded the bAP by an interstimulus interval of 20 ms. When the EPSP was followed by the bAP (50 ms interstimulus interval) the amplitude was larger ($A_{CabAP\text{-}EPSP}$ = 138%) then the Ca^{2+} peak evoked by the EPSP alone, but close to the linear sum of an EPSP (A_{CaEPSP} = 100%) and a bAP (A_{CabAP} = 22%) (Fig. 5.5G).

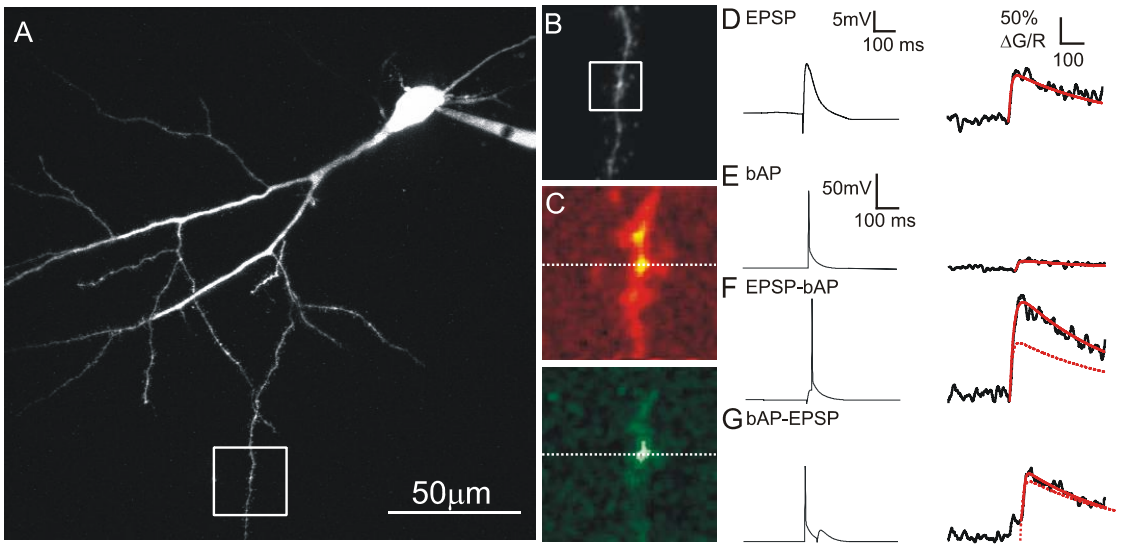

Figure 5.5. *Ca^{2+} **transients evoked by paring of EPSPs and bAPs in spines.***

***(A)** Two-photon image of a hippocampal CA1 pyramidal cell filled with 30 µM Alexa-fluor 594 and 600 µM Fluo5F.*

***(B)** Magnified view of the boxed region in A with the active spine.*

***(C)** Synaptically evoked spine Ca^{2+} transients. For ration measurements, the cell was filled with a green Ca^{2+}-sensitive dye (Fluo5F) and a red dye (Alexa-Fluor 594). Ca^{2+} signals were measured in line-scan mode. The position of the line scan through the active spine is indicated by the vertical line.*

***(D)** The somatic whole-cell recording of an EPSP (left) and the corresponding synaptically evoked Ca^{2+} transient (right) in the active spine.*

***(E)** The somatic recording (left) and the corresponding Ca^{2+} transient (right) in the same spine evoked by a bAP.*

***(F)** Pairing of an EPSP with a following bAP at a stimulus interval of 20 ms (somatic voltage recording, left) and the corresponding Ca^{2+} transient (right). The dotted red lines indicate the sum of the bAP evoked and the synaptically evoked Ca^{2+} transients.*

***(G)** Pairing of a bAP preceding an EPSP by 50 ms (somatic voltage recording, left). The resulting Ca^{2+} transient is shown to the right. The dotted red lines indicate the sum of the bAP evoked and the synaptically evoked Ca^{2+} transients.*

Discussion

Modifications of synaptic strength can be induced by the coincidence of an AP with a synaptic input (Magee and Johnston, 1997; Markram et al., 1997; Bi and Poo, 1998; Debanne et al., 1998). The direction of change is dependent on the relative timing of postsynaptic APs and EPSPs (Markram et al., 1997; Bi and Poo, 1998) (Feldman, 2000; Sjostrom et al., 2001). For the induction of change in synaptic strength postsynaptic Ca^{2+} elevation is essential (Lisman, 1989). The magnitude of the change in synaptic strength has been shown to depend on the volume-averaged elevation of Ca^{2+} in a spine (Nevian and Sakmann, 2006). We tested the effect of the spine neck resistance on the elevation of Ca^{2+} after coincident activity. The results show that the Ca^{2+} transients in spines with higher spine neck resistance are strongly enhanced after paring an EPSP with an AP. Further more, our results indicate that the peak Ca^{2+} transients in spines with a high spine neck resistance are more sensitive to the precise timing the presynaptic and the postsynaptic action potentials then in spine with low neck resistance.

The amplitude of the Ca^{2+} influx evoked by the backpropagation of APs decayed very fast with distance form soma, especially in the thin oblique dendrites, where most of the synapses are located. VDCCs have a variable density and function along the dendrites of CA1 pyramidal neurons (Isomura et al., 2002). Therefore, we can not exclude that the AP is able to electrically propagate to even more distal dendrites where we did not detect any Ca^{2+} signals. But for our study we decided to study coincident activity in the first oblique dendrites where we could measure a Ca^{2+} signal after current injection at the soma.

In hippocampal pyramidal neurons, coincident bAP and EPSP can induce spine Ca^{2+} transients larger than the linear sum of the individual signals (Yuste and Denk, 1995; Koester and Sakmann, 1998; Schiller et al., 1998). Here we show that only in spines with a high spine neck resistance the pairing of an EPSP with an AP can cause strong supralinear Ca^{2+} transients. The NMDA receptors are thought to account for a large fraction of the supralinearity of the Ca^{2+} increase during coincident activity (Schiller et al., 1998). The voltage dependence of NMDA receptor mediated Ca^{2+} influx is steepest at a membrane potential of -20 mV (Grunditz et al., 2008). A high spine neck

resistance leads to strong depolarization of the spine head by the AMPA current. During the EPSP, NMDA receptors in the spine head are exquisitely sensitive to additional depolarization. Only in spine with a high spine neck resistance the depolarization provided by coincidence of bAP and EPSP is sufficient to unblock enough NMDA receptors to cause a supralinear Ca^{2+} transient. In a shaft synapse or spine with a low neck resistance, the activation threshold of NMDA receptors can only be reached if multiple neighboring synapses are activated simultaneously. Therefore, it is likely that the rules for the induction of long-term plasticity (cooperativity vs. independence) depend on the spine neck resistance. Not only the NMDA receptors are responsible for the supralinearity in the Ca^{2+} transients also VDCCs play a crucial role. The R-type VDCCs are high voltage activated Ca^{2+} channels and need a strong depolarization to get activated. Thus, only in spines with a high neck resistance the depolarization is strong enough to open a significant number of R-type VDCCs and only in these spines the R-type VDCCs contribute significantly to the Ca^{2+} transient.

How can a spine change the properties of its neck? In a previous study, we have shown that spines increase their neck resistance in response to high Ca^{2+} elevation (Grunditz et al., 2008). In this study, the spine with low neck resistance (120 MΩ) represents a spine that has only experienced low level of spontaneous activity and the spine with a high neck resistance (1.2 GΩ) represents a spine that have experienced activity that led to high Ca^{2+} elevation. Only in a spine with a high neck resistance the peak Ca^{2+} transients are strongly dependent on the timing between the action potentials of the presynapse and of the postsynapse. Changing the spine neck resistance after Ca^{2+} elevation allows the spine to work as a perfect detector for the precise timing of coincident activity. Isolation of the spine induced by a high neck resistance could be an important step in STDP.

Conclusions and Outlook

Most excitatory synapses are made onto dendritic spines, yet their function is still unclear. The main focus during my PhD work has been to assess the role of the spine during synaptic transmission. In the following chapter I have summarized the main findings of this work and discussed them with respect to previous studies.

1. Spine Ca^{2+} transients depend on electrical synergism between AMPA receptors, NMDA receptors, and VDCCs

We have shown that dendritic spines with a high spine neck resistance are able to generate NMDA receptor-dependent Ca^{2+} transients following glutamate release in an autonomous fashion, without the need of additional depolarization of the postsynaptic cell. At depolarized potentials, Ca^{2+} responses were dependent on NMDA receptor activity, but not on AMPA receptor function. At the resting membrane potential Ca^{2+} transients were inhibited by blocking NMDA receptors, AMPA receptors or R-type Ca^{2+} channels. The pharmacological experiments combined with numerical simulations indicated the following:

1) AMPA receptor activity is necessary to trigger spine Ca^{2+} transients.
2) NMDA receptors and voltage-dependent Ca^{2+} channels act together to prolong the depolarization of the spine head and boost the Ca^{2+} influx. Thus, we provide evidence for graded electrical amplification in spines which operates below the threshold for a spine spike.
3) The strong depolarization of the spine head (~55 mV) brings NMDA and R-type channels briefly to the steepest part of their activation curve, making the entire spine highly sensitive to additional depolarization.

2. The voltage-dependence of synaptic NMDA receptors is steep

To ensure realistic model simulations, we characterized the voltage-dependence of NMDA receptors experimentally. When comparing postsynaptic Ca^{2+} transients at different membrane potentials (with AMPA receptors pharmacologically blocked), the residual Ca^{2+} influx at the resting potential was barely detectable, in spite of the very high driving force for Ca^{2+} ions. This demonstrates an almost perfect Mg^{2+} block

of NMDA receptors at -65 mV. Our measurements were well fit using a combination of the Boltzmann equation and the GHK current equation, but indicated a stronger Mg^{2+} block than previously reported.

Two reasons can account for the discrepancy with previous measurements. Firstly, many measurements were performed on excised patches, that i) have a bias towards extrasynaptic receptors, and ii) strip the NMDA receptors from the many binding partners within the PSD. Therefore, it is conceivable that NMDA receptors have different properties *in situ*. Secondly, in previous optical Ca^{2+} measurements without AMPA receptor block, imperfect control over the spine membrane potential during AMPA receptor activity could have led to an underestimate of the Mg^{2+} block (Kovalchuk et al., 2000). In voltage clamp experiments without AMPA receptor block, we measured much larger Ca^{2+} signals in the spines, indicating voltage escape of the spine membrane. For these reasons, we used our new measurements to set the voltage-dependence of the NMDA conductance in all our model simulations.

3. Ca^{2+}-silent spines differ pre- and postsynaptically from their functional neighbors

Our Ca^{2+} imaging experiments revealed a distinct group of spines that showed hardly any Ca^{2+} influx at resting potential. Ca^{2+}-silent spines have been described in a previous study (Ward et al., 2006) where the authors equated Ca^{2+}-silent spines with silent synapses. We show that a lack of AMPA receptors is not the only possible explanation for Ca^{2+}-silence. Spines can also be Ca^{2+}-silent due to insufficient electrical isolation from the parent dendrite through a short and wide spine neck. These synapses would be generating AMPA-EPSCs at the resting membrane potential, but appear Ca^{2+}-silent in imaging experiments. Interestingly, many Ca^{2+}-silent spines were contacted by presynaptic terminals that did not release glutmate after a single AP. Such an ultra-low release probability was never observed in any of the functional spines, indicating a matching of pre- and postsynaptic properties at individual synapses (‘deaf-mute’ synapses).

4. High Ca^{2+} levels trigger changes in the spine neck resistance

We have shown that postsynaptic depolarization leads to reduction in the diffusional coupling between spine head and parent dendrite which is likely to be accompanied by an increase in the electrical resistance of the spine neck. Spine neck plasticity was not dependent on synaptic activity, but was completely blocked in Ca^{2+} free solution. Thus, elevated Ca^{2+} levels during the dendritic depolarization triggered changes in the spine neck resistance.

We compared the diffusional resistance of spine necks *in vivo* and *in vitro*. In naive slices, spine necks had lower resistances compared to the *in vivo* situation, but after depolarization, they were considerably higher. The wide range of spine neck diffusional resistances *in vivo* suggests that some spines act as electrical amplifiers, while others behave like the Ca^{2+}-silent spines described in our slice experiemnts.

Surprisingly, the actively amplified depolarization in spines with high spine neck resistance did not result in larger EPSPs at the soma, a finding that was fully reproduced in our modeling study. Thus, active changes in spine neck resistance are a powerful mechanism to modulate Ca^{2+} signaling in spines, but with little effect on the somatic EPSPs.

Outlook: Is spine neck plasticity essential for functional synaptic plasticity?

Although spine neck plasticity does not change synaptic strength by itself, it could still be an essential step in the induction of LTP. A commonly used protocol for inducing LTP in the hippocampus is to give 'tetanic' stimulation (a high frequency stimulation of the Schaffer collaterals (3 x 1 s, 100 Hz). This synaptic input produces postsynaptic depolarization. Also the pairing protocol, i.e. low frequency of synaptic stimulation paired with postsynaptic depolarization, has been shown to successfully induce LTP (Gustafsson et al., 1987; Malinow, 1991). In a study by Chen et al., they show that the pairing protocol only leads to LTP when presynaptic stimulation occurs at the end of a long depolarization pulse but not if paired at the beginning (Chen et al., 1999). An explanation for this finding could be that the active change in the spine

neck resistance triggered by the high Ca^{2+} elevation during the depolarization pulse enables synaptic plasticity.

A high spine neck resistance (R_{neck}) could facilitate potentiation by at least 3 mechanisms: Firstly, only spines with high R_{neck} show large Ca^{2+} transients in response to synaptic activation, due to strong depolarization of the spine heads. Secondly, upon pairing pre- and postsynaptic activity, our model predicts further boosting of Ca^{2+} transients in high R_{neck} spines, since they are highly sensitive to additional depolarization. Peak Ca^{2+} elevation determines the magnitude of long-term changes in synaptic strength (Nevian and Sakmann, 2006). Thus, only spines with high neck resistance are 'primed' to act as a coincidence detector of pre- and postsynaptic activity. Thirdly, signaling molecules downstream of Ca^{2+}, e.g. CaMKII, will be trapped close to the synapse by a high resistance spine neck, increasing the probability of phosphorylation of target proteins.

Testing this possible connection between spine neck morphology and synaptic plasticity would be a logical next step, but it is not trivial in terms of the experimental strategy. Methods for the non-invasive potentiation of single synapses will be needed to address this question. Most promising is currently a combination of optogenetic methods (Channelrhodopsin-2) and two-photon uncaging of glutamate.

We have shown that the spine neck can change its properties upon depolarization. But for how long does the neck resistance stay high? The modification of the spine neck is most likely reversible because most spines in acute slices showed low neck resistance before the depolarization step, in contrast to the *in vivo* situation. But what molecules are involved in the signal transduction cascade that triggers spine neck changes? These questions remain to be investigated.

Methods

Two-photon excitation fluorescence microscopy was combined with whole-cell patch clamp recordings to measure Ca^{2+} transients in single spines of CA1 pyramidal cells in acute hippocampal slices. Based on the data from the Ca^{2+} imaging experiments we build a model of a single spine attached to a neuron using the NEURON simulation environment. FRAP experiments were used to estimate the resistance of the spine neck. The methods of the brain slice preparation, the patch-clamp recordings, measurement of the Ca^{2+} indicator, FRAP experiments and the parameters for the model are explained in detail in this chapter.

Acute slice preparation

Acute hippocampal brain slices were prepared from Sprague Dawley rats (postnatal day 16-20) in accordance with the animal care and use guidelines of the Veterinary Department Basel-Stadt. Following isofluorane anesthesia and decapitation, horizontal slices (350 μm thick) were cut on a vibroslicer (Leica) in ice-cold solution containing (in mM): 110 choline chloride, 25 NaHCO3, 25 D-glucose, 11.6 sodium ascorbate, 7 MgSO4, 2.5 KCl, 1.25 NaH2PO4 and 0.5 CaCl2. Slices were incubated at 34°C for 30 min in oxygenated artificial CSF (ACSF), containing (in mM) 127 NaCl, 25 NaHCO3, 25 D-glucose, 2.5 KCl, 1 MgCl2, 2 CaCl2, 1.25 NaH2PO4 and then stored at room temperature until used. Experiments were done at 32° C in ACSF containing 10 μM bicuculline, 30 μM serine and 2 μM thapsigargin to block GABAA receptors, glycine-dependent desensitization, and to deplete intracellular Ca2+ stores.

Organotypic slice culture

(used in FRAP experiments to compare acute slices with in vivo data)
Organotypic hippocampal slices were prepared from Sprague Dawley rats at postnatal day 5 as described (Stoppini et al., 1991). To compare in vivo FRAP data (YFP bleach, Fig. S4.2) to slice data (Alexa-Fluor 594 bleach), we transfected cultures biolistically with YFP ‘Venus’, using a Helios Gene Gun (BioRad). 2 weeks

after transfection, YFP-expressing pyramidal cells were filled with Alexa-Fluor 594 through a patch pipette. Two-photon FRAP experiments were performed at 940 nm, and the recovery of both fluorophores in individual spines was recorded in separate color channels. In a sample of 30 spines, the FRAP time constants τYFP and τAlexa-Fluor were correlated and well fit by a linear function:

$$\tau YFP = 4.85 \cdot \tau Alexa\text{-}Fluor$$

Thus, we divided the time constants measured in vivo by 4.85 to compare them with our measurements in acute and cultured slices (Fig. 4.1A). To generate the FRAP data set labeled 'organotypic culture' in Fig. 4.1A. , untransfected CA1 pyramidal cells (14-16 DIV) were filled with Alexa-Fluor 594 via patch pipette and bleached using two-photon excitation at 810 nm.

Electrophysiology

Whole-cell recordings from CA1 pyramidal cells were made with a Multiclamp 700B amplifier (Axon Instruments), using 4-6 MΩ pipettes filled with (in mM): 130 K-methylsulfonate (or 135 cesium methanesulfonate), 10 HEPES, 10 sodium phosphocreatine, 3 sodium ascorbate, 4 MgCl2, 4 Na2-ATP, 0.4 Na-GTP, 0.6 Fluo5F and 0.03 Alexa-Fluor 594 (pH 7.2). Schaffer collaterals were stimulated with a monopolar glass electrode filled with 1M NaCl, positioned 15-25 μm from an oblique dendrite, using brief hyperpolarizing pulses (0.2 ms, -3 to -5 V) delivered by a stimulus isolator (NPI Electronics). Paired pulses (ISI = 40 ms) and single pulses were alternated every 8 seconds.

Pharmacology

In order to characterize the channels determining the Ca^{2+} influx into the spine drugs which specifically block certain ion channels were perfused or diluted in the patch pipette. The drugs applied to the bath were washed in for at least 4 min. The glutamate receptors of the AMPA type were blocked with 10 μM NBQX (Tocris). To reduce the desensitization of the AMPA receptors 40 μM cyclothiazide (Anawa) was used. The NMDA receptors were blocked with 10 μM dCPP (Tocris). 5nM lidocaine

N-ethyl bromide (QX-314, Tocris) was used to block fast Na^+ channels. A low concentration of Ni2+ (10 μM) partially blocks R- and T-type voltage-dependent Ca^{2+} channels. The selective blocker SNX-482 (0.1 μM, Peptides International) was used to separately block high-voltage activated R-type Ca^{2+} channels.

Two-photon laser scanning microscopy

We used a custom-built 2-photon laser scanning microscope based on a BX51WI microscope (Olympus) and a pulsed Ti:Sapphire laser (Chameleon XR, Coherent) tuned to $\lambda = 810$ nm, controlled by the open source software package ScanImage (Pologruto et al., 2003). Fluorescence was detected in epifluorescence (LUMPlan W-IR2 60X 0.9 NA, Olympus) and transfluorescence modes (achromatic aplanatic condenser, 1.4 NA, Olympus) using 4 photomultiplier tubes (R3896, Hamamatsu). We used 725DCXR dichroic mirrors and E700SP blocking filters to reflect emitted photons into a secondary beamsplitter, containing a 560DCXR dichroic, 525/50 (green) and 610/75 (red) band pass filters (AHF Analysentechnik). The principle and advantages of a two photon excitation microscopy are explained in a paper by Svoboda and Yasuda (Svoboda and Yasuda, 2006) (Fig. 7.1).

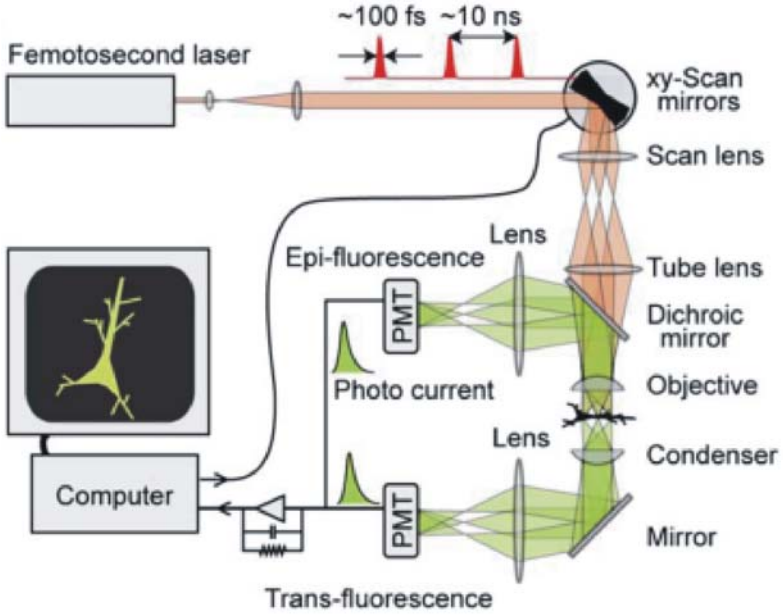

Figure 7.1. ***Two-photon excitation microscopy.***

Schematic drawing of a two-photon microscope with epifluorescence and transfluorescence detection. (Adapted from Svoboda and Yasuda, 2006).

Ca^{2+} imaging

A large number of Ca^{2+} ion sensitive indicator dyes can be used for functional Ca^{2+} imaging. These dyes change their spectral properties upon binding to Ca^{2+} ions. We used Fluo5F as a Ca^{2+} indicator dye (0.6 mM, Kd = 0.8 μM under physiological conditions, Molecular Probes) and for the back propagating action potential experiments Fluo4 (0.2 mM, Kd = 0.5 μM under physiological conditions, Molecular Probes). Fluo5F has a very low basal fluorescence; therefore Alexa-Fluor 594 (Molecular Probes) was used to label the fine structures of the cell. The two dyes can be well separated because there is little overlap in the emission spectra.

Responsive spines on oblique dendrites 100-200 μm (average 170 μm) from the soma were identified using frame scans (4 Hz). For a quantitative measurement of the Ca^{2+} transients, line scans (500 Hz) were used. After background subtraction, we calculated the ratio of green/red fluorescence intensity (*G/R*) (Yasuda et al., 2004).

Data analysis

To quantify the amplitude of noisy fluorescence transients, we first generated a response template for each spine by fitting the difference of two exponentials to the average response. This response template was scaled in amplitude to fit each individual response (scaling factor * template amplitude = response amplitude). Summary data are reported as mean ± SEM. The Wilcoxon signed-rank test with $\alpha = 0.1$ was used to test for significance.

Dye saturation

The comparison of Ca^{2+} transients under depolarized conditions and in current clamp makes great demands on brightness and dynamic range of the Ca^{2+} sensitive dye. To estimate dye saturation in our experiments, we compared fluorescence transients following single (f1) and paired stimulation (f2). Under current clamp conditions, f2/f1 was larger than under depolarized conditions (f2'/f1'), indicating partial dye saturation under depolarized conditions (Fig. 7.2). Assuming that the ratio of the Ca^{2+}

transients was similar in current clamp and at 0 mV (r2/r1 = r2'/r1'), we fitted an exponential saturation curve to our measurements. The asymptotic value of 0.93 was close to the highest G/R ratios we observed experimentally (0.88, synaptic stimulation in Mg^{2+}-free recording solution, data not shown). We would like to point out that responses to paired stimulation under depolarized conditions (f2'), where free Ca^{2+} levels exceeded the K_D of Fluo5F, were not used for any quantitative analysis.

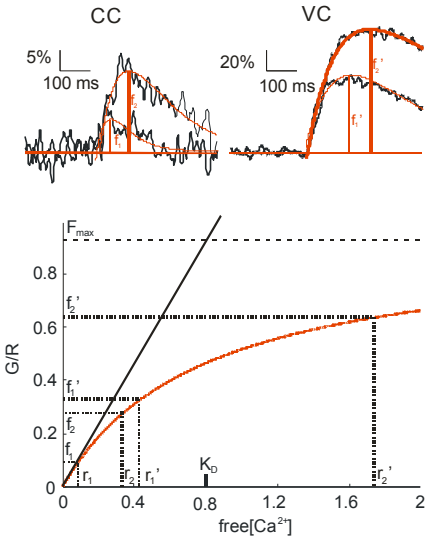

Figure 7.2. ***Non-linearity of Ca^{2+} measurements.***

We compared spine fluorescence changes (G/R) after single pulse stimulation (f_1) and paired pulse stimulation (f_2, 40 ms I.S.I.) under current clamp conditions (CC) and in voltage clamp (VC, depolarized to the synaptic reversal potential). The ratio in CC (f_2 / f_1) was larger than the ratio in VC (f_2' / f_1'), indicating partial dye saturation under depolarized conditions. Assuming that the ratio of the underlying Ca^{2+} transients was similar under both conditions (r_2 / r_1 = r_2' / r_1'), we used the relationship

$$\frac{(G/R)}{(G/R)_{\max}} = \frac{[Ca^{2+}]}{K_D + [Ca^{2+}]} \qquad \textit{(Eq. 1)}$$

to estimate dye saturation (red curve). The asymptotic value (G/R = 0.93) was similar to the highest G/R ratio we observed in a spine (paired stimulation in Mg^{2+} free saline, G/R = 0.88, data not shown). Since f_2' responses were not used for quantitative analysis, and $[Ca^{2+}]_{free} < K_D$ in all other conditions, we used the linear approximation (black line) to convert our fluorescence measurements into Ca^{2+} concentrations.

Estimation of spine volume

Assuming homogenous distribution of Alexa-Fluor 594 in the cytoplasm, the integrated fluorescence intensity (red channel) of a spine is proportional to its cytoplasmic volume (Svoboda, 2004) (Holtmaat et al., 2005). For each cell, a calibration measurement was taken by scanning the laser across the proximal apical dendrite, a cellular compartment large enough to contain the entire point-spread function (PSF) of our microscope, to get the maximum fluorescence intensity (f_{max}). This calibration measurement was typically taken at a different depth (z_{cal}) than the spine image (z_{spine}), and attenuation of the laser was corrected using an experimentally determined attenuation function

$f(z) = f_{\max} \cdot \exp(a \cdot (z_{cal} - z_{spine}))$, with a = -0.015 µm-1 (attenuation coefficient).

To measure the absolute volume of a spine (V_{spine}), we first calculated the Gaussian intensity distribution a hypothetical PSF-sized object would produce if imaged at the same zoom factor and the same depth than the spine (f_{sim}). The integrated intensity of fsim (sum of all pixel values within a region of interest, $\iint f_{sim}$) was then compared to the integrated intensity of the spine image in the center plane ($\iint f_{spine}$). The volume of the spine is related to the spine intensity as follows:

$V_{spine} = \iint f_{spine} * V_{PSF} / \iint f_{sim}$

The volume of the PFS (V_{PSF} = 0.38 µm3) was determined using fluorescent beads (0.1 µm, Molecular Probes).

Estimation of spine neck resistance

To get information about the diffusional resistance of the spine neck, we took advantage of the fact that under depolarized conditions, the time constant of decay of the spine Ca^{2+} signal (τ_{decay}) was largely due to diffusion of Ca^{2+}-bound dye molecules into the dendrite. Extrusion of free Ca^{2+} from the cytoplasm was compromised under these conditions, because

i) the spine membrane was clamped above the reversal potential of the Na^{+}-Ca^{2+} exchanger (Blaustein and Lederer, 1999a),

ii) plasma membrane Ca^{2+} pumps had to compete with 600 µM Fluo5F for free Ca^{2+} ions, and

iii) SERCA pumps were blocked by thapsigargin. These three effects resulted in very long lasting fluorescence transients (τ_{decay} = 900 ms, average of excitable spines).

Therefore, we could use τ_{decay} to estimate the spine neck length to cross section ratio (L/A) according to the equation

$$L/A = \tau \cdot D / V = 900\ [\text{ms}] \cdot 0.1\ [\mu\text{m}^2/\text{ms}] / 0.11\ [\mu\text{m}^3] = 818\ [\mu\text{m}^{-1}]$$

(Bloodgood and Sabatini, 2005)where D is the diffusion coefficient of Fluo5F in cytoplasm (100 $\mu m^2/s$) and V is the average spine volume of our sample (0.11 μm^3). We estimated the resistance of the spine neck according to the cable equation

$$R_{neck} = R_i \cdot L / A = 150 \cdot 10^4\ [\Omega\ \mu\text{m}] \cdot 818\ [\mu\text{m}^{-1}] = 1.2 \cdot 10^9\ [\Omega]$$

assuming an internal resitivity Ri = 150 Ωcm.

FRAP measurements in acute slices

Transport through the spine neck can be directly probed by measuring diffusion using fluorescence recovery after photobleaching (FRAP) in the spine. The freely diffusible fluorophore Alexa-Fluor 594 was bleached in the spine head and the time for fluorescence recovery by diffusion from the parent dendrite was measured. The diffusional exchange between spine and dendrite was in the range of x-x, about a factor of 100 slower than expected for free diffusion over the small distance between spine and dendrite.

In vivo FRAP measurements

Transgenic mice expressing yellow fluorescent protein (B6.Cg-Tg(Thy1-YFPH)2Jrs/J, Jackson Laboratory) were anesthetized by IP injection (17 mg/ml ketamine, 1.7 mg/ml xylasine). The skull was exposed and thinned with a dental drill as described (Grutzendler et al., 2002). For imaging and photobleaching, an Ultima 2-photon microscope (Prairie Technologies) with a 60x/1.1NA Objective (Olympus) was used at 920 nm excitation wavelength (Mai Tai HP, Spectra Physics). Of each spine, 40 images (64x64 pixels) were taken at 13 Hz according to the following protocol: 10 frames baseline, bleach pulse (0.5 s), 10 frames, 5 s wait, 10 frames, 10 s

wait, 10 frames (Fig. S4.2). Laser power was adjusted to bleach the spine to 30-40% of its original intensity. Custom-written software (Matlab) was used to measure the spine fluorescence intensity, compensating for small movements by centering the region of interest (ROI) on the spine in every frame. The fluorescence recovery was fit with a single exponential function (Fig. S3.2). To compare YFP and Alexa-Fluor 594 measurements, we performed calibration experiments in organotypic slice culture.

Compartmental modeling

We used the NEURON simulation environment (Hines and Carnevale, 1997) to model a single dendritic spine of 0.11 μm^3 volume (average volume of all functional spines in our sample), equipped with NMDA and AMPA receptors and voltage-dependent Ca^{2+} channels. To ensure a realistic EPSP time course in the spine head, we connected the spine through a thin neck (Rneck = 1.2 GΩ) to the dendrite of a multi-compartment model of a CA1 pyramidal cell taken from the NEURON database (Golding et al., 2001). The model possessed three active conductances: a voltage-gated sodium conductance (gNa), a delayed rectifying potassium conductance [gK(DR)], and an A-type potassium conductance [gK(A)]. The biophysical parameters of these conductances were implemented as described in (Migliore et al., 1999) and were inserted and in all compartments of the cell excluded the spine and distributed as described in (Golding et al., 2001). When the model was used for studying the interactions of glutamatergic receptor and voltage-dependent Ca^{2+} channel in the spine all active conductances were removed from soma and dendrites. The membrane time constant (τm) was 30 ms (Rm = 40 kΩ cm2, Cm = 0.75 μF/cm2). The original model had no spines, but was compensated for the presence of spines by increasing Cm by a factor of 2 and decreasing Rm by a factor of 2 beyond 100 μm from the soma. An intracellular resistivity of Ri = 150 Ω cm (Ri = 50 Ω cm in the axon) and a membrane resting potential of Vrest = -65 mV were used.

AMPA receptor current

The kinetic equations for the AMPA and NMDA mechanism were taken from (Franks et al., 2002). The synaptic AMPA current I_{AMPA} was calculated as

$$I_{AMPA} = g_{AMPA}(V - E_{AMPA})$$

where g_{AMPA} is the total conductance of the AMPA receptors, V is the membrane potential, and E_{AMPA} is the reversal potential of the AMPA receptors.

The time course of the AMPA conductance g_{AMPA} was modeled as the difference of two exponentials

$$g_{AMPA}(t) = g_{AMPA\_max}(e^{-t/\tau 2} - e^{-t/\tau 1})$$

with $\tau 1$ = 0.206 ms, $\tau 2$ = 0.26 ms (Franks et al., 2002) and where g_{AMPA_max} is the maximal conductance of the AMPA receptors (single channel conductance = 10 pS).

NMDA receptor current

The NMDA receptor current I_{NMDA} was calculated as

$$I_{NMDA} = g_{NMDA}G(V - E_{NMDA})$$

where g_{NMDA} is the total NMDA conductance, G describes the voltage-dependent Mg^{2+} block, V is the membrane potential, and E_{NMDA} is the reversal potential of the NMDA receptor.

The time course of the NMDA conductance was modeled as the sum of 3 exponentials:

$$g_{NMDA}(t) = g_{NMDA\_max}(0.88e^{-t/\tau 2} + 0.12e^{-t/\tau 3} - e^{-t/\tau 1})$$, (Franks et al., 2002)

with $\tau 1$ = 3.18 ms, $\tau 2$ = 57.14 ms, $\tau 3$ = 2000 ms (Spruston et al., 1995a) (Hestrin et al., 1990), and where g_{NMDA_max} is the maximal conductance of the NMDA receptors (single channel conductance = 45 pS).

.

The equation describing the voltage-dependent Mg^{2+} block G (Jahr and Stevens, 1990) contains two empirically defined constants which we modified to fit our voltage clamp experiments (Fig. S4.3):

$$G = \frac{1}{1 + e^{-0.08V}(C/0.69)}$$

where C is the extracellular Mg^{2+} concentration (1 mM).

Approximately 10% of the current through NMDA channels is carried by Ca^{2+} (Jahr and Stevens, 1993). Therefore, we calculated $P_{Ca,NMDA}$ to be 10% of the total NMDA channel conductance (g_{NMDA}). The NMDA receptor current carried by Ca^{2+} was described as

$$I_{Ca\_NMDA} = P_{Ca,NMDA} G(V - E_{NMDA,Ca})$$

where $E_{NMDA,Ca}$ is the reversal potential of the NMDA channels for Ca^{2+} (40 mV) (Schneggenburger et al., 1993) (Spruston et al., 1995b).

Voltage-dependent Ca^{2+} channels

A voltage-dependent Ca^{2+} conductance was simulated using a Hodgkin-Huxley-like formalism adapted from Foehring et al. The current $I_{R\text{-}type}$ was described as

$$I_{R-type} = g_{R-type\_max} m^3 h (V - E_{Ca})$$

where m and h are the activation and inactivation variables, $g_{R\text{-}type\_max}$ is the total VDCCs conductance (single channel conductance = 17 pS), and E_{Ca} the reversal potential of the VDCCs. Activation and inactivation kinetics for $I_{R\text{-}type}$ were given by

$$\tau_m \frac{dm(t)}{dt} = -m(t) + m_\infty,\ \tau_h \frac{dh(t)}{dt} = -h(t) + h_\infty,\ \text{with } \tau_m = 3.6 \text{ ms},\ \tau_h = 200 \text{ ms},$$

and corresponding steady-state equations (Foehring et al., 2000) for m_{inf}, h_{inf}

$$m_\infty = \frac{1}{1 + e^{-\frac{V - V_{m\_half}}{k_m}}},\ h\infty = \frac{1}{1 + e^{\frac{V - V_{h\_half}}{k_h}}}$$

with V_{m_half} = -14 mV, k_m = 6.7 mV^{-1}, V_{h_half} = -65 mV, k_m = -11.8 mV^{-1}

Active conductance

Active conductance (I_{Na}, $I_{KA(prox)}$,$I_{KA(dist)}$, I_{KDR} and I_h) in the soma and dendrites were inserted and distributed as described by (Migliore et al., 1999).

The sodium current (I_{Na})

$$I_{Na} = g_{Na\_max} m^3 hs (V - E_{Na})$$

where m and h are the activation and inactivation variables, g_{Na_max} is the total sodium channel conductance, and E_{Na} the reversal potential of the sodium channel. The additional variable s was introduced to account for the dendritic location-dependent slow attenuation along the apical dendrite as a function of distance from the soma. Activation and inactivation kinetics for I_{Na} were given by

$$\tau_m \frac{dm(t)}{dt} = -m(t) + m_\infty, \tau_h \frac{dh(t)}{dt} = -h(t) + h_\infty,\ \tau_s \frac{ds(t)}{dt} = -s(t) + s_\infty \text{ with}$$

$$m_\infty = \frac{\alpha_m}{\alpha_m + \beta_m},\ \tau_m = \frac{0.5}{\alpha_m + \beta_m}$$

$$\alpha_m = \frac{0.4(V+30)}{1-e^{\frac{-(V+30)}{7.2}}},\ \beta_m = \frac{0.124(V+30)}{e^{\frac{V+30}{7.2}}-1}$$

$$h\infty = \frac{1}{1+e^{\frac{V-V_{h\_half}}{k_h}}} \text{ with } V_{\text{h\_half}} = \text{ 50mV, } k_{\text{m}} = \text{ 4mV}$$

$$\tau_h = \frac{0.5}{\alpha_m+\beta_m},\ \alpha_h = \frac{0.03(V+45)}{1-e^{\frac{-(V+45)}{1.5}}},\ \beta_h = \frac{0.01(V+45)}{e^{\frac{V+45}{1.5}}-1}$$

$$s\infty = \frac{1+b_s e^{\frac{V+58}{2}}}{1+e^{\frac{V-58}{2}}},\ \tau_s = \frac{3\cdot 10^4 \beta_s}{1+\alpha_s}$$

$b_s = 0.5$ in the apical dendrites, $b_s = 0.8$ in the soma and $b_s = 1$ elsewhere

$$\alpha_s = e^{0.45(V+60)},\ \beta_s = e^{0.09(V+60)}$$

A-type potassium current ($I_{KA(prox)}$) and ($I_{KA(dist)}$)

$$I_{KA} = g_{KA\_\max} mh(V - E_{KA})$$

where m and h are the activation and inactivation variables, $g_{\text{KA\_max}}$ is the total potassium channel conductances, and E_{KA} the reversal potential of the potassium channels. The maximal conductances for both channels vary as a function of distance from the soma.

$$g_{KA(prox)\_\max} = \begin{cases} 48\frac{1+d}{100} \\ 0 \end{cases} \text{ for d} \le 100 \text{ µm resp. for d} > 100 \text{ µm from soma}$$

$$g_{KA(dist)\_\max} = \begin{cases} 0 \\ 48\frac{1+d}{100} \end{cases} \text{ for d} \le 100 \text{ µm resp. for d} > 100 \text{ µm from soma}$$

Activation and inactivation kinetics for $I_{\text{KA(prox)}}$ were given by

$$\tau_m \frac{dm(t)}{dt} = -m(t) + m_\infty,\ \tau_h \frac{dh(t)}{dt} = -h(t) + h_\infty$$

$$m_\infty = \frac{1}{\alpha_m + 1},\ \tau_m = \frac{4\beta_m}{1+\alpha_m}$$

$$\alpha_m = e^{-0.038\frac{1.5+1}{1+\frac{e^{V+40}}{5}}(v-11)},\ \beta_m = e^{-0.038\frac{0.825+1}{1+\frac{e^{V+40}}{5}}(v-11)}$$

$$h\infty = \frac{1}{1 + ek_h \cdot (V - V_{h\_half})} \text{ with } V_{\text{h\_half}} = \text{ -56 mV, } k_{\text{m}} = 0.11 \text{ mV}^{-1}$$

$$\tau_m = \frac{2\beta_m}{1 + \alpha_m}$$

Activation and inactivation kinetics for $I_{\text{Na(dist)}}$ were given by

$$\tau_m \frac{dm(t)}{dt} = -m(t) + m_\infty, \ \tau_h \frac{dh(t)}{dt} = -h(t) + h_\infty$$

$$m_\infty = \frac{1}{\alpha_m + 1}, \ \tau_m = \frac{2\beta_m}{1 + \alpha_m}$$

$$\alpha_m = e^{-0.038\frac{1.8+1}{1+\frac{e^{V+40}}{5}}(v+1)}, \ \beta_m = e^{-0.038\frac{0.7+1}{1+\frac{e^{V+40}}{5}}(v+1)}$$

$$h\infty = \frac{1}{1 + ek_h \cdot (V - V_{h\_half})} \text{ with } V_{\text{h\_half}} = \text{ -56 mV, } k_{\text{m}} = 0.11 \text{ mV}^{-1}$$

$$\tau_h = 0.26 \cdot (V + 50)$$

Noninactivating potassium current (I_{KDR})

$$I_{kdr} = g_{KDR\_\max} n (V - E_{KDR})$$

where n is the activation variable, $g_{\text{KDR\_max}}$ is the total potassium conductance, and E_{KDR} the reversal potential of the potassium channel. Activation kinetics for I_{KDR} were given by

$$\tau_n \frac{dn(t)}{dt} = -n(t) + n_\infty$$

$$n_\infty = \frac{1}{1 + e^{(-k_n (V - E_{Kdr}))}}, \text{ with } V_{\text{n\_half}} = 13 \text{ mV, } k_{\text{m}} = 0.11 \text{ mV}^{-1}$$

Noninactivating, nonspecific cation current (I_h)

$$I_h = g_{h\_\max} n (V - E_{rev})$$

where n is the activation variable, $g_{\text{h\_max}}$ is the total conductance, and E_{rev} the reversal potential. Activation kinetics for I_{h} were given by

$$\tau_n \frac{dn(t)}{dt} = -n(t) + n_\infty$$

$$n_\infty = \frac{1}{1 + e^{\frac{-(V + V_{n\_half})}{k_n}}}, \text{ with } V_{\text{n\_half}} = \text{ 81mV, } k_{\text{n}} = 8\text{mV}$$

Simulation of spine Ca^{2+} transients

The increase of intracellular Ca^{2+}, $[Ca^{2+}]_i$, is given by

$$\frac{d[Ca^{2+}]_i}{dt} = -\frac{I_{Ca}}{2FV},$$

where I_{Ca} is the net Ca^{2+} current, F is Faraday's constant and V is the volume of the spine head. The net Ca^{2+} current I_{Ca} is described by $I_{Ca} = I_{R-type} + I_{Ca\_NMDA}$

$I_{R\text{-}type}$ is the Ca^{2+} current through R-type VDCCs, and I_{Ca_NMDA} the Ca^{2+} current through NMDA receptors. Since all our experiments were performed under conditions of high buffer concentration (600 μm Fluo5F), we used the simplifying assumption that all Ca^{2+} ions that enter the spine were immediately bound by dye molecules. The diffusion of Ca^{2+}-bound dye molecules through the spine neck was implemented as described (Carnevale, 2006), assuming D = 100 $\mu m^2/s$ (diffusion coefficient of Fluo5F-Ca^{2+} in cytoplasm) (Michailova et al., 2002) and $[Ca^{2+}]^{\infty}_i$ = 50 nM (resting intracellular Ca^{2+} concentration). Without introduction of any additional free parameters (Ca^{2+} removal mechanisms), the experimentally measured time course of the fluorescence transients under different conditions was well captured by the simulation (Fig. 3.3A and B).

The free parameters of our model were the numbers of AMPA receptors, NMDA receptors, and R-type Ca^{2+} channels in the spine head. We adjusted the current densities (Table 7.1) to reproduce the Ca^{2+} amplitude of the pharmacological experiments (Fig. S3.5), and then systematically explored the parameter space locally (Fig. S3.6). In the best fitting model, the depolarization in the spine had a high amplitude (55.2 mV), which was attenuated by dendritic filtering to 1.1 mV at the soma (Fig. 3.3C and Table 7.2). We would like to emphasize that the absolute channel numbers needed to reproduce our experimental findings are dependent on other parameters of the model, e.g. spine neck geometry, cytoplasmic resistivity. The basic mechanism of amplification, positive feedback by voltage-dependent conductances, is a robust feature of any model compatible with our experimental findings.

	AMPA receptor	NMDA receptor	R-type VDCC
Number of channels present in spine	240	110	100
Number of channels open at peak of current	240	18	10

Table 7.1: ***Channel activation during EPSP in model spine***

	EPSC amplitude (VC)	EPSP amplitude (CC)
spine head	41 pA	54.8 mV
spine base	n/a	22.2 mV
soma	24 pA	1.1 mV

Table 7.2: ***Attenuation of current and voltage in CA1 pyramidal cell model***

References

Abraham RT (1996) Phosphatidylinositol 3-kinase related kinases. Curr Opin Immunol 8:412-418.

Amaral DG, Witter MP (1989) The three-dimensional organization of the hippocampal formation: a review of anatomical data. Neuroscience 31:571-591.

Bi GQ, Poo MM (1998) Synaptic modifications in cultured hippocampal neurons: dependence on spike timing, synaptic strength, and postsynaptic cell type. J Neurosci 18:10464-10472.

Blackstad TW (1956) Commissural connections of the hippocampal region in the rat, with special reference to their mode of termination. J Comp Neurol 105:417-537.

Blackstad TW (1958) On the termination of some afferents to the hippocampus and fascia dentata; an experimental study in the rat. Acta Anat (Basel) 35:202-214.

Blaustein MP, Lederer WJ (1999a) Sodium-calcium exchange: Its physiological implications. Physiological Reviws 79:763-854.

Blaustein MP, Lederer WJ (1999b) Sodium/calcium exchange: its physiological implications. Physiol Rev 79:763-854.

Bliss TV, Collingridge GL (1993) A synaptic model of memory: long-term potentiation in the hippocampus. Nature 361:31-39.

Bloodgood BL, Sabatini BL (2005) Neuronal activity regulates diffusion across the neck of dendritic spines. Science 310:866-869.

Bloodgood BL, Sabatini BL (2007a) Ca(2+) signaling in dendritic spines. Curr Opin Neurobiol 17:345-351.

Bloodgood BL, Sabatini BL (2007b) Nonlinear Regulation of Unitary Synaptic Signals by CaV(2.3) Voltage-Sensitive Calcium Channels Located in Dendritic Spines. Neuron 53:249-260.

Burnashev N, Monyer H, Seeburg PH, Sakmann B (1992) Divalent ion permeability of AMPA receptor channels is dominated by the edited form of a single subunit. Neuron 8:189-198.

Busetto G, Higley MJ, Sabatini BL (2008) Developmental presence and disappearance of postsynaptically silent synapses on dendritic spines of rat layer 2/3 pyramidal neurons. J Physiol.

Carlisle HJ, Kennedy MB (2005) Spine architecture and synaptic plasticity. Trends Neurosci 28:182-187.

Carnevale NTaH, M.L. (2006) The NEURON Book. Cambridge, UK: Cambridge University Press.

Catterall WA (2000) Structure and regulation of voltage-gated Ca2+ channels. Annu Rev Cell Dev Biol 16:521-555.

Catterall WA, Perez-Reyes E, Snutch TP, Striessnig J (2005) International Union of Pharmacology. XLVIII. Nomenclature and structure-function relationships of voltage-gated calcium channels. Pharmacol Rev 57:411-425.

Chang HT (1952) Cortical neurons with particular reference to the apical dendrites. Cold Spring Harb Symp Quant Biol 17:189-202.

Chen HX, Otmakhov N, Lisman J (1999) Requirements for LTP induction by pairing in hippocampal CA1 pyramidal cells. J Neurophysiol 82:526-532.

Choi S, Klingauf J, Tsien RW (2000) Postfusional regulation of cleft glutamate concentration during LTP at 'silent synapses'. Nat Neurosci 3:330-336.

Conti R, Lisman J (2003) The high variance of AMPA receptor- and NMDA receptor-mediated responses at single hippocampal synapses: evidence for multiquantal release. Proc Natl Acad Sci U S A 100:4885-4890.

Cooney JR, Hurlburt JL, Selig DK, Harris KM, Fiala JC (2002) Endosomal compartments serve multiple hippocampal dendritic spines from a widespread rather than a local store of recycling membrane. J Neurosci 22:2215-2224.

Coss RG, Perkel DH (1985) The function of dendritic spines: a review of theoretical issues. Behav Neural Biol 44:151-185.

Crick F (1982) Do dendritic spines twitch? Trends in Neuroscience 12:44-46

Czurko A, Czeh B, Seress L, Nadel L, Bures J (1997) Severe spatial navigation deficit in the Morris water maze after single high dose of neonatal x-ray irradiation in the rat. Proc Natl Acad Sci U S A 94:2766-2771.

Debanne D, Gahwiler BH, Thompson SM (1998) Long-term synaptic plasticity between pairs of individual CA3 pyramidal cells in rat hippocampal slice cultures. J Physiol 507 (Pt 1):237-247.

DeRobertis ED, Bennett HS (1955) Some features of the submicroscopic morhpology of synapses in frog and earthworm. J Biophys Biochem 1:47-58.

Dingledine R, Borges K, Bowie D, Traynelis SF (1999) The glutamate receptor ion channels. Pharmacol Rev 51:7-61.

Durand GM, Kovalchuk Y, Konnerth A (1996) Long-term potentiation and functional synapse induction in developing hippocampus. Nature 381:71-75.

Emptage N, Bliss TV, Fine A (1999) Single synaptic events evoke NMDA receptor-mediated release of calcium from internal stores in hippocampal dendritic spines. Neuron 22:115-124.

Feldman DE (2000) Timing-based LTP and LTD at vertical inputs to layer II/III pyramidal cells in rat barrel cortex. Neuron 27:45-56.

Fifkova E (1985) A possible mechanism of morphometric changes in dendritic spines induced by stimulation. Cell Mol Neurobiol 5:47-63.

Fifkova E, Delay RJ (1982) Cytoplasmic actin in neuronal processes as a possible mediator of synaptic plasticity. J Cell Biol 95:345-350.

Foehring RC, Mermelstein PG, Song WJ, Ulrich S, Surmeier DJ (2000) Unique properties of R-type calcium currents in neocortical and neostriatal neurons. J Neurophysiol 84:2225-2236.

Franks KM, Bartol TM, Jr., Sejnowski TJ (2002) A Monte Carlo model reveals independent signaling at central glutamatergic synapses. Biophys J 83:2333-2348.

Gasparini S, Saviane C, Voronin LL, Cherubini E (2000) Silent synapses in the developing hippocampus: lack of functional AMPA receptors or low probability of glutamate release? Proc Natl Acad Sci U S A 97:9741-9746.

Geiger JR, Melcher T, Koh DS, Sakmann B, Seeburg PH, Jonas P, Monyer H (1995) Relative abundance of subunit mRNAs determines gating and Ca2+ permeability of AMPA receptors in principal neurons and interneurons in rat CNS. Neuron 15:193-204.

Golding NL, Kath WL, Spruston N (2001) Dichotomy of action-potential backpropagation in CA1 pyramidal neuron dendrites. J Neurophysiol 86:2998-3010.

Gray EG (1959) Electron microscopy of synaptic contacts on dendrite spines of the cerebral cortex. Nature 183:1592-1593.

Gray EG, Guillery RW (1963) A Note on the Dendritic Spine Apparatus. J Anat 97:389-392.

Gray NW, Weimer RM, Bureau I, Svoboda K (2006) Rapid redistribution of synaptic PSD-95 in the neocortex in vivo. PLoS Biol 4:e370.

Grutzendler J, Kasthuri N, Gan WB (2002) Long-term dendritic spine stability in the adult cortex. Nature 420:812-816.

Gustafsson B, Wigstrom H, Abraham WC, Huang YY (1987) Long-term potentiation in the hippocampus using depolarizing current pulses as the conditioning stimulus to single volley synaptic potentials. J Neurosci 7:774-780.

Harris KM, Stevens JK (1988) Dendritic spines of rat cerebellar Purkinje cells: serial electron microscopy with reference to their biophysical characteristics. J Neurosci 8:4455-4469.

Harris KM, Stevens JK (1989) Dendritic spines of CA 1 pyramidal cells in the rat hippocampus: serial electron microscopy with reference to their biophysical characteristics. J Neurosci 9:2982-2997.

Harris KM, Kater SB (1994) Dendritic spines: cellular specializations imparting both stability and flexibility to synaptic function. Annu Rev Neurosci 17:341-371.

Harvey CD, Svoboda K (2007) Locally dynamic synaptic learning rules in pyramidal neuron dendrites. Nature 450:1195-1200.

Hebb DO (1949) The organization of behavior: A neuropsychological thoery: John Wiley & Sons Inc

Hestrin S, Sah P, Nicoll RA (1990) Mechanisms generating the time course of dual component excitatory synaptic currents recorded in hippocampal slices. Neuron 5:247-253.

Hines ML, Carnevale NT (1997) The NEURON simulation environment. Neural Comput 9:1179-1209.

Holmes WR (1990) Is the function of dendritic spines to concentrate calcium? Brain Res 519:338-342.

Holtmaat AJ, Trachtenberg JT, Wilbrecht L, Shepherd GM, Zhang X, Knott GW, Svoboda K (2005) Transient and persistent dendritic spines in the neocortex in vivo. Neuron 45:279-291.

Imredy JP, Yue DT (1994) Mechanism of Ca(2+)-sensitive inactivation of L-type Ca2+ channels. Neuron 12:1301-1318.

Isaac JT, Nicoll RA, Malenka RC (1995) Evidence for silent synapses: implications for the expression of LTP. Neuron 15:427-434.

Isomura Y, Fujiwara-Tsukamoto Y, Imanishi M, Nambu A, Takada M (2002) Distance-dependent Ni(2+)-sensitivity of synaptic plasticity in apical dendrites of hippocampal CA1 pyramidal cells. J Neurophysiol 87:1169-1174.

Jahr CE, Stevens CF (1990) Voltage dependence of NMDA-activated macroscopic conductances predicted by single-channel kinetics. J Neurosci 10:3178-3182.

Jahr CE, Stevens CF (1993) Calcium permeability of the N-methyl-D-aspartate receptor channel in hippocampal neurons in culture. Proc Natl Acad Sci U S A 90:11573-11577.

Kaczmarek L, Kossut M, Skangiel-Kramska J (1997) Glutamate receptors in cortical plasticity: molecular and cellular biology. Physiol Rev 77:217-255.

Kasai H, Matsuzaki M, Noguchi J, Yasumatsu N, Nakahara H (2003) Structure-stability-function relationships of dendritic spines. Trends Neurosci 26:360-368.

Kennedy MJ, Ehlers MD (2006) Organelles and trafficking machinery for postsynaptic plasticity. Annu Rev Neurosci 29:325-362.

Kim CH, Lisman JE (1999) A role of actin filament in synaptic transmission and long-term potentiation. J Neurosci 19:4314-4324.

Knott GW, Holtmaat A, Wilbrecht L, Welker E, Svoboda K (2006) Spine growth precedes synapse formation in the adult neocortex in vivo. Nat Neurosci 9:1117-1124.

Koch C (1999) Biophysics of Computation. New York: Oxford Univ. Press

Koch C, Poggio T (1985) The biophysical properties of spines as a basis for their electrical function: a comment on Kawato & Tsukahara (1983). J Theor Biol 113:225-229.

Koch C, Zador A (1993) The function of dendritic spines: devices subserving biochemical rather than electrical compartmentalization. J Neurosci 13:413-422.

Koester HJ, Sakmann B (1998) Calcium dynamics in single spines during coincident pre- and postsynaptic activity depend on relative timing of back-propagating action potentials and subthreshold excitatory postsynaptic potentials. Proc Natl Acad Sci U S A 95:9596-9601.

Kohr G (2006) NMDA receptor function: subunit composition versus spatial distribution. Cell Tissue Res 326:439-446.

Korkotian E, Segal M (1999) Release of calcium from stores alters the morphology of dendritic spines in cultured hippocampal neurons. Proc Natl Acad Sci U S A 96:12068-12072.

Kovalchuk Y, Eilers J, Lisman J, Konnerth A (2000) NMDA receptor-mediated subthreshold Ca(2+) signals in spines of hippocampal neurons. J Neurosci 20:1791-1799.

Kullmann DM (2003) Silent synapses: what are they telling us about long-term potentiation? Philos Trans R Soc Lond B Biol Sci 358:727-733.

Li Z, Okamoto K, Hayashi Y, Sheng M (2004) The importance of dendritic mitochondria in the morphogenesis and plasticity of spines and synapses. Cell 119:873-887.

Liao D, Malinow R (1996) Deficiency in induction but not expression of LTP in hippocampal slices from young rats. Learn Mem 3:138-149.

Liao D, Hessler NA, Malinow R (1995) Activation of postsynaptically silent synapses during pairing-induced LTP in CA1 region of hippocampal slice. Nature 375:400-404.

Linden DJ (1999) The return of the spike: postsynaptic action potentials and the induction of LTP and LTD. Neuron 22:661-666.

Lisman J (1989) A mechanism for the Hebb and the anti-Hebb processes underlying learning and memory. Proc Natl Acad Sci U S A 86:9574-9578.

Losi G, Prybylowski K, Fu Z, Luo JH, Vicini S (2002) Silent synapses in developing cerebellar granule neurons. J Neurophysiol 87:1263-1270.

Magee JC, Johnston D (1997) A synaptically controlled, associative signal for Hebbian plasticity in hippocampal neurons. Science 275:209-213.

Malenka RC, Nicoll RA (1999) Long-term potentiation--a decade of progress? Science 285:1870-1874.

Malinow R (1991) Transmission between pairs of hippocampal slice neurons: quantal levels, oscillations, and LTP. Science 252:722-724.

Markram H, Lubke J, Frotscher M, Sakmann B (1997) Regulation of synaptic efficacy by coincidence of postsynaptic APs and EPSPs. Science 275:213-215.

Matsuzaki M, Honkura N, Ellis-Davies GC, Kasai H (2004) Structural basis of long-term potentiation in single dendritic spines. Nature 429:761-766.

Matsuzaki M, Ellis-Davies GC, Nemoto T, Miyashita Y, Iino M, Kasai H (2001) Dendritic spine geometry is critical for AMPA receptor expression in hippocampal CA1 pyramidal neurons. Nat Neurosci 4:1086-1092.

Matus A, Ackermann M, Pehling G, Byers HR, Fujiwara K (1982) High actin concentrations in brain dendritic spines and postsynaptic densities. Proc Natl Acad Sci U S A 79:7590-7594.

Mayer ML, Westbrook GL, Guthrie PB (1984) Voltage-dependent block by Mg2+ of NMDA responses in spinal cord neurones. Nature 309:261-263.

Michailova A, DelPrincipe F, Egger M, Niggli E (2002) Spatiotemporal features of Ca2+ buffering and diffusion in atrial cardiac myocytes with inhibited sarcoplasmic reticulum. Biophys J 83:3134-3151.

Migliore M, Hoffman DA, Magee JC, Johnston D (1999) Role of an A-type K+ conductance in the back-propagation of action potentials in the dendrites of hippocampal pyramidal neurons. J Comput Neurosci 7:5-15.

Miller JP, Rall W, Rinzel J (1985) Synaptic amplification by active membrane in dendritic spines. Brain Res 325:325-330.

Miller SG, Kennedy MB (1986) Regulation of brain type II Ca2+/calmodulin-dependent protein kinase by autophosphorylation: a Ca2+-triggered molecular switch. Cell 44:861-870.

Morris RG, Anderson E, Lynch GS, Baudry M (1986) Selective impairment of learning and blockade of long-term potentiation by an N-methyl-D-aspartate receptor antagonist, AP5. Nature 319:774-776.

Moser EI, Krobert KA, Moser MB, Morris RG (1998) Impaired spatial learning after saturation of long-term potentiation. Science 281:2038-2042.

Moser MB, Trommald M, Andersen P (1994) An increase in dendritic spine density on hippocampal CA1 pyramidal cells following spatial learning in adult rats suggests the formation of new synapses. Proc Natl Acad Sci U S A 91:12673-12675.

Moses SN, Cole C, Ryan JD (2005) Relational memory for object identity and spatial location in rats with lesions of perirhinal cortex, amygdala and hippocampus. Brain Res Bull 65:501-512.

Mulkey RM, Malenka RC (1992) Mechanisms underlying induction of homosynaptic long-term depression in area CA1 of the hippocampus. Neuron 9:967-975.

Muller W, Connor JA (1991) Dendritic spines as individual neuronal compartments for synaptic Ca2+ responses. Nature 354:73-76.

Nakamura T, Barbara JG, Nakamura K, Ross WN (1999) Synergistic release of Ca2+ from IP3-sensitive stores evoked by synaptic activation of mGluRs paired with backpropagating action potentials. Neuron 24:727-737.

Nevian T, Sakmann B (2004) Single spine Ca2+ signals evoked by coincident EPSPs and backpropagating action potentials in spiny stellate cells of layer 4 in the juvenile rat somatosensory barrel cortex. J Neurosci 24:1689-1699.

Nevian T, Sakmann B (2006) Spine Ca2+ signaling in spike-timing-dependent plasticity. J Neurosci 26:11001-11013.

Nimchinsky EA, Sabatini BL, Svoboda K (2002) Structure and function of dendritic spines. Annu Rev Physiol 64:313-353.

Noguchi J, Matsuzaki M, Ellis-Davies GC, Kasai H (2005) Spine-neck geometry determines NMDA receptor-dependent Ca2+ signaling in dendrites. Neuron 46:609-622.

Nowak L, Bregestovski P, Ascher P, Herbet A, Prochiantz A (1984) Magnesium gates glutamate-activated channels in mouse central neurones. Nature 307:462-465.

Nusser Z, Lujan R, Laube G, Roberts JD, Molnar E, Somogyi P (1998) Cell type and pathway dependence of synaptic AMPA receptor number and variability in the hippocampus. Neuron 21:545-559.

O'Keefe J, Dostrovsky J (1971) The hippocampus as a spatial map. Preliminary evidence from unit activity in the freely-moving rat. Brain Res 34:171-175.

Palay SL (1956) Synapses in the central nervous system. J Biophys Biochem Cytol 2:193-202.

Paulsen O, Sejnowski TJ (2000) Natural patterns of activity and long-term synaptic plasticity. Curr Opin Neurobiol 10:172-179.

Perkel DH, Perkel DJ (1985) Dendritic spines: role of active membrane in modulating synaptic efficacy. Brain Res 325:331-335.

Petersen CC, Malenka RC, Nicoll RA, Hopfield JJ (1998) All-or-none potentiation at CA3-CA1 synapses. Proc Natl Acad Sci U S A 95:4732-4737.

Petralia RS, Esteban JA, Wang YX, Partridge JG, Zhao HM, Wenthold RJ, Malinow R (1999) Selective acquisition of AMPA receptors over postnatal development suggests a molecular basis for silent synapses. Nat Neurosci 2:31-36.

Pettit DL, Perlman S, Malinow R (1994) Potentiated transmission and prevention of further LTP by increased CaMKII activity in postsynaptic hippocampal slice neurons. Science 266:1881-1885.

Pologruto TA, Sabatini BL, Svoboda K (2003) ScanImage: Flexible software for operating laser scanning microscopes. Biomed Eng Online 2:13.

Pozzan T, Rizzuto R, Volpe P, Meldolesi J (1994) Molecular and cellular physiology of intracellular calcium stores. Physiol Rev 74:595-636.

Raghavachari S, Lisman JE (2004) Properties of Quantal Transmission at CA1 Synapses. J Neurophysiol.

Rall W, Shepherd GM (1968) Theoretical reconstruction of field potentials and dendrodendritic synaptic interactions in olfactory bulb. J Neurophysiol 31:884-915.

Ramon y Cajal S (1888) Estructura de los centros nerviosos de les aves. Rev Trim Hisol Norm Pat 1:1-10.

Ramon y Cajal S (1891) Signification fisiologica de las expansiones protoplasmicas y nerviosas de la substancia gris. In: Congreso Medico Valenciano.

Ramon y Cajal S (1893) Neue darstellung vom histologischen bau des centralnervensystem. Arch Anat Entwick:319-428.

Ramon y Cajal S (1991) New ideas on the structure of the nervous system of man and vertebrates. From: Lcs nouvelles idees sur la structure du systeme nerveux chez l'homme et chez les vertebres (Swanson N, Swanson LM, transl). Cambridge, MA: MIT Press.

Rempel-Clower NL, Zola SM, Squire LR, Amaral DG (1996) Three cases of enduring memory impairment after bilateral damage limited to the hippocampal formation. J Neurosci 16:5233-5255.

Rhodes P (2006) The properties and implications of NMDA spikes in neocortical pyramidal cells. J Neurosci 26:6704-6715.

Sabatini BL, Maravall M, Svoboda K (2001) Ca(2+) signaling in dendritic spines. Curr Opin Neurobiol 11:349-356.

Sabatini BL, Oertner TG, Svoboda K (2002) The life cycle of Ca(2+) ions in dendritic spines. Neuron 33:439-452.

Santamaria F, Wils S, De Schutter E, Augustine GJ (2006) Anomalous diffusion in Purkinje cell dendrites caused by spines. Neuron 52:635-648.

Schiller J, Schiller Y (2001) NMDA receptor-mediated dendritic spikes and coincident signal amplification. Curr Opin Neurobiol 11:343-348.

Schiller J, Schiller Y, Clapham DE (1998) NMDA receptors amplify calcium influx into dendritic spines during associative pre- and postsynaptic activation. Nat Neurosci 1:114-118.

Schneggenburger R, Zhou Z, Konnerth A, Neher E (1993) Fractional contribution of calcium to the cation current through glutamate receptor channels. Neuron 11:133-143.

Scoville WB, Milner B (1957) Loss of recent memory after bilateral hippocampal lesions. J Neurol Neurosurg Psychiatry 20:11-21.

Segev I, Rall W (1988) Computational study of an excitable dendritic spine. J Neurophysiol 60:499-523.

Senn W (2002) Beyond spike timing: the role of nonlinear plasticity and unreliable synapses. Biol Cybern 87:344-355.

Shepherd GM, Brayton RK, Miller JP, Segev I, Rinzel J, Rall W (1985) Signal enhancement in distal cortical dendrites by means of interactions between active dendritic spines. Proc Natl Acad Sci U S A 82:2192-2195.

Silva AJ, Stevens CF, Tonegawa S, Wang Y (1992) Deficient hippocampal long-term potentiation in alpha-calcium-calmodulin kinase II mutant mice. Science 257:201-206.

Sjostrom PJ, Turrigiano GG, Nelson SB (2001) Rate, timing, and cooperativity jointly determine cortical synaptic plasticity. Neuron 32:1149-1164.

Sobczyk A, Scheuss V, Svoboda K (2005) NMDA receptor subunit-dependent [Ca2+] signaling in individual hippocampal dendritic spines. J Neurosci 25:6037-6046.

Song S, Abbott LF (2001) Cortical development and remapping through spike timing-dependent plasticity. Neuron 32:339-350.

Sourdet V, Debanne D (1999) The role of dendritic filtering in associative long-term synaptic plasticity. Learn Mem 6:422-447.

Spacek J, Harris KM (1997) Three-dimensional organization of smooth endoplasmic reticulum in hippocampal CA1 dendrites and dendritic spines of the immature and mature rat. J Neurosci 17:190-203.

Spruston N, Jonas P, Sakmann B (1995a) Dendritic glutamate receptor channels in rat hippocampal CA3 and CA1 pyramidal neurons. J Physiol 482 (Pt 2):325-352.

Spruston N, Schiller Y, Stuart G, Sakmann B (1995b) Activity-dependent action potential invasion and calcium influx into hippocampal CA1 dendrites. Science 268:297-300.

Stepanyants A, Hof PR, Chklovskii DB (2002) Geometry and structural plasticity of synaptic connectivity. Neuron 34:275-288.

Stevens CF (1979) The neuron. Sci Am 241:54-65.

Steward O, Falk PM (1985) Polyribosomes under developing spine synapses: growth specializations of dendrites at sites of synaptogenesis. J Neurosci Res 13:75-88.

Steward O, Reeves TM (1988) Protein-synthetic machinery beneath postsynaptic sites on CNS neurons: association between polyribosomes and other organelles at the synaptic site. J Neurosci 8:176-184.

Stoppini L, Buchs PA, Muller D (1991) A simple method for organotypic cultures of nervous tissue. J Neurosci Methods 37:173-182.

Stuart GJ, Sakmann B (1994) Active propagation of somatic action potentials into neocortical pyramidal cell dendrites. Nature 367:69-72.

Stuart GJ, Hausser M (2001) Dendritic coincidence detection of EPSPs and action potentials. Nat Neurosci 4:63-71.

Svoboda K (2004) Do spines and dendrites distribute dye evenly? Trends Neurosci 27:445-446.

Svoboda K, Yasuda R (2006) Principles of two-photon excitation microscopy and its applications to neuroscience. Neuron 50:823-839.

Svoboda K, Tank DW, Denk W (1996) Direct measurement of coupling between dendritic spines and shafts. Science 272:716-719.

Svoboda K, Helmchen F, Denk W, Tank DW (1999) Spread of dendritic excitation in layer 2/3 pyramidal neurons in rat barrel cortex in vivo. Nat Neurosci 2:65-73.

Swindale NV (1981) Dendritic spines only connect. Tends Neurosci 4:240-241.

Tada T, Sheng M (2006) Molecular mechanisms of dendritic spine morphogenesis. Curr Opin Neurobiol 16:95-101.

Takumi Y, Ramirez-Leon V, Laake P, Rinvik E, Ottersen OP (1999) Different modes of expression of AMPA and NMDA receptors in hippocampal synapses. Nat Neurosci 2:618-624.

Tanaka J, Matsuzaki M, Tarusawa E, Momiyama A, Molnar E, Kasai H, Shigemoto R (2005) Number and density of AMPA receptors in single synapses in immature cerebellum. J Neurosci 25:799-807.

Toni N, Buchs PA, Nikonenko I, Bron CR, Muller D (1999) LTP promotes formation of multiple spine synapses between a single axon terminal and a dendrite. Nature 402:421-425.

Voronin LL, Cherubini E (2004) "Deaf, or mute and whispering" silent synapses: their role in synaptic plasticity. J Physiol.

Walikonis RS, Jensen ON, Mann M, Provance DW, Jr., Mercer JA, Kennedy MB (2000) Identification of proteins in the postsynaptic density fraction by mass spectrometry. J Neurosci 20:4069-4080.

Ward B, McGuinness L, Akerman CJ, Fine A, Bliss TV, Emptage NJ (2006) State-dependent mechanisms of LTP expression revealed by optical quantal analysis. Neuron 52:649-661.

Whitlock JR, Heynen AJ, Shuler MG, Bear MF (2006) Learning induces long-term potentiation in the hippocampus. Science 313:1093-1097.

Wickens J (1988) Electrically coupled but chemically isolated synapses: dendritic spines and calcium in a rule for synaptic modification. Prog Neurobiol 31:507-528.

Wilson CJ (1984) Passive cable properties of dendritic spines and spiny neurons. J Neurosci 4:281-297.

Yasuda R, Sabatini BL, Svoboda K (2003) Plasticity of calcium channels in dendritic spines. Nat Neurosci 6:948-955.

Yasuda R, Nimchinsky EA, Scheuss V, Pologruto TA, Oertner TG, Sabatini BL, Svoboda K (2004) Imaging calcium concentration dynamics in small neuronal compartments. Sci STKE 2004:pl5.

Yuste R, Denk W (1995) Dendritic spines as basic functional units of neuronal integration. Nature 375:682-684.

Yuste R, Majewska A, Cash SS, Denk W (1999) Mechanisms of calcium influx into hippocampal spines: heterogeneity among spines, coincidence detection by NMDA receptors, and optical quantal analysis. J Neurosci 19:1976-1987.

Zola-Morgan S, Squire LR, Amaral DG (1986) Human amnesia and the medial temporal region: enduring memory impairment following a bilateral lesion limited to field CA1 of the hippocampus. J Neurosci 6:2950-2967.

Zucker RS (1999) Calcium- and activity-dependent synaptic plasticity. Curr Opin Neurobiol 9:305-313.

List of Abbreviations

ACSF	artificial cerebrospinal fluid
AMPA	α-Amino-3-hydroxy-5-methyl-4-isoxazolepropionic acid
AP	action potential
bAP	backpropagating action potential
CA1	cornu ammoni 1
CICR	Ca^{2+}-induced Ca^{2+}-release
EPSP	excitatory postsynaptic potential
HVA	High-Voltage Activated Ca^{2+} channels
IP_3R	inositol-1,4,5-triphosphate receptor
LTD	long-term depression
LTP	long-term potentiation
LVA	Low-Voltage Activated Ca^{2+} channels
NMDA	N-Methyl-D-aspartic acid
p_r	release probability
PSD	postsynaptic density
RyR	Ryanodine-receptor
sER	Smooth endoplasmatic reticulum
STDP	spike-timing-dependent plasticity
VDCC	voltage-dependent Ca^{2+} channel

Acknowledgments

I would like to thank my advisor, Dr. Thomas G. Oertner, for giving me the opportunity to work on this fascinating project in his laboratory and for his support and guidance during this time. His suggestions and his proofreading have been crucial to this thesis.

Thanks to my committee members, Prof. Denis Monard and Prof. Andreas Lüthi for their scientific advice. I gratefully acknowledge their critical questions and helpful advice.

Thanks to Lei Tian for his help with the biophysical model.

I would like to thank all members of the Oertner laboratory, especially Yan-Ping Zhang, Daniela Gerosa Erni, Niklaus Holbro, Tobias Rose and Philipp Schoenenberger for their support. It was always most enjoyable to work in this group and I had a wonderful time. Thanks to all of them.

Finally, I would like to thank my family, especially my husband Thomas and my son Niklas, for their love and support. I thank my mother Helena, father Hans and Åse for looking after Niklas and for their support and encouragement.

Curriculum Vitae

Name	Åsa Müller-Grunditz
Address	Wasserwerkstrasse 14
	CH-4332 Stein
Phone	+41 (0)62 875 14 95
Mobil	+41 (0)79 506 53 19
e-mail	asa.grunditz@fmi.ch
Nationality	Swedish
Date of Birth	17th of September 1976

Education

2003 – 2008	PhD in Neurobiology, Friedrich Miescher Institute in Basel, Switzerland
1998 – 2003	Master of Science (Biology), University of Basel, Switzerland
1997 – 1998	Certificate in psychology with medical orientation, University of Basel, Switzerland
1993 – 1997	High school (Kantonsschule, Matura Typus C, mathematical) in Baden, Switzerland

Research Experience

Sept. 2003 –	PhD Thomas Oertner's laboratory at the Friedrich Miescher Institute in Basel, Switzerland Title/Project: Dendritic spines act as chemical and electrical compartments: A two-photon imaging study in the hippocampus of the rat
Aug. 2002 – Mai 2003	MSc project , neuroscience, Novartis Pharma AG in Basel, Switzerland Title/Project: Establishment of an assay for α-secretase activity in cell cultures and pharmacological testing of potential inhibitors of α-secretase.

April 2002 – Aug. 2002	Practical course Prof. Dr. Esther Stoeckli's laboratory at the University of Basel, Switzerland Title/Project: Identification of different cell populations and potential changes in the cell using marker genes to investigate differentiation in the developing spinal cord of chick embryos

Information Technology

Programming languages:	Java, Matlab
Data and Mathematics treatment tools	Matlab, Imaris, Image Access , NEURON
User and operator skills in Operating systems	Windows XP/2000
Document edition	Word, Excel, PowerPoint, CorelDraw

Experimental, Technical and other Experiences

Two-photon calcium imaging and electrophysiology

Development of an assay (ELISA and Western blot) for alpha-secretase activity in Alzheimer's disease

Immunostaining, in sity hybridisation, and RNAi

Teaching physics at the high school in Oberwil, Switzerland

Supervising undergraduate students at the FMI using the microscopy and imaging tools

Publications

Grunditz A, Holbro N, Tian L, Zuo Y, Oertner TG, Spine neck plasticity as a mechanism to dissociate electrical and chemical signaling, *Manuscript submitted*

Schoenenberger P, Grunditz A, Rose T, and Oertner TG, Optimizing the spatial resolution of channelrhodopsin-2 activation, *Manuscript submitted*

Bourikas D, Pekarik V, Baeriswyl T, Grunditz A, Sadhu R, Nardo M, Stoeckli ET, Sonic hedgehog guides commissural axons along the longitudinal axis of the spinal cord, Nat Neurosci. 2005 Mar; 8 (3): 297-304

Lipscher J, Burger D, Grunditz Å, Kaiser P, Kamber S, Nicca M, Petrick A, Spycher M, Chemie und Verbrechen, Chemie in unser Zeit Juni 1998; 32(3): 143-149

Presentations

Grunditz A., T. G. Oertner, Interactions between AMPA and NMDA receptors in individual dendritic spines, Program No. A191.4. Vienna, Austria: Forum of European Neuroscience, 2006. Online

Grunditz A., T. G. Oertner, Visualizing interactions between AMPA and NMDA receptors in individual dendritic spines, Program No. 493.13. Washington: Society for Neuroscience, 2005. Online

March 2007 Swiss Society for Neuroscience Meeting in Bern: The amplitude of excitatory potentials in individual spines

Jan. 2006 ELTEM NEUREX Workshop, Centre of Neuroscience in Strasbourg: Visualizing silent versus functional spines in CA1 pyramidal cells

Honors / Adwards

2006	MBL course Scholarship of the Boehringer Ingelheim Fonds
1997	Award for the team work ”Chemie und Verbrechen” of the University of Fribourg, Switzerland